NUMERICAL AND THERMODYNAMIC ANALYSIS OF EXTERNAL FLOW OVER TUBE BANKS FOR WASTE HEAT RECOVERY

by

MUSTAFA ERGUVAN

DAVID W.MACPHEE, COMMITTEE CHAIR
MUHAMMAD ALI ROB SHARIF
PAUL G. ALLISON

A THESIS

Submitted in partial fulfillment of the requirements for
the degree of Master of Science in the Department
of Mechanical Engineering in the
Graduate School of The
University of Alabama

TUSCALOOSA, ALABAMA

2018

Copyright Mustafa Erguvan 2018
ALL RIGHTS RESERVED

ABSTRACT

This study will involve numerical energy and exergy analyses for unsteady cross flow over heated circular cylinders. Several simulations were conducted using Ansys FLUENT 18.2 with different values of Reynolds number, inlet temperatures, number of in-line cylinders, pitch ratios, as well as the heat transfer coefficient of artificial heat leakages. Heat leakages were considered as the source terms for the concerned domain. The comparison of the numerical results with published data was favorable with regard to values of Nusselt number and pressure drop.

It was found that the energy efficiency varies from 72%–99% for all cases, while viscous dissipation had a highly limited effect on the energy efficiency of cases with low Reynolds number values. The exergy efficiency ranged from 26%–70%, while the entropy generation due to heat transfer was found to have a significant effect on exergy efficiency. Furthermore, while heat leakage had a considerable effect on energy efficiency, its effect was more prominent in the exergy analysis, especially for low Reynolds number and high pitch ratio cases. It was observed that while energy efficiency increases with increasing inlet temperature, exergy efficiency demonstrates a decreasing trend. Therefore, inlet temperature was determined as the most influential parameter in this analysis.

The results suggest that energy and exergy efficiencies can be maximized through the selection of specific pitch ratios for various Reynolds number values. The results of this study could be useful in designing more efficient heat recovery systems, especially for low, medium, and high temperature applications.

LIST OF ABBREVIATIONS AND SYMBOLS

A	Surface area (m^2)
C	Specific heat (J/kg K)
D	Tube diameter (m)
$\dot{E}$	Energy (W)
f	Friction factor
h	Enthalpy (J)
k	Thermal conductivity of the heat transfer fluid (W/m K)
$\dot{m}$	Mass flow rate (kg/s)
Nu	Nusselt number
P	Pressure (Pa)
Pr	Prandtl number
Pr_s	Prandtl number at the surface temperature
$\dot{Q}$	Total heat transfer (W)
$\dot{Q}_l$	Heat leakage (W)
$\dot{Q}_w$	Total heat transfer over the tubes (W)
R_0	Ideal gas constant (J/kg K)
Re	Reynolds number
$\dot{S}_{in}$	Total entropy flow into system (W/K)
$\dot{S}_{out}$	Total entropy flow out of system (W/K)
$\dot{S}_{gen}$	Entropy generation (W/K)

$\dot{S}_{gen,\ heattrans}$	Entropy generation due to heat transfer (W/K)
$\dot{S}_{gen,\ vis.diss}$	Entropy generation due to viscous dissipation (W/K)
$\dot{S}_{gen,\ heat\text{-}leakage}$	Entropy generation due to heat transfer (W/K)
S_D	Transverse pitch ratio
S_L	Longitudinal pitch ratio
T_o	Ambient temperature (K)
$\bar{T}_d$	Average bulk temperature (K)
$\bar{T}_{in}$	Average inlet temperature (K)
$\bar{T}_{out}$	Average outlet temperature (K)
$\bar{T}_w$	Tube surface temperature (K)
U	Overall heat transfer coefficient (W/m^2K)
U_{max}	Maximum velocity (m/s)
U_{in}	Approach velocity (m/s)
ρ	Density (kg/m^3)
μ	Dynamic viscosity of the heat transfer fluid (Ns/ m^2)
$\dot{V}$	Volume flow rate (m^3/s)
Ξ_d	Exergy destroyed due to internal irreversibilities (W)
Ξ_{in}	Total exergy entering system (W)
Ξ_{out}	Total exergy exiting system (W)
Ξ_Q	Total exergy (W)
$\Xi_{Q,\ l}$	Exergy destroyed due to heat leakage (W)
$\Xi_{Q,w}$	Exergy due to convective heat transfer (W)
ΔT_{ln}	Log mean temperature difference

ΔP	Pressure drop (Pa)
X	Friction factor
η	Energy efficiency
Ψ	Exergy efficiency
HTF	Heat transfer fluid

ACKNOWLEDGEMENTS

I would like to express my gratitude first to Dr. David W. MacPhee for the help he has given me during the production of this thesis, I believe that I would not have been able to do it without him. I have learned a lot and gained experience in different areas during my graduate education, it is due to Dr. MacPhee's vast array of knowledge in many engineering fields as well as his excellent teaching and research skills. I am also thankful to my committee members, Dr. Sharif and Dr. Allison, for helping and guiding me along the way.

To the other graduate students whom have helped me along the way, I am grateful for their help. I would like to thank Roohany Mahmood, Lalit Roy and Kellis Kincaid, who have been in the lab since the beginning of my graduate studies, for their companionship and support and for making the lab an enjoyable place.

To the many other in the office of mechanical engineering who have helped me; Betsy Singleton, who has been very helpful in organizing my documents, and Cris Porter, who has provided technical support when I needed access to the HR251 computational laboratory. I am grateful for your assistance.

I owe an immense thank to Ministry of Turkish National Education who has provided me a highly competitive scholarship. I believe that it was not possible for me to go abroad and pursue a master degree without this scholarship program. I am also thankful to my Turkish advisor, Cemalettin Aygun, who is an Assistant Professor in Gumushane University, Turkey, for his guidance when in selecting my graduate program.

Lastly, and most importantly, I would like to thank my family, especially my brother Halim; for always believe and encourage me to go further in my carrier. To my wife, my life would not be as exciting without your company and support.

CONTENTS

LIST OF TABLES

LIST OF FIGURES

1 INTRODUCTION

In this thesis, a numerical investigation is conducted for a fluid flow over tube bundles in cross flow. The primary part of the study is concerned with the thermodynamic performance of different systems with varying parameters, such as Reynolds number, inlet temperature, number of in-line cylinders, pitch ratio, and heat leakage. All simulations are performed using a computational fluid dynamics tool, ANSYS Fluent 18.2. Furthermore, this software was not only used for simulations, but it was also used to generate the desired geometry and mesh.

External forced convection around circular cylinders has numerous applications such as heat exchangers, for space heating, in power generators, condensers, electrical equipment, and many other thermal applications. In order to determine the thermodynamic efficiency of a heat transfer process, both energy and exergy analyses require to be examined. It is commonly known that entropy generation exerts a considerable influence on the exergy destruction of a system and can occur as a result of heat transfer (temperature gradients) and/or fluid friction (viscous dissipation). Thus, high entropy generation will result in a less exergetically efficient system. Therefore, investigating parameters that reduce entropy generation and systems' irreversibility presents a significant research area.

Computer-aided analyses have contributed to the enhancement of engineering designs in many areas of interests. With the increasing use of technology in numerical methods, techniques of Computational Fluid Dynamics (CFD) offer powerful and reliable designs and solutions for industrial process. Numerical studies are more popular with researchers compared to experimental studies, since experimental setups introduce cost constraints. On the contrary, in

numerical methods, a single powerful computer can perform simulations and obtain the desired results, which can possibly show a high level of agreement with existing research.

In this section, the three basic heat transfer modes will be explained before further detailed information about convection heat transfer and the main subject, tube banks, is discussed in the literature review.

1.1 Background

Heat transfer constitutes a physical process caused due to temperature differences across systems. This phenomenon continues until the mediums reach the same temperature, and its direction is always from high temperature towards low temperature (Cengel and Ghajar, 2015). With the increasing use of technological equipment, heat transfer theories have witnessed development at a very fast pace due to the high accuracy offereed by analytical and numerical solutions reached with these tools. Since the last three decades, numerical methods have been employed to gain extreemly accurate results in comparison to experimental results.

There are three primary heat transfer modes: conduction, convection, and radiation. As mentioned earlier, there must be a temperature difference between systems for the transfer of heat as a form of energy to take place. More detailed information for each mode have been provided below.

1.1.1 Conduction

Conduction comprises a form of heat transfer from more energetic particles of a substance to its less energetic particles due to interactions between the particles (Bergman et al, 2011). In gases and liquids, conduction takes place due to collision and diffusion of molecules during random motion. However, the mechanism of conduction for solids is different from that

of gases and liquids. Conduction of heat in a solid object takes place due to the vibration of molecules (atomic motion) and the energy transfer of free electrons.

The conduction heat transfer ratio can be calculated using Fourier's law for one-dimensional objects:

$$Q = -kA\frac{dT}{dx} \tag{1.1}$$

According to Fourier's law (1.1), the ratio of conduction depends on the thermal conductivity of the material, its cross-sectional area, temperature gradient, and thickness.

1.1.2 Convection

Convective heat transfer takes place between a solid surface and an adjacent fluid in motion due to conduction and the motion of the flows. There are two types of convection heat transfer: forced convection and free or natural convection. In forced convection, the flow is produced by external sources, such as a fan or pump. In this type of heat transfer, convection and conduction occur simultaneously; however, conduction is relatively low compared to convection. Hence, conduction can be neglected in convection heat transfer applications. Conversely, free convection happens if the flow is induced by buoyancy forces due to temperature variation in the fluid leading to density differences.

The first expression of convective heat transfer was provided by Newton in 1701 (Welty et al, 2013), and it is known as Newton's law of cooling, expressed below:

$$Q = hA\left(\mathrm{T} - \mathrm{T}_s\right) \tag{1.2}$$

where h and A represent the convective heat transfer coefficient and heat transfer area respectively.

In this thesis, heat transfer and flow characteristics of tube banks will be examined; hence, further details regarding external forced convection will be provided later.

1.1.3 Radiation

Thermal radiation refers to the energy emitted by all matter whose temperature is greater than absolute zero. Radiation heat transfer occurs as a result of changes in the electronic configurations of atoms or molecules of matter (Cengel and Ghajar, 2015). Although it takes place in solid and gases, it can also transpire between solid surfaces frequently (Dincer and Kanoglu, 2010). While conduction and convection heat transfer methods require the presence of a material medium, radiation does not.

The rate of radiation heat transfer between the two surfaces is expressed with equation (1.3):

$$Q_{rad} = \varepsilon \sigma A_s \left(T_s^4 - T_{surr}^4 \right) \tag{1.3}$$

where σ, ε, A_s, T_s, T_{surr} represent the Stefan-Boltzmann constant, the emissivity of the surface, surface temperature, and surrounding temperature, respectively.

2 MOTIVATION AND OBJECTS

The motivation behind this study is recovering the heat wasted in power generation and utilize this heat for the production of a hot fluid. A Heat Recovery Steam Generator (HRSG) can be employed to generate steam or electricity, and these systems can increase a power plant's energy efficiency up to 85%–90%. Hence, HRGS systems serve a significant function, especially in power plants. They can also be used in public facilities or universities; for instance, a gas turbine can be used to produce a reliable electricity supply; further, this system can also recover the heat wasted by the turbine and use it to produce hot water for district heating. Another important consideration for an HRSG is that they contribute to decrease of using fossil fuel consumption.

In this study, tube banks will be analyzed as simplified version of an HSRG system, as they provide excellent heat transfer performance. Furthermore, although all HRSG's are efficient, the thermal efficiency of the HRSG in question with regard to different parameters will be illustrated. Using a CFD and heat transfer software program, the objectives provided below will be addressed:

- Energy and exergy efficiency of tube banks
- Effect of Reynolds number on energy and exergy efficiencies
- Effect of pitch ratio on energy and exergy efficiencies
- Effect of number of in-line cylinders on energy and exergy efficiencies
- Effect of heat leakage on energy and exergy efficiencies
- Effect of inlet temperature on energy and exergy efficiencies

3 LITERATURE REVIEW

In this chapter, previous studies will be presented starting with convective heat transfer. While internal forced convection and natural convection will be briefly addressed, the primary concentration will be on external forced convection, especially on tube banks in cross flow. In the literature, there is a considerable amount of research available which investigate heat transfer, fluid flow, and pressure drop over the tube bundles. In order to evaluate flow and heat transfer characteristics, experimental, analytical, and numerical studies are investigated. While some empirical relations are assessed using experimental data, others are performed using numerical methods due to the relative case when compared to experimental analysis. General correlations for Nusselt number, pressure drop, and friction factor are proposed for each solution method. Moreover, in the last subsection, entropy generation-based studies using numerical techniques are introduced, which is a crucial parameter for this study, when we examine exergy destruction of the system. A more detailed flowchart of the convective heat transfer modes is indicated in Figure 3.1, which will guide the readers through the literature review.

As it can be seen from Figure 3.1, convection can be classified into natural and forced convection, and, furthermore, forced convection is classified as external and internal. Whereas tube banks are the main topic of this study, internal forced convection, and natural convection will be discussed in detail in this chapter.

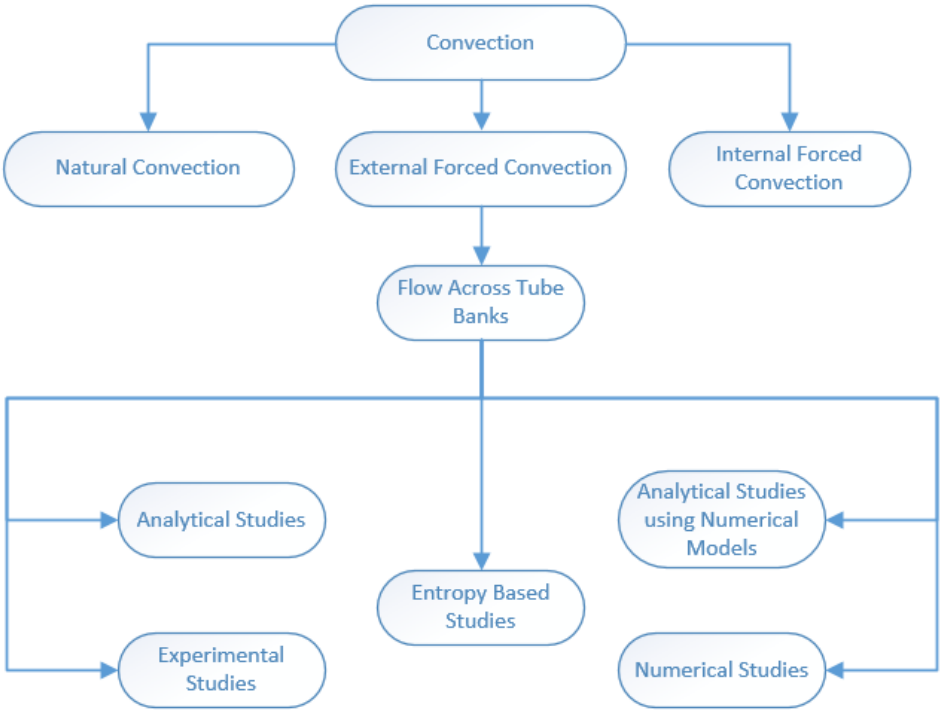

Figure 3. 1 Literature review flowchart

3.1 Natural Convection

Natural convection is a primary mechanism of heat transfer which can be seen in many applications, such as cooling of electronic equipment, heat transfer from steam radiators, refrigeration coils, the bodies of animals, human beings, and many, many others.

Unlike forced convection, in natural convection, fluid motion occurs by natural means i.e., buoyancy. Buoyancy causes fluid motion due to a difference in body force acts on fluid and resulting from differences in density, this causes advection near heated or cooled surfaces (Cengel and Ghajar, 2015). In practice, temperature gradients and gravitational fields result in the density gradient and body force, respectively. Whereas fluid motion is quite noticeable in forced convection, it is not easily noticeable for free convection due to low velocities. Although

velocity plays a crucial role in evaluating convective heat transfer coefficients, it is not required for natural convection.

Churchill and Chu (1975) have developed an expression to calculate the Nusselt number for a flow over the vertical plate which depends on the Rayleigh and Prandtl Number. The authors claimed that the expression could apply under uniform heat flux as well as uniform wall temperature boundary conditions. McAdams' (1954) correlations are widely known for horizontal plates, with different correlations depending on whether the fluid is hot or cold compared with the adjacent surface. Churchill and Chu (1975) have developed a Nusselt Number correlation for horizontal cylinders, and Churchill (2002) also developed another correlation for spheres.

3.2 Internal Forced Convection

Internal forced convection correlations are one of the most commonly used tools to evaluate heating and cooling systems, and an external power supply such as a pump or fan is required to force the flow. The main difference between external and internal flow is the boundary layer. In external flow, fluid does not have a constrained boundary layer, and this boundary layer over the surface can grow indefinitely. In internal flow, boundary layer growth is limited by the inner surface of the tube; therefore, the boundary layer cannot grow as it does in external convection.

Although most fluids are transported in circular pipes, non-circular ducts are usually used to transport air in cooling and heating application due to the low-pressure difference between the inlet and outlet of the fluid.

Leo Graetz (1885) was the scientist who introduced the first analytical solution for laminar forced convection in a tube. In the literature, there are two different solution approaches,

the first one with hydrodynamically developed flow and the second one with thermally developed flow. There are a few Nusselt number correlations for a boundary condition which has a constant surface temperature. Edwards et al. (1974) developed a correlation for a circular tube which has a constant surface temperature for the thermal entrance region. This correlation can be used to calculate Nusselt number for internal forced convection applications, which have low-temperature differences between the wall surface and the fluid. Sieder and Tate (1936) introduced an average Nusselt number correlation for a hydrodynamically developed flow and inside a circular pipe. This expression is more applicable for the high-temperature difference between the wall surface and the fluid. The equations provided by Tate and Sieder may results in a 25% error; therefore, another correlation developed by Gnielinski (1976) which may be more reliable due to high accuracy with less than a 10% error.

The correlations mentioned above are valid for laminar flow; however, there are some other correlations for turbulent internal flow. The flow in a smooth tube is considered as fully turbulent for Re>10,000. Dittus and Boelter (1985) proposed a correlation for fully turbulent flow.

3.3 External Forced Convection

In external forced convection, heat is transferred between a solid surface and a fluid. As mentioned previously, there is no limitation for the boundary layer which can grow indefinitely over the surface. Therefore; there is a region in which temperature and velocity gradients are negligible outside of the boundary layer. There are numerous example of external flow importance, such as automobile radiators, power lines, airplane wings, heated pipes, cooling of electronic equipment, etc.

There is a significant amount of research regarding heat transfer in external flow, and the most commonly studied geometries are: flat plate, cylinders, spheres, and tube banks. Churchill and Bernstein (1977) developed a correlation for cross flow over a cylinder, and it is available for RePr > 0.2. There is another correlation recommended by Whitaker (1972) for a flow over a sphere. In the literature, there are some other correlations for different geometries in cross flow, but are not considered further in this study.

3.3.1 Flow across tube banks

Crossflow over tube banks is one of the most common example of external forced convection. It can be seen in numerous industrial applications, such as heat exchangers, condensers, evaporators, air conditioners, and refrigerators. In these applications, where one fluid moves over the tubes another fluid moves through the tubes and heat is transferred due to a temperature difference between these fluids. In some cases, the surface temperature of the tube is assumed to be constant, and in others, uniform surface heat flux can also be assumed.

Tube banks can be designed in two different configurations; in-line, or staggered in the direction of the fluid. The diameter of the tubes, transverse pitch, and longitudinal pitch are the parameters to characterize the arrangements of the tube banks. Longitudinal pitch is defined as the distance between two adjacent tubes in the horizontal direction, and transverse pitch refers to the vertical direction. Flow characteristics around the first cylinder in a tube bank are very similar to that a flow in a single cylinder in crossflow. Typically, the heat transfer coefficient is enhanced from the first row until the fifth row; however, after that the heat transfer coefficient does not change considerably. In tube banks, the Reynolds number depends on the maximum velocity which occurs between the tubes, in most cases, as well as depending on the transverse pitch and the diameter of the tubes.

It is a known fact that flow over the tube banks is investigated using numerical or experimental methods due to the complexity of analytical studies. In this study, the average heat transfer coefficient is examined for the overall tube banks, and it depends on the diameter of the tubes, number of tubes in the horizontal direction, and the tube arrangement.

After this point, research will be reviewed for flow through tube banks in cross-flow experimentally, numerically, and analytically. Beside the heat and flow characteristics, some other studies will also be reviewed regarding entropy generation and exergy efficiency due to the fact that the primary purpose of this study is to investigate energy and exergy efficiencies of tube banks.

3.3.1.1 Experimental studies

There is a large number of experimental studies regarding fluid flow and heat transfer over tube banks in cross-flow. In 1933, Colburn (1933) presented a simple correlation in terms of heat transfer for a flow across tube banks and this correlation is suitable for more than ten rows of tubes and Reynolds numbers ranging from 10 to 40,000. Moreover, Huge (1937), Pierson (1937), and Bergelin et al. (1949) have significant experimental studies to investigate pressure drop and heat transfer of in-line and staggered arrangement of tube banks in cross-flow.

Aiba et al. (1982a) conducted an experimental study to investigate heat transfer and fluid flow over the cylinders of in-line tube banks in cross-flow. The authors used seven cylinders in the horizontal direction, and the range of the Reynolds number changed from 10^4 to 6×10^4. The dimensionless ratio was selected as 1.2 and 1.6 for both transverse and longitudinal pitches. They found that the average heat transfer coefficient of the first cylinder change considerably with the cylinder spacing; however, there is a small marked change for the second and subsequent cylinders in the downstream direction. Moreover, they claimed that the flow over the tube banks for a case of 1.2×1.2 pitch ratio was entirely deflected. Aiba et al. (1982b) conducted another

experimental study to investigate heat transfer and flow over the tube bundles in staggered arrangements. They have performed experiments using the same pitch ratios as the previous study for a Reynolds number between 8,600 and 36,000. They determined that the maximum heat transfer rate was obtained for the third cylinder in the case of a 1.6×1.6 pitch ratio. They explained that it might be because of high flow velocity over the third cylinder, along with its high turbulence intensity. Furthermore, they claimed that even though the local heat transfer coefficients varied for downstream cylinders, the mean heat transfer coefficient was almost equal for both the cases of a 1.2×1.2 and 1.6×1.6 pitch ratio at the same Reynolds number.

Fujii et al. (1972) performed an experimental study to investigate heat transfer and pressure drop for a system circulating saturated steam at a low pressure through a bundle of tubes. The authors proposed an expression for the heat transfer coefficient over the tubes and pressure drop through the tube banks. They performed experiments for a pitch ratio of 22/14, and they found that the Nusselt number for a staggered arrangement is 20% more than that of an in-line arrangement. It was also determined that the drag coefficient for in-line arrangement was nearly half of that for staggered one.

Ljungkrona and Sunden (1993) conducted an experiment to investigate the flow around and the pressure through two tubes in in-line and tandem arrangement. The measurements for the flow visualization and the pressure were recorded for a range of Reynolds numbers from 3.3×10^3 to 12×10^3 and 3.3×10^3 to 4×10^4, respectively. The dimensionless pitch ratios were varied from 1.25 to 4.0 for both measurements. The authors found that the Strouhal number increases with the Reynolds number, for a value of a Reynolds number more than 12×10^3, and a dimensionless pitch ratio of 1.25.

Zukauskas (1972) studied experimentally for a staggered and in-line arrangement of tube banks. It was found that heat transfer was considerably higher for an arrangement of staggered tubes than in-line ones. Pressure drop, it increased with decreasing dimensionless pitch ratio for both staggered and in-line tubes.

Balabani (1996) carried out a series of experiments in a water tunnel to examine the velocity characteristics and pressure drops of tube bundles in cross-flow for two different staggered and one in-line tube arrangements. The configurations of the bundles were 3.6×1.6 and 3.6×2.1 for staggered, and 3.6×2.1 for in-line. Here, it was found that turbulence levels and pressure drop were higher for staggered arrangements than those of in-line.

In order to enhance heat transfer rate, some research has been conducted for different geometries such as elliptic tubes, wing-shaped, cam shaped, and spheres. Even though the purpose of this study is to investigate cylindrical tubes, this literature review will be touch an these studies briefly. Ota et al. (1984) performed an experiment to examine heat transfer and flow characteristics of an elliptic cylinder with an axis ratio of 1:3. The authors varied the angle of attack from 0° to 90° and the Reynolds number from 8,000 to 79,000. It was found that the minimum Nusselt number was still higher for an elliptic cylinder than that of a circular cylinder of equal circumferential length. Ibrahim and Gomaa (2009) have also carried out an experimental and numerical study to investigate the thermofluid characteristics of the elliptic tube bundle in cross-flow. In this experiment, the Reynolds number varied from 5,600 to 40,000, the axis ratio from 0.25 to 1, and the flow angles of attack from 0° to 150°. The results indicated that heat transfer coefficients increased considerably with increasing of the angle of attack up to 90°. Whereas the maximum thermal performance was obtained at an angle of attack of zero, the minimum thermal performance occurred at an angle of attack 90°. They claimed that the best

thermal performance was obtained for the lower values of angle of attack, Reynolds number, and axis ratio.

Ahmed et al. (2015) conducted an experimental and numerical study to examine fluid flow characteristics and pressure drop for a bundle of wing-shaped tubes in a staggered arrangement. Here, the angle of attack and the Reynolds number were varied, and the results indicated that pressure drop increased with the angle of attack from 0° to 45°, and decreased with angle of attack from 135° to 180°. Another experimental study for a bundle of isothermal spheres in cross-flow was conducted by Will et al. (2017). Here, experiments for a range of Reynolds numbers between 7.8×10^{3} and 3.3×10^{5} were conducted. They expressed a correlation regarding the Nusselt number, and also accounted for the thermal radiation and natural convection. The authors found a sudden increase in the Nusselt number above the Reynolds number of about 2.9×10^{5}. Lavasani et al. (2014) studied experimentally the heat transfer and drag coefficient for a bundle of cam-shaped tube banks in in-line arrangements. Experiments were performed for a Reynolds number ranging from 27,000 to 42,500 with pitch ratios of 1.5 and 2.0. Minimum and maximum drag coefficients were obtained in the first and second columns for each Reynolds number, respectively. Also, the friction factor of circular tube banks was 5 and 7% higher than that of cam-shaped ones. Moreover, increasing the pitch ratio from 1.5 to 2.0 increased heat transfer by between 7-14%. Due to aerodynamic characteristics of cam-shaped tube banks, the thermal hydraulic performance of cam-shaped tube bundles was approximately six times higher than that of circular tube banks. Hence, cam-shaped tube banks can have a significant effect to enhance energy conservation and minimize the size of a heat exchanger.

There have also been several studies considering fins attached to the tubes. Jang et al. (1996) performed an experimental and numerical study to investigate fluid flow and heat transfer

over a multi-row plate fin and tube heat exchanger in cross-flow. Here, the tube arrangement, tube row number, and pitch ratio was varied for a Reynolds number ranging from 600 to 900. The results indicated that the heat transfer coefficient and pressure drop for a staggered arrangement was 15%-27% and 20%-25% higher than that of in-lined arrangements, respectively. Furthermore, it was claimed that whereas the average Nusselt number decreased as the number of the row increased from 1 to 6, the effect of row number was relatively small on heat transfer coefficient for the cases, which had more than four rows. Mangrulkar et al. (2017) performed an experimental and numerical study to compare the thermal performance of tube banks with and without splitter plate attachments. Longitudinal and transverse pitch ratios were kept constant at 1.75 and 2.0, respectively and Reynolds numbers were varied between 5,500 and 14,500. The authors found that thermal performance of the tube banks with fin was much greater than that of bare cylinders due to higher heat transfer with a lower friction factor.

3.3.1.2 Analytical correlations using experimental data

In the literature, there exists a significant amount of experimental data regarding heat transfer and pressure drop along the tube banks; however, these data should be correlated with some parameter to understand how selected variables affect heat transfer rate and pressure drop.

As mentioned previously, Colburn (1933) developed a correlation to calculate the Nusselt number over the tube banks in cross-flow. Grimison (1937) proposed a correlation using the experimental data from Huge (1937) and Pierson (1937). This equation can be applied to tube banks which have more than ten rows in the flow direction. Kays and London (1964) generated a correction factor for the Grimison (1937) correlation to find the Nusselt number for a tube bank of fewer than ten rows. Hausen (1983) modified the correlation of Grimison (1937), and added another term to account pitch ratios for the correlation. There is another correlation

formulated by Zukauskas (1972), which is widely used to calculate average heat transfer and pressure drop for the application of tube banks.

Wilson and Bassiouny (2000) applied a mathematical procedure to predict the heat transfer characteristics and pressure drop of turbulent and laminar flow for a bundle of tubes. They used an implicit finite volume procedure to solve the partial equations of conservation of mass, momentum, and energy. They varied Reynolds numbers and the pitch ratios as well as the numbers of rows for staggered and in-line arrangements. It was found that the highest Nusselt number was obtained for a longitudinal pitch ratio of 3 for the in-line arrangement. Pressure drop, on the other hand, increased with increasing longitudinal pitch ratio; hence, it was recommended to use a longitudinal pitch ratio less than 3 to obtain the best performance. In case of a staggered arrangement, longitudinal pitch ratio should be selected equal or less than 1.5 to reduce friction factor and enhance the Nusselt number.

Mandhani et al. (2002) presented a mathematical model to investigate heat transfer characteristics for an incompressible, steady, and Newtonian fluid flow over a bundle of circular tubes. Reynolds numbers varied from 1 to 500, and the voidage of the assemblage ranged from 0.4 to 0.99. The authors determined that the average Nusselt number over the surface of the tube increased when increasing the values of Prandtl and Reynolds number and decreasing the value of porosity.

Khan et al. (2006;2006) conducted an analytical study to investigate heat transfer from tube bundles in cross-flow for both staggered and in-line arrangement under an isothermal boundary condition. They suggested a general correlation of the Nusselt number that can be applied for a wide range of Reynolds and Prandtl numbers as well as longitudinal and transverse pitch ratios. The authors found that the heat transfer rate was higher for compact banks than that

of widely spaced ones. Moreover, the staggered arrangement produced higher heat transfer rate than the in-line arrangements.

3.3.1.3 Analytical correlations using numerical methods

In the previous section, some of the most famous correlations obtained by experimental studies for cross-flow in tube banks were discussed. On the other hand, there are some other numerical studies which produced general correlations of the Nusselt number and pressure drop using computational fluid dynamics tools, which can often be completed with greater ease than experiments.

Tahseen et al. (2015) introduced an extensive review of thermal and flow characteristics of un-finned and finned tube banks. They presented 15 different research correlations based on analytical, experimental, and numerical studies for the Nusselt number, friction factor, and Sherwood number. They summarized their review as heat transfer coefficient and pressure drop increased with increasing the velocity of the fluid. Moreover, staggered arrangement tube banks had a higher heat transfer coefficient than that of an in-line configuration.

Miyatake and Iwashita (1991) carried out a numerical study to investigate the heat transfer characteristics of a bundle of tubes in triangular or square configurations in laminar flow conditions. They assumed uniform heat flux boundary conditions on the wall of the tubes and uniform inlet temperature for the fluid. The authors presented two correlations for local Nusselt and Graetz numbers. Another transient numerical simulation of fluid flow and heat transfer over a bundle of flat tube banks is presented by Benarji et al. (2008). The authors studied both in-line and staggered configurations with isothermal and isoflux boundary conditions. They used a commercial software, FLUENT 6.2, to solve the governing equations of continuity, fluid flow, and energy. The results indicated that an in-line arrangement performs better than a staggered one in terms of heat transfer. Also, the pressure drop is higher in the case of in-line

configurations. The Nusselt number and pressured drop correlations are proposed by the authors, and they also determined the optimum configuration for in-line and staggered arrangements. Ziskind et al. (2011) performed an analytical study in a PCM-air heat exchanger and generated a formula for heat transfer rate compared with a numerical solution conducted by Letan and Ziskind (2006). Bacellar et al. (2014) used the Parallel Parameterized CFD method to present CFD-based correlation for finned and finless tube heat exchangers, using a k-ε realizable turbulence model with enhanced wall functions. Varying air velocity and geometry, the authors conducted 1392 simulations, and they obtained a proposed correlation that gives more than 90% accuracy for the bare cylinders. Another numerical study was carried out by Rehim (2013) to predict the pressure drop and heat transfer characteristics of laminar and turbulent flow for a flat-tube bank in a staggered configuration. He investigated how aspect ratio affects the pressure drop, temperature, and velocity contours for laminar and turbulent flow. Using multiple linear regression, the author generated two correlations for the overall Nusselt number and dimensionless pressure drop as a function of Reynolds number and aspect ratio under the isothermal boundary condition. There was a good agreement between this analytical model and previously published experimental data of different authors.

Kim (2013) carried out an analytical study using a CFD code to investigate the effect of longitudinal pitch ratio on the heat transfer characteristics of tube bundles in cross-flow. Symmetric and periodic boundary conditions, were used, and various turbulence models were evaluated and compared with the well-known correlation from Zukauskas (1972).

3.3.1.4 Numerical studies without analytical correlation

Though a great number of experimental data and correlations regarding heat transfer and pressure drop over tube banks are available in the literature, numerical studies are preferred due to the increasing availability of high computer performance, better algorithms that cause fewer

errors, and higher efficiency of energy and momentum equation convergence. In computational fluid dynamics, there are three fundamental methods for solving a problem: the finite difference method, finite element method, and finite volume method. Whereas a computational domain is divided into control volumes in the finite volume method, it is discretized into a series of grid points in the finite difference method, and a series of elements in the finite element method. In this section, some important numerical studies using these three methods regarding heat transfer over tube banks will be reviewed.

Fujii et al. (1984) proposed a numerical method, called the one step forward and half step backward iteration method, to investigate heat transfer and friction factor over in-line tube banks configuration. Another numerical study was conducted by Grannis and Sparrow (1991) to examine heat transfer characteristics of an array of diamond-shaped pin fins using the finite difference method, whereby the solution domain was divided into an assemblage of two dimensional, nine-noded quadrilateral elements. Two other numerical solutions based on finite element method were carried out in (Buyruk, 2002) and (Krishne Gowda et al., 1998).

Beale (1992) conducted an extensive numerical study to explore a steady laminar flow and heat transfer in two-dimensional tube banks, in three-dimensional fin and tube exchangers using a finite volume-based numerical scheme. Here a constant wall flux is applied as well as constant wall temperature boundary conditions. Alongside steady flow, he also investigated transient two-dimensional flow over the tube bundles in in-line and staggered configurations. The author presented extensive data for overall and local pressure drop as well as heat transfer and skin friction. Bahaidarah (2004) and Bahaidarah et al. (2005) developed a finite volume-based FORTRAN code to solve governing equations for a steady laminar two-dimensional incompressible flow over in-line and staggered flat tube bank configurations. They investigated

the effect of Reynolds number, Prandtl number, length ratio, and height ratio on the pressure drop and heat transfer through the tube bundles. The authors used the SIMPLE algorithm method as a solver as well as a line-by-line method and Gauss-Seidel procedure to solve the results of discretization equations. In those two studies, it was summarized that while pressure drop decreases with increasing Reynolds number, average Nusselt number increases with Reynolds number. They recommended two optimum length pitch ratios for in-line configuration from an overall performance point of view.

Shaboury and Ormiston (2005) performed a numerical investigation for forced convection heat transfer in a bundle of tubes in square and non-square in-line arrangements. They used a finite volume method with a nonorthogonal, boundary-fitted grid and co-located storage variable. The results of this study agreed well with published experimental studies and empirical correlations in terms of overall heat transfer and pressure drop. Ambesi and Kleijn (2012) studied heat transfer over a single row of equidistantly and non-equidistantly spaced parallel cylindrical wires for a range of Reynolds numbers from 0.001 to 600. They used a SIMPLE algorithm and QUICK scheme to solve and to discretize the equations, respectively. The authors discussed in detail the effect of Prandtl number, Reynolds number, and open frontal for equidistance and non-equidistance arrangements.

Yilmaz et al. (2016) used ANSYS Fluent to investigate heat transfer and pressure drop of tube banks with axial fins. It was assumed that the flow over the tubes was under constant wall temperature, laminar, steady, and incompressible. They varied the pitch ratios, fin length, Prandtl number, and dimensionless pressure drop. It was summarized that, whereas axially finning brought about an increase in the heat transfer for low dimensionless pressure drop values, it does not increase the heat transfer for high dimensionless pressure drop values. Gholami et al. (2016)

conducted a study to compare heat transfer characteristics of finned tube banks in different geometries for a laminar flow. They investigated flat, oval, and circular tubes and found that a flat tube has a better thermal-hydraulic performance than circular and oval tubes.

Tahseen et al. (2013) carried out a numerical study to investigate velocity fields, temperature contours, and the local and average Nusselt numbers for a bundle of staggered arrangement in cross-flow under incompressible, two-dimensional, and steady-state conditions. They used FORTRAN-90 and a SIMPLER algorithm to calculate strong coupling of pressure and velocity in the cross-section. In this study, the authors varied the Reynolds number and longitudinal pitch ratio from 25 to 250 and from 1.25 to 2, respectively. It was found that the heat transfer increases when decreasing the longitudinal tube diameter; also, the temperature distribution and flow form mainly depends on Reynolds number. Beale and Spalding (1998) performed a computational study using a modified version of the SIMPLE algorithm and PHOENICS software program. Heat transfer and fluid flow equations were solved assuming laminar, fully-developed cross-flow for in-line square, rotated square, and equilateral triangle configurations. The authors varied Reynolds numbers from 10 to 1,000, pitch ratios from 1.25 to 2, Prandtl numbers from 1-100, as well as constant heat flux and constant wall temperature boundary conditions. They found that the local heat transfer distributions are qualitatively similar for different geometries in constant heat flux and constant wall temperature conditions and the ratio of local Nusselt number to overall Nusselt number is greater for constant heat flux than for constant wall temperature.

The following two studies indicated the optimum design of finned staggered tube banks and un-finned in-line tube banks configurations. In these investigations conducted by Selma et al. (2014) and Yilmaz and Yilmaz (2016), the authors performed their studies using OpenFOAM

and ANSYS Fluent, respectively. Another study using OpenFOAM was conducted by Valikangas (2015), wherein the author examined the convective heat transfer for two types of fin-and-tube heat exchangers.

Turbulent flow has also been investigated by some researchers. For example, Paul et al.(2008), and Iacovides et al. (2013). Iacovides et al. (2013) used alternative strategies for modeling turbulent flow and heat transfer over in-line tube bundles. They examined the suitability and accuracy of wall-resolved Large Eddy Simulation (LES) and Unsteady Reynolds-Averaged Navier Stokes (URANS) for this application. It was indicated that LES flow patterns for a value of pitch ratio 1.6 with URANs computations was disappointing since a simple wall function was employed, causing issues predicting local heat transfer rates. Nagamani and Reddy (2015) analyzed the turbulent and incompressible flow in a cross-flow tube bank using ANSYS Fluent with a periodic boundary condition.

Some studies provide applications of tube bundle heat transfer. For example, in aero engines (Kritikos et al., 2010), and heat recovery systems (Torresi et al., 2008),(Lee et al., 2013). Lee et al. (2013) conducted a numerical study to investigate heat transfer rate of a heat recovery steam generator (HRSG). FLUENT was used for the simulations varying longitudinal and transverse pitch distances, Reynolds numbers from 500 to 2,000, and the uniformity of the tube bundles in an in-line arrangement. The authors summarized that the overall heat transfer increased when increasing the longitudinal pitch space for uniformly distributed cylinders. However, if the longitudinal pitch ratio was not uniform, the individual heat transfer coefficient tends to oscillate. Moreover, a general correlation was proposed for the local Nusselt number by considering an additional effect from the uneven longitudinal pitch ratio.

Some other studies (Zhang et al., 2011) for finned plates to investigate flow oscillations and vortex shedding. Another (Chakrabarty and Wankhede, 2012) focused on reviewing the effect of longitudinal and transverse tube spacing, Reynolds number, stagnation point, and surface roughness on wake size and vortex shedding in experimental, numerical, and analytical studies.

There are also many other studies in which tube banks are used for nanofluid applications. Lavasani and Bayat (2016) used ANSYS Fluent to compare the effect of nanofluid volume fraction on the heat transfer and pressure drop of cam-shaped and circular tube banks with staggered and in-line configurations. The authors summarized that adding Al_2O_3 nanoparticles to pure water increased the friction factor for both cam-shaped and circular tube bundles. Comparing the effect of geometries on the friction factor, they found that heat fraction factors across cam-shaped tube banks are 71% and 74% lower than those of circular tube banks for in-line and staggered configurations, respectively. Ahmed et al. (2017) studied laminar convective heat transfer using Al_2O_3 over staggered tube banks under constant wall temperature boundary conditions using a finite volume approach. They varied longitudinal and transverse pitch ratios, Reynolds number from 100 to 600, and nanoparticle volume fractions ranging from 0 to 0.05. The authors obtained an optimal arrangement at longitudinal pitch ratio of 1.5, transverse pitch ratio of 2.5, and nanoparticles volume fraction of 5% over each Reynolds numbers.

3.3.1.5 Entropy-based studies

In order to investigate the thermodynamic efficiency of a heat-transfer process, both energy and exergy analyses should be conducted. It is a well-known fact that entropy generation has a great influence on the exergy destruction of a system, which can occur as a result of heat transfer and fluid friction. High entropy generation causes a less exergetically efficient system;

thus, it has been a crucial subject to explore the parameters which reduce entropy generation and irreversibility. In this section, some studies based on entropy generation using tube banks are reviewed.

Fowler and Bejan (1994) proposed a correlation to determine the optimal size of bodies with specified external forced convection to minimize entropy generation and cost. Three different objects were considered, cylinder, sphere in cross-flow, and flat plate in parallel flow. The authors found that there was a monotonic increase in the optimal size with the heat transfer duty parameter. Korukcu (2015) investigated a numerical study to solve Navier-Stokes and energy equations as well as to explore the effect of Reynolds number on the energy and exergy characteristics of laminar steady flow over a square cylinder in cross-flow. He determined that heat transfer and temperature drops are more sensitive in the earlier section of the upstream region for the flows with a low Reynolds number. Furthermore, the author summarized the exergy characteristic that the most notable frictional entropy generation in the upstream generation is obtained at the inlet section of the throat, especially on the corner of the throat. Melhem et al. (2017) conducted an analytical study to investigate the effect of blockage, Reynolds and Prandtl numbers on the laminar-flow entropy generation for flow across a cylinder confined between parallel plates. The authors reported that whereas entropy generation decreases with decreasing blockage ratio, it increases as the Reynolds and Prandtl numbers increase. Another numerical investigation was carried out by Hijleh (1998) to explore the entropy generation due to laminar mixed heat convection from an isothermally heated cylinder in a cross-flow for different values of Reynolds numbers, buoyancy parameter, and cylinder diameter. The author found that large cylinder diameters produced lower entropy generation compared to small cylinders. It was also claimed that the difference between the entropy generation caused by

mixed and pure convection reduced with increasing cylinder diameter. Poulikakos and Johnson (1989) also investigated a general expression for the entropy generation for conductive heat and mass transfer combination in external laminar and turbulent flow. The expression took into account three types of irreversibilities: heat transfer across finite temperature difference, mass transfer across finite difference in chemical potential, and flow friction.

Apart from circular cylinders, there are some studies concerned with for different geometries, such as elliptic or square cylinders. Ibrahim and Moawed (2009) carried out an experimental study to investigate heat transfer characteristics and entropy generation for individual elliptic tubes with fins. They used electrically heated elliptic tubes in a wind tunnel, with air as the fluid. They varied the position of the fins on the tube and Reynolds number which ranged from 4.75×10^{3} to 3.96×10^{4}. The authors proposed that the Nusselt number and friction factor were decreasing depending on the order of front and back fin, front fin, back fin, and without a fin. Moreover, the irreversibility ratio decreased depending on the order of without a fin, front fin, back fin, front and back fin. Khan et al. (2007) investigated an optimization study for tube banks using entropy generation minimization method in terms of dimensionless pitch ratio, velocity, tube diameters, and heat load. The authors proposed a general dimensionless expression for the entropy generation rate regarding a control volume over a tube bank. They claimed that staggered configuration performs better for lower approach velocities and longer tubes, while in-line configurations give better performance for higher approach velocities and larger dimensionless pitch ratios. Moreover, they presented that compact tube banks were more efficient for both configurations and smaller tube diameters. Gharbi et al. (2015) carried out a numerical study using the finite volume discretization method to compare the performance of different tube bundles configurations: circular, ellipsoidal, and wing-shaped. The authors

investigated the effect of pressure drop, exergy, and enthalpy balance, and used entropy generation as a criterion to find the best bundle arrangement. They proposed general correlations for Nusselt and Euler numbers for each geometry for Reynolds numbers ranging from 5×10^3 to 2.4×10^4. The results showed that there was no best geometric shape for all flow conditions; however, circular tube shapes give the worst performance when $Re>1.5\times10^4$, and elliptic shape tube bundles perform best when $Re>2.3\times10^4$. Another analytical study has been conducted by Khan et al. (2006) to investigate the effect of thermal performance regarding with different fin geometries, rectangular plate fins, square, circular, and elliptical fins. The authors obtained a general dimensionless entropy generation expression in terms of aspect ratio, Reynolds number, Nusselt number, and drag coefficient. They found that the worst performance was obtained for a geometry of square from the point of view of heat transfer and drag force; hence, total entropy generation. Moreover, in situations of dimensionless total entropy generation for smaller perimeters, larger aspect ratios, and lower Reynolds numbers, circular geometry performed better, whereas rectangular plate fin gives the best performance from the point of view of total entropy generation rate for higher Reynolds numbers, smaller aspect ratios, and large perimeters.

An extensive review of heat transfer and flow characteristics, as well as entropy generation for tube banks, has been introduced in detail. First, experimental studies were presented, then analytical studies using experimental and numerical methods. Numerical studies were explained in terms of solution and discretization methods as well as laminar and turbulence models. Besides circular tube banks, non-circular tube bundles were also reviewed and compared with the circular bundles. Second law analysis studies were presented regarding entropy generation due to heat transfer and fluid flow.

With the development of numerical codes, the study of heat transfer and flow characteristics, as well as entropy generation on the tube banks has progressed significantly. For this reason, Erguvan and MacPhee investigate a numerical study using a commercial software, ANSYS Fluent 18.2. Not only are heat transfer and flow characteristics examined, but also entropy generation due to heat transfer and fluid flow were explored. Air is selected as a fluid for each simulation, and Reynolds number, row numbers, dimensionless pitch ratio, inlet temperature and the amount of heat leakage are varied. Energy and exergy analysis is conducted for each simulation, and optimum Reynolds number and pitch ratios are obtained for each domain. This study differs from other studies due to the fact that it considers not only energy efficiency, but also exergy destruction. Another important point is that an artificial heat leakage is applied to each domain.

4 ANALYSIS

This chapter provides a detailed explanation of the problem specifications, solution methods, as well as thermodynamic analysis and case studies. In order to use numerical methods, governing equations and boundary conditions are introduced to address fluid flow and heat transfer equations. ANSYS Fluent 18.2, geometry and mesh generation, as well as governing equations, are presented.A common numerical procedure to solve Navier-Stokes equations and k-ε RNG turbulence model, SIMPLEC (Semi-Implicit Method for Pressure Linked Equations-Consistent), is also explained in this section.

Before introducing the thermodynamic results of the simulations, different domain descriptions are presented, varying dimensionless pitch ratios and row numbers. Furthermore, to obtain a reasonable numerical model, grid and time independence tests are conducted, also explained herein.

4.1 Problem Specification

In the design of tube banks, as mentioned in the previous sections, a number of tubes are arranged using in-line or staggered arrangement. The arrangement of tube bundles are characterized by geometric parameters: the tube diameter d, the longitudinal pitch S_L, and transverse pitch S_T, the distances between the adjacent tubes. However, while designing tube bundles, dimensionless longitudinal (S_L/D) and transverse (S_T/D) pitch ratios are considered instead of the pitches. The typical geometry of the given two-dimensional problem is illustrated in Fig.4.1.

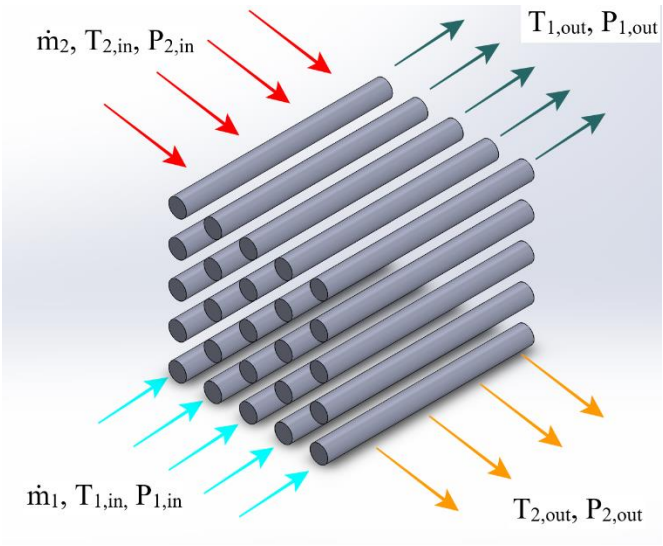

Figure 4. 1 A schematic of tube banks

In the literature, tube bundles configurations are considered as follows: in-line square, equilateral triangle, and rotated square, as illustrated in Fig.4.2. However, in this study, only the in-line square configuration is investigated. Tube banks are generally classified as widely spaced and compact for a dimensionless pitch ratio of $S/d>3$ and $S/d<1.25$, respectively. In order to be somewhere between those two limitations, dimensionless pitch ratios are varied between 1.3 to 3.0 for three different rows. 12 different geometries are investigated for this study; more information will be furnished in section 4.2.2. In order to reduce the effect of outlet location on solution parameters, the inlet and outlet of the domain have been extended by three times and six times of the tube diameters before the first row and last row, respectively.

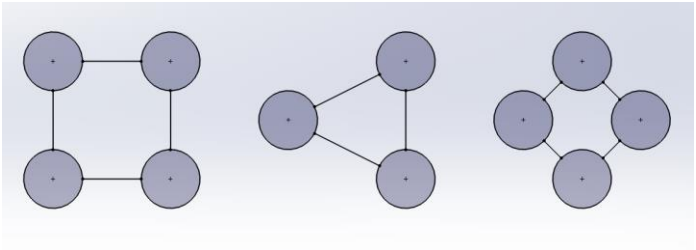

Figure 4. 2 Configuration of in-line square (left), equilateral triangle (middle), and rotated square (right)

Before discussing heat transfer and fluid flow analyses, a number of assumptions have been made for the flow:

- Flow is two-dimensional and transient;
- Inlet velocity of the fluid is uniform;
- Thermophysical properties of the fluid are constant;
- Free convection and radiation heat transfer effects are negligible;
- Conduction and radiation effects are negligible;
- Flow incompressible with constant density; and
- Thermodynamic reversibility inside pipes are neglected for simplicity

Table 4.1 illustrates the thermophysical properties of the fluid at constant temperatures of 393K, 465K, and 550K. These temperatures are determined as the mean temperature of the inlet and outlet temperature of the fluid for three different inlet temperatures. The properties of the air are obtained from Cengel's (2015)

Table 4.1 Thermophysical properties of heat transfer fluid

Temperatures of Air [K]	C [J/kg.K]	ρ [kg/m^3]	k [W/m^2.K]	μ [kg/m.s]
393	1011	0.8969	0.0324	2.27e-05
465	1021	0.7593	0.0372	2.55e-05
550	1039	0.6418	0.0428	2.86e-05

4.2 Heat Transfer and Fluid Flow Analysis

There has been considerable development in CFD (Computational Fluid Dynamics) codes over the last several decades. ANSYS Fluent provides a system to create geometries, to generate meshes, and to solve complex simulations. In this chapter, first, the fundamental governing equations to solve heat transfer and fluid flow problems will be outlined. Then, the

computational procedure of the FLUENT 18.2 will be explained in terms of the solution algorithm, discretization methods, and the turbulence model.

4.2.1 Governing equations

Three governing equations—energy, continuity, and momentum—must be solved to accurately describe the problem. All three equations are formulated according to the assumptions listed in the previous section. In most cases, viscous dissipation is negligible, although it was not neglected in this study; hence, the energy equations for the heat transfer fluid become more complicated. Equation (4.1) indicates the energy equation:

$$\rho \frac{Dh}{Dt} = \frac{Dp}{Dt} + k\nabla^2 T + \Phi \tag{4.1}$$

Here, $\alpha = k / \rho C_p$ is the thermal diffusivity, and Φ is the viscous dissipation, which is defined as heat generation due to shear stress in the fluid:

$$\Phi = \mu\left[2\left(\frac{\partial u}{\partial x}\right)^2 + 2\left(\frac{\partial v}{\partial y}\right)^2 + 2\left(\frac{\partial w}{\partial z}\right)^2 + \left(\frac{\partial v}{\partial x} + \frac{\partial u}{\partial y}\right)^2 + \left(\frac{\partial w}{\partial y} + \frac{\partial v}{\partial z}\right)^2 + \left(\frac{\partial u}{\partial z} + \frac{\partial w}{\partial x}\right)^2\right] \tag{4.2}$$

In order to include velocity and pressure term into the energy equation, some other equations must be introduced. First, the continuity equation (mass conservation) will be outlined with the assumptions of the incompressible heat transfer fluid:

$$\nabla . \vec{V} = 0, \tag{4.3}$$

The above equation states that the total mass at the inlet and the outlet is equal. Now, the last equation is commonly referred to as Navier-Stokes or momentum equation, as given below:

$$\rho \frac{D\vec{V}}{Dt} = -\nabla p + \mu\nabla^2 \vec{V} \tag{4.4}$$

As observed from the momentum equation, the total mass depends on the velocity vector and the pressure gradient in the velocity field. The pressure gradient, ∇p, at any point in the fluid causes

velocity change and viscous dampening as well; $\mu\nabla^2\vec{V}$, has the same effect on the velocity change.

After governing equations are introduced, fluid domain and the boundary conditions with the governing equations will be addressed.

4.2.2 Fluid domain and boundary conditions

Figure 4.3 illustrates the fluid domain of the given two-dimensional tube banks problem. Although 12 different geometries are investigated for different pitch ratios and different tube rows, only one has been demonstrated here, since all geometries have identical shape. Detailed geometry configurations are provided in Table 4.2.

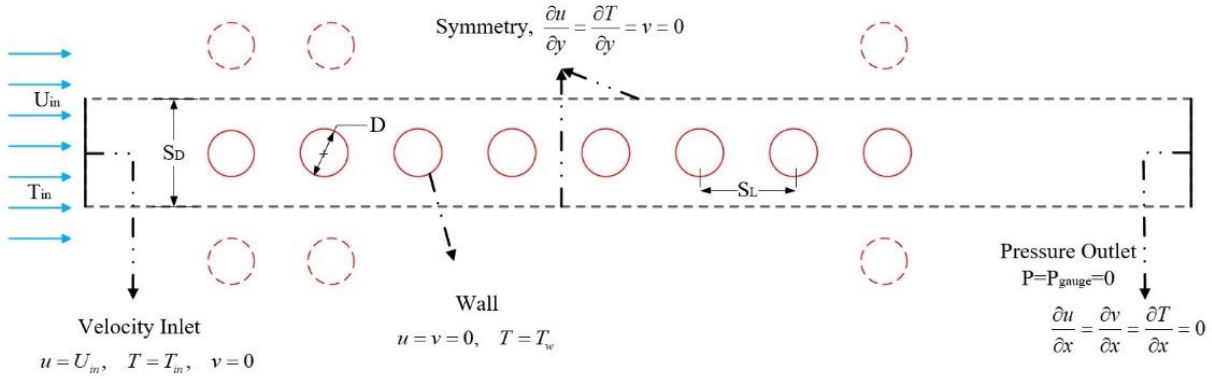

Figure 4. 3 Fluid domain with boundary conditions

Table 4. 2 List of geometries

Dimensionless Pitch Ratio	Number of In-line Tubes
1.3	3, 4, 8
1.6	3, 4, 8
2.0	3, 4, 8
3.0	3, 4, 8

As considered before, the geometries are created using a commercial software program ANSYS Fluent 18.2. The diameter of the in-line tubes is 15 mm, which has been selected since it is suitable for the widely available tubing used in various applications. The longitudinal and

transverse pitches are determined based on this tube diameter. Since fully developed velocity is considered in the inlet, the entrance region is extended by three times of the tube diameter. It is again applied six times longer than the tube diameter for the outlet region to lead the fully developed flow and to avoid oscillations. Owing to symmetry boundary conditions, only one of the rows is used to investigate the heat transfer and fluid flow characteristics.

After designing the domain, boundary conditions can then be applied. A non-slip boundary condition, where the velocity components are set to zero, was applied for the tubes with a constant temperature of 350K. This temperature is applicable for low-heat recovery applications such as boiler exhaust. A uniform velocity boundary condition was applied to the inlet, and the velocity of the fluid is calculated, corresponding to various Reynolds number and pitch ratio using equations (4.5) and (4.6).

$$\mathrm{Re} = \frac{\rho U_{\max} D}{\mu} \tag{4.5}$$

$$U_{\max} = U_{in} \frac{S_D}{S_D - D} \tag{4.6}$$

The temperature of the inlet was also assumed to be constant and a range of temperature was set from 400K to 600K. Symmetry boundary conditions is selected for the top and bottom walls of the domain. In symmetry boundary conditions, no flow can cross these boundaries, and the velocity of the components are set to zero. A pressure-outlet boundary condition is applied for the outlet of the domain with a value of zero pressure gauge pressure, since the outlet of the domain is assumed to be open to the atmosphere. In order to apply an artificial heat leakage to the systems, source terms are applied to Fluent, and the sources are calculated using equation (4.23) for a value of heat transfer coefficient 10, 50, and 100 W/m^{2}K, corresponding to different

geometries. Also, the author is not basing this on the fluid temperature rather the equation that was used. Therefore it is not exactly "heat leakage" in a strict sense but acts in the same way.

Along with boundary conditions, initial conditions should be indicated. The temperature of the heat transfer fluid is initialized as equal to its inlet temperature.

$$T_{htf}(t=0)=T_{in}$$

The velocity of the heat transfer fluid is set to a value corresponding Reynolds number and dimensionless pitch ratio. The velocity of the air is assumed to be uniform over the inlet, and the mass flow rate is equal at the inlet and outlet of the domain. A summary of the boundary conditions of the given domain is illustrated in Table 4.3.

Table 4.3 Boundary conditions of the computational domain

	Flow simulation	Heat transfer simulation
Inlet	Fully developed	Uniform temperature at 400K, 500K, 600K
Outlet	Zero gauge pressure	dT/dx=0 (zero gradient)
Wall of the tube	No-slip wall	Constant temperature at 350K
Up and down wall	Symmetry	Symmetry

4.2.3 Mesh generation

High-quality grid generation performs a vital role in the accuracy of numerical solutions as well as the computational time of simulations. A small change in the step size of the mesh will create a high increase in the number of volumes. Therefore, an adequate study must be conducted to select a proper mesh type and to obtain optimum mesh size. In section 4.4.1, grid independence study is demonstrated to examine the minimum numbers of cells that would require accurate results for the given domains.

In this study, a 2D structured and quadrilateral mesh type has been used for the given geometries with an increased density in the vicinity of the cylinders; and as mentioned before,

ANSYS Fluent 18.2 was used to generate the mesh. The computational domain is divided into three regions: inlet, tube banks, and exit regions. While a uniform mesh is used for the inlet and exit regions, a non-uniform mesh is applied to the tube banks region to increase the density of the mesh over the cylinders. Figure 4.4 displays the mesh for a 4-cylinder simulation, and a more detailed view of one such cylinder is shown in Fig. 4.5.

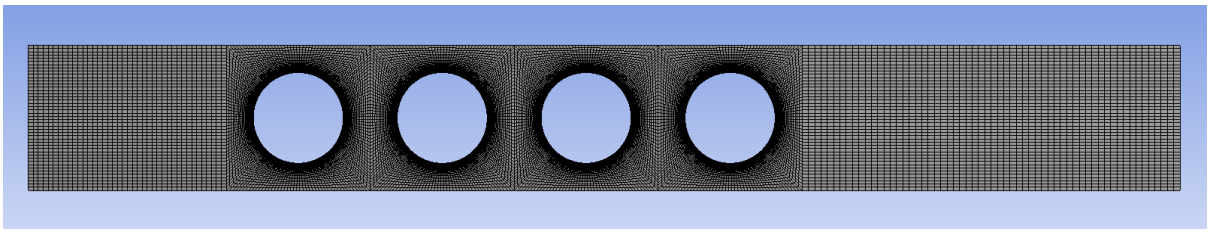

Figure 4. 4 Overall mesh generation for 1.6x1.6 pitch ratio.

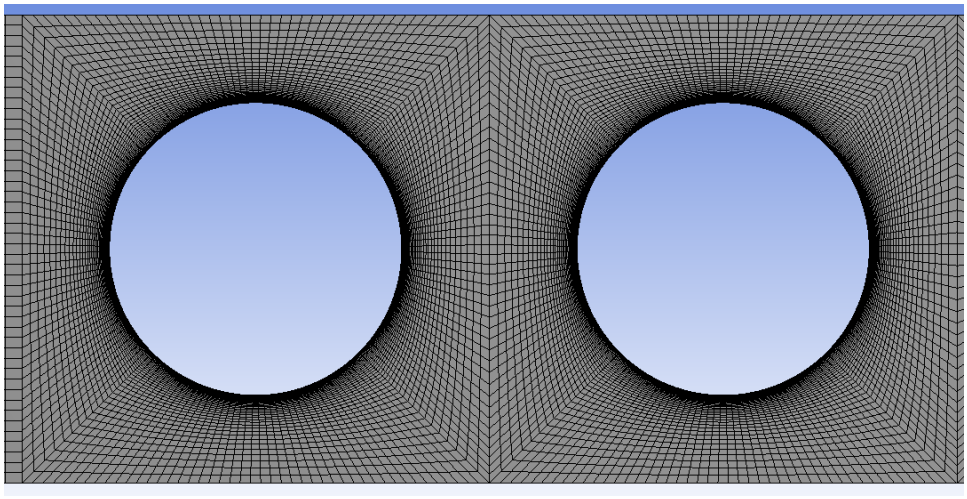

Figure 4. 5 Close-up of mesh near cylindrical surface

Although this method is very time consuming, it can be applied to simple geometries since the different areas of the mesh can be changed separately and the changes to the mesh do not affect the other parts of the model.

4.2.4 Computational procedure

In this study, a finite volume method has been used to solve governing equations of mass, momentum, and energy through ANSYS Fluent 18.2. In the finite volume method, the domain is

divided into small volumes or cells, and the equations are integrated in each volume; then the equations are transformed into an integral form. The pressure-based solver is selected as a solver in this numerical solution since it is assumed that the flow is incompressible and it is governed only by pressure differentials. In this case, the pressure-based solver applies an algorithm that belongs to a general class of methods termed projection methods (Chorin, 1968). In this projection method, solving a pressure correction equation provides the achievement of the conversation of mass or the continuity of the velocity field. The pressure equation is derived from the mass and momentum equation; consequently, the continuity equation is satisfied with the pressure and velocity profile. Due to the fact the differential equations are nonlinear by nature and are coupled, they must be repeatedly solved until the required convergence solution is achieved. Figure 4.6 illustrates the schematic of the solution process, which is taken from Fluent 14.0 Theory Guide (2011).

In the pressure-based segregated algorithm, the governing equations are solved sequentially to obtain the solution variables, such as u, v, w, p, T, k, ε, etc. Despite the solution convergence being relatively slow for the segregated algorithm compared to the coupled algorithm, the segregated algorithm is preferred since it is memory-efficient, and since high-speed computers can alleviate the slow convergence problems. Thus, a widely-known algorithm method, the SIMPLEC (Semi-Implicit Method for Pressure-Linked Equations-Consistent) (Doormaal and Raithby, 1984) algorithm is used for the pressure-based segregated solvers.

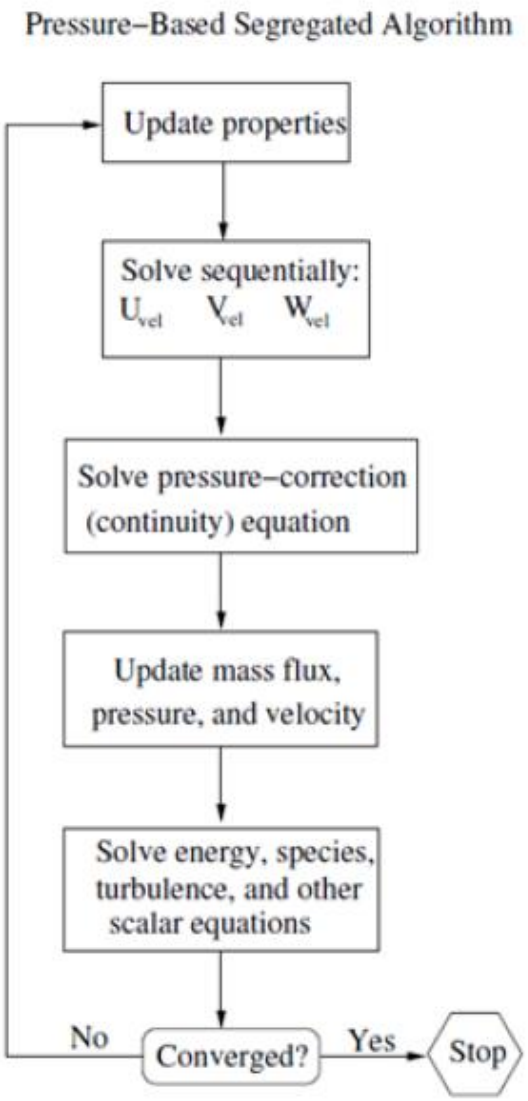

Figure 4. 6 Solution procedure for the Pressure-Based Segregated Solution Algorithm (*ANSYS FLUENT Theory Guide*, 2011)

4.2.4.1 SIMPLEC Algorithm

In order to solve two dimensional, incompressible and laminar as well as turbulent flow over a cylinder, the SIMPLEC algorithm based on a finite volume discretization method is applied. This algorithm follows the steps illustrated in Figure 4.6; however, each step is quite complicated. In this section, the concept of SIMPLEC algorithm will be outlined.

Before providing more details about the SIMPLEC algorithm, it should be noted that all variables are not solved at all locations and times. Instead, the computational domain is divided

or, discretized into sections or “cells”. The velocity vectors, temperature, density, and any other important properties for the user are stored in the centroid of each cell. As governing equations are all continuous, they must be discretized to be utilized in the computational procedure. In other words, due to the fact that the variables are stored in the centroid of each cell, the governing equations must be applied to cell facets instead of the centroids. To do so, a second order upwind scheme was used to discretize the convective terms in the energy and momentum equations, and second-order implicit method was used to discretize the time derivative. Furthermore, Green-Gauss method is used to calculate the arithmetic average of the required variables at the adjacent cell centers.

$$\overline{\Phi_f} = \frac{\Phi_{c0} + \Phi_{c1}}{2} \tag{4.7}$$

Although SIMPLEC algorithm has been used in this study, the SIMPLEC and SIMPLE (Semi-Implicit Method for Pressure-Linked Equations) algorithms are identical except for the omitting of the velocity correction equation in the SIMPLEC algorithm. The first step of this algorithm is to solve the momentum equation using a predicted pressure field, p*. Since the pressure field p* is generally mispredicted, the solution loop continues to update the pressure field until the solution is achieved within the required convergence criteria. Moreover, if the pressure field p* is not predicted correctly at the beginning of the solution, the continuity equation is not satisfied. In order to obtain a satisfied continuity equation, face fluxes are corrected by introducing a correction factor, and the fluxes for each cell are applied to a separate continuity equation. This method yields a separate equation for pressure correction in each cell. The primary purpose of this step is to solve the pressure correction equation through the algebraic multigrid method. After solving the pressure correction equation, this equation is used

to correct all cell pressure values and velocity components along with the under-relaxation factors.

The next step is to solve energy equations, which is crucial for any heat transfer applications, using the corrected continuity and momentum equations. Once these equations are solved, the last step in the SIMPLEC algorithm is to check the residuals error of the conservation equations.

The residual error represents the total combined difference in the governing equations through each iteration step. It should be noted that it is not possible to solve the equation with infinite precision for the cells in the computational domain; thus, the errors invariably occur when updating solutions. So, a converged solution is obtained when the residuals errors are below than that of the required convergence criteria or tolerance. However, if the results are above the tolerance, the solution is not converged, and the whole process repeats from the step one with a new approximate pressure field p*.

In order to obtain a converged solution, the residuals were set at $1e^{-6}$ for x, y, and z velocity values as well as continuity and energy equations.

4.2.4.2 k-ε turbulence model

In this study, each simulation is run transient and the k-ε RNG turbulence model is utilized, as is customary in similar applications (Ibrahim and Gomaa, 2009; Mangrulkar et al., 2017; Sayed Ahmed et al., 2015; Sayed Ahmed et al., 2015). This section will provide detailed information about RNG k-ε.

A statistical technique known as renormalization group theory is used in order to derive the RNG k-ε model. Although the standard k-ε model and the RNG k-ε model are similar, there are some refinements, which include swirl, separation, and recirculation of the fluid, on the RNG model, making this model more accurate and reliable for more extensive applications of flow. The transport equations for the RNG k-ε model is provided in equations (4.8) and (4.9)

$$\frac{\partial}{\partial t}(\rho k)+\frac{\partial}{\partial x_i}(\rho k u_i)=\frac{\partial}{\partial x_j}\left(\alpha_k \mu_{eff}\frac{\partial k}{\partial x_j}\right)+G_k+G_b-\rho\varepsilon-Y_M+S_k \quad (4.8)$$

$$\frac{\partial}{\partial t}(\rho \varepsilon)+\frac{\partial}{\partial x_i}(\rho \varepsilon u_i)=\frac{\partial}{\partial x_j}\left(\alpha_\varepsilon \mu_{eff}\frac{\partial \varepsilon}{\partial x_j}\right)+C_{1\varepsilon}\left(G_k+C_{3\varepsilon}G_b\right)-C_{2\varepsilon}\rho\frac{\varepsilon^2}{k}-R_\varepsilon+S_\varepsilon \quad (4.9)$$

In the two equations above, G_k and G_b represent the generation of turbulence kinetic energy due to the mean velocity gradients and buoyancy, respectively. Y_M is the fluctuating dilatation in compressible turbulence to the overall dissipation rate. The values of α_k and α_ε denote the inverse of the effective Prandtl numbers for k and ε, respectively; whereas, S_k and S_ε are the user-defined source terms.

Generation of turbulence kinetic energy due to the mean velocity gradients G_k is described as follows:

$$G_k=\mu_t\left(\frac{\partial u_i}{\partial x_j}+\frac{\partial u_j}{\partial x_i}\right)\frac{\partial u_i}{\partial x_j} \quad (4.10)$$

The μ_{eff} is the effective turbulent viscosity and is calculated as $\mu_{eff}=\mu+\mu_t$. Here, μ_t represent the turbulent viscosity and is calculated as;

$$\mu_t=\rho C_\mu\frac{k^2}{\varepsilon} \quad (4.11)$$

With C_μ=0.0845, $C_{\varepsilon 1}$ and $C_{\varepsilon 2}$ are 1.42, and 1.68, respectively. The primary difference between standard k- ε model and RNG k- ε model is the turbulent viscosity and an additional term R_ε

$$R_\varepsilon=\frac{C_\mu\rho\eta^3(1-\eta/\eta_0)}{1+\beta\eta^3}\frac{\varepsilon^2}{k} \quad (4.12)$$

Here, η_o= 4.38, β= 0.012, and $\eta= Sk/\varepsilon$, and S represents the modulus of the mean rate of the strain sensor,

$$S\equiv\sqrt{2S_{ij}S_{ij}} \quad (4.13)$$

$$S_{ij} = \frac{1}{2}\left(\frac{\partial u_i}{\partial x_j} + \frac{\partial u_j}{\partial x_i} \right) \tag{4.14}$$

The effect of the additional term R_ε will be more noticeable when rearranging the right hand side terms in equation (4.9) for ε, which can be rewritten as,

$$\frac{\partial}{\partial t}(\rho\varepsilon) + \frac{\partial}{\partial x_i}(\rho\varepsilon u_i) = \frac{\partial}{\partial x_j}\left(\alpha_\varepsilon \mu_{eff} \frac{\partial \varepsilon}{\partial x_j} \right) + C_{1\varepsilon}(G_k + C_{3\varepsilon}G_b) - C^*_{2\varepsilon}\rho\frac{\varepsilon^2}{k} \tag{4.15}$$

$$C^*_{2\varepsilon} \equiv C_{2\varepsilon} + \frac{C_\mu \rho \eta^3 (1 - \eta/\eta_0)}{1 + \beta\eta^3} \tag{4.16}$$

In the case of $\eta < \eta_0$, R_ε term is positive; so, $C^*_{2\varepsilon}$ is higher than $C_{2\varepsilon,}$ which shows that the RNG model produces higher μ_t results than the standard k- ε model. Moreover, in the case of large strain rate ($\eta > \eta_0$), the RNG model produces lower turbulent viscosity than the standard k- ε model. This feature is unique for this model and is not utilized in any other turbulence model.

4.2.4.3 Numerical solution

Once the solution is accomplished at each time step, some parameters are monitored as time progresses. The parameters monitored and saved are as follows: inlet and outlet pressures, velocities, temperatures, and heat flux over the tube bundles, and average volumetric bulk temperatures within the computational domains. Parameters are saved to file every time step size, which was selected as 0.01 seconds.

In this study, 24 Dell workstations were used to obtain the solutions in a computing laboratory at the University of Alabama. Although the computational power of these computers are quite high, the computational time for each simulation took between 1 and 2 hours, depending on the number of cells. Even though 24 computers were used for the simulations, each computer was run for about 30 hours to obtain solutions for 576 simulations.

Before starting on the grid size and time independence study, the parameters obtained using Fluent during the simulations should be addressed.

Once the computational solution was accomplished, it was easy to obtain and monitor the parameters—the average temperatures and pressures of the heat transfer fluid at the inlet and outlet of the domain, heat flux over the tube banks, and the volumetric average temperature of the HTF (Heat Transfer Fluid)—to evaluate thermodynamics analyses. The average values of the bulk temperature of the heat transfer fluid was obtained by conducting a volume-weighted average over the domain. This method is reasonable since the fluid is assumed incompressible and holding constant specific heat. The volume-weighted average of bulk temperature is computed by dividing the summation of the product of temperature and the cell volume by the total volume of the cell zone:

$$\overline{T} = \frac{1}{V}\int T dV = \frac{1}{V}\sum_{i=1}^{n} T_i \left| V_i \right| \tag{4.17}$$

The average values of the pressure and temperatures at the inlet and outlet of the domain were met by performing a mass-weighted average over the selected surfaces. The volume-weighted average method was not valid for the evaluation of the average inlet and outlet temperatures and pressures, since the velocity of the fluid may vary over the flow field. The mass-weighted average of pressure or temperature is computed by multiplying density and the absolute dot product of the facet area and the velocity vector, representing the surface mass flux. In order to obtain average pressure, mass flux is multiplied by the summation of the pressure over the n cells and then divided by the total mass flux entering the surface. The formulation of the mass-weighted average temperature and mass-weighted average pressure are given by euqations (4.18) and (4.19).

$$\overline{P} = \frac{\sum_{i=1}^{n} P_i \rho_i \left| \vec{V} . \vec{A} \right|}{\sum_{i=1}^{n} \rho_i \left| \vec{V} . \vec{A} \right|} \tag{4.18}$$

$$\overline{T} = \frac{\sum_{i=1}^{n} T_i \rho_i \left| \vec{V} . \vec{A} \right|}{\sum_{i=1}^{n} \rho_i \left| \vec{V} . \vec{A} \right|} \tag{4.19}$$

With the required parameters to evaluate thermodynamics analysis now discussed, the thermodynamic analysis section now follows

4.3 Thermodynamic Analysis

Thermodynamic analyses are as crucial as heat transfer and fluid flow numerical analyses for evaluating the performance of the systems and to determine the losses. There are two main methods, energy and exergy analyses, which are commonly used to investigate thermal performance. In this section, these two analyses will be introduced and discussed.

4.3.1 Energy Analysis

To begin with, the steady-state energy balance for the control mass, assuming negligible kinetic and gravitational effects, and negligible control volume work is presented as follows:

$$\dot{Q} = \dot{m}\left(h_2 - h_1\right) \tag{4.20}$$

Here, $\dot{Q}$ represents the heat transfer rate between the control volume and its surroundings. In this system, there are two heat transfer sources. The first one is due to convection over the cylinders, and the second is due to heat leakage:

$$\dot{Q} = \dot{Q}_w + \dot{Q}_l = \dot{m} C \Delta T + \dot{V}\left(\overline{P}_{in} - \overline{P}_{out}\right) \tag{4.21}$$

Here, $\dot{V}$ and $\overline{P}$ represent the volumetric flow rate and average thermodynamic pressure respectively. As observed from equation (4.21), the balance of energy depends on the mass flow

rate of heat transfer fluid in the simulation, specific heat, and the average temperature and pressure difference between the inlet and the outlet. There is also a dependence on heat leakage, which has been artificially introduced to account for heat leakage from the ambient into the domain. The leakage, $\dot{Q}_l$, is applied as follows:

$$\dot{Q}_l = UA\left(\Delta T\right)_l \tag{4.22}$$

Here, U, A and ΔT_l denote the overall heat transfer coefficient, surface area, and temperature difference, calculated as follows:

$$\left(\Delta T\right)_l = \frac{T_{in} + T_w}{2} - T_0 \tag{4.23}$$

Finally, the energy efficiency can be defined as the ratio of desired energy extracted from the fluid and the total energy required by the flow. It is expressed as follows:

$$\eta = \frac{\dot{Q}_w}{\dot{m}C\Delta T + \dot{V}\left(\bar{P}_{in} - \bar{P}_{out}\right)} \tag{4.24}$$

4.3.2 Exergy Analysis

The exergy efficiency can be calculated using equations (4.25)–(4.36). The exergy balance equation is similar to energy equation but includes a term for exergy destruction due to the irreversibility of the system, $\dot{\Xi}_d$:

$$\dot{\Xi}_Q - \dot{W} + \dot{m}\left(\psi_1 - \psi_2\right) - \dot{\Xi}_d = 0 \tag{4.25}$$

The first term of the equation (4.25) represents the exergy gained due to heat transfer and has two sources, similar to the energy balance.

$$\dot{\Xi}_Q = \dot{\Xi}_{Q,w} + \dot{\Xi}_{Q,\mathrm{l}} \tag{4.26}$$

$$\dot{\Xi}_{Q,w} = \dot{Q}_w\left(1 - \frac{T_o}{T_w}\right) \tag{4.27}$$

$$\dot{\Xi}_{Q,1} = \dot{Q}_l \left(1 - \frac{T_o}{T_d}\right) \tag{4.28}$$

Here, T_o, T_w and T_d are the surrounding temperature of the domain, tube surface temperature (assumed constant), and the average bulk temperature, respectively. The flow exergy difference between the inlet and outlet is determined as follows and can be calculated by monitoring the temperature difference at the inlet and the outlet:

$$\dot{\Xi}_{in} - \dot{\Xi}_{out} = \dot{m}\left(\psi_{in} - \psi_{out}\right) = \dot{m}\left[C\left(\bar{T}_{in} - \bar{T}_{out}\right) - T_0 \ln\left(\frac{\bar{T}_{in}}{\bar{T}_{out}}\right)\right] \tag{4.29}$$

To evaluate the exergy destruction, equation (4.30), an entropy balance is required, equation (4.31):

$$\dot{\Xi}_d = T_0 \dot{S}_{gen} \tag{4.30}$$

$$\Delta S_{sys} = \dot{S}_{in} - \dot{S}_{out} + \dot{S}_{gen} \tag{4.31}$$

For the given problem, there are three different sources of entropy generation: viscous dissipation, heat transfer to the cylinder, and heat transfer to the environment due to heat leakage. They are evaluated in equations (4.32)–(4.34):

$$\dot{S}_{gen} = \dot{S}_{gen,\text{heattrans}} + \dot{S}_{gen,vis.diss} + \dot{S}_{gen,heat-leakage} \tag{4.32}$$

$$\dot{S}_{gen,heattrans} = \dot{m}\left[C \ln\left(\frac{\bar{T}_{out}}{\bar{T}_{in}}\right) - R_0 \ln\left(\frac{\bar{P}_{out}}{\bar{P}_{in}}\right)\right] - \frac{\dot{Q}_w}{T_w} \tag{4.33}$$

$$\dot{S}_{gen,heat-leakage} = \frac{\dot{Q}_l}{\bar{T}_d} \tag{4.34}$$

Here, $\dot{Q}_w$, $\dot{Q}_l$ represent the total heat transfer from the fluid to tubes and heat leakage from the system to the environment, respectively.

$$\dot{S}_{gen,vis.diss} = \frac{\dot{V}\left(\bar{P}_{in} - \bar{P}_{out}\right)}{\bar{T}_d} \tag{4.35}$$

In order to calculate entropy generation due to viscous dissipation, average pressure drop and domain temperature are monitored, which are readily calculated in Fluent. It is then possible to evaluate the exergy efficiency of the system. The exergy efficiency gives a measure of how thermodynamically efficient a system is as compared to a perfect (reversible) one under the same conditions.

$$\Psi = \frac{\dot{\Xi}_{Q,w}}{\dot{\Xi}_{in} - \dot{\Xi}_{out}} = \frac{\dot{\Xi}_{Q,w}}{\dot{\Xi}_{Q} + \dot{\Xi}_{d}} \tag{4.36}$$

Once the required equations to analyze thermodynamic characteristics of the system are introduced, the effect of the inlet velocity, inlet temperature, dimensionless pitch ratio, number of in-line cylinders, and the amount of heat leakage can be investigated.

4.4 Spatial and Temporal Independence Study

As mentioned earlier, grid independence and time independence tests must be completed in order to obtain satisfactory results for the simulations. These tests are the first steps after mesh generation. Once independence tests are completed successfully, parametric studies can be initiated. The next two sections discuss the grid and temporal independence studies conducted in this study.

4.4.1 Grid independence study

A grid size independence study is essential to ensure computational accuracy and tractability. When creating a control volume, it should be ensured that the domain is divided adequately into cells in order to obtain accurate results. If the computational domain is discretized into too many volumes, the computational time required will considerably increase. Therefore, an optimum number of cells should be generated in order to obtain not only accurate

results but also as minimal a computational time as possible. In order to achieve this, a grid size independence test is carried out by varying the number of volumes in the domain.

In this study, the grid independence test is performed for a pitch ratio of 1.6. The highest Reynolds number, 30,000, is chosen for grid independence. The inlet temperature is 400K and the tube wall temperature is 350K. Starting with a coarse mesh, cell count was increased by about 20,000 volumes at each step until no further changes in Nusselt number is observed, see Fig. 4.7. It is obvious from Fig. 4.7 that a mesh count of around 65,000 is sufficient for the simulation process.

As it can be observed from Figure 4.7, Nusselt number was chosen as a criterion to study grid size independence; and this parameter was recorded at intervals of 0.01s.

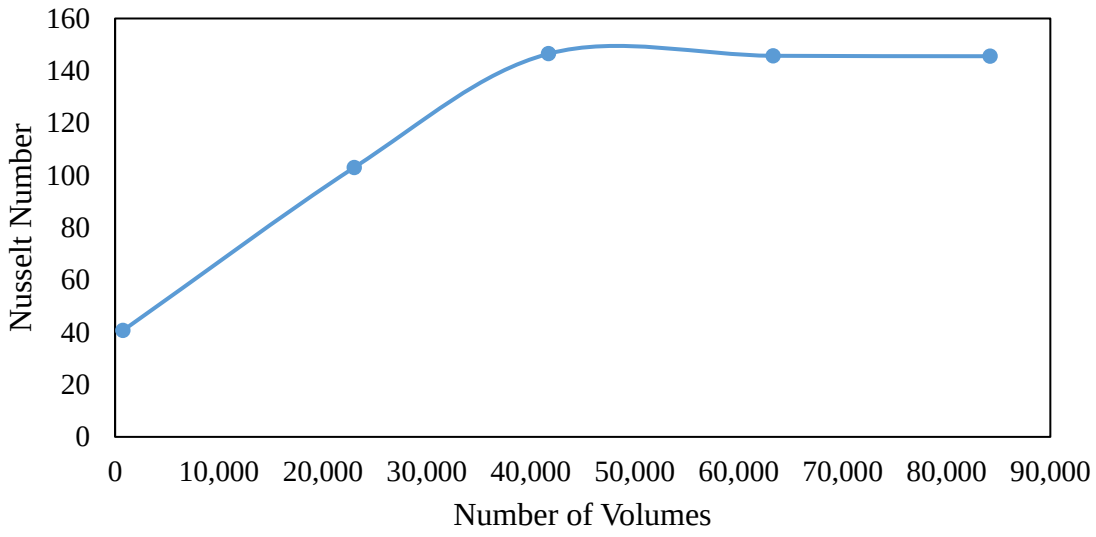

Figure 4. 7 Grid size independence study

4.4.2 Time step independence study

In transient flow problems, time independence is as crucial as grid size independence when evaluating fluid flow and heat transfer characteristics for numerical solutions. As mentioned in the previous section, larger volumes may not indicate accurate results, and the same situation can be seen if the time step size is considerably large. Conversely, if a very small

time step size is employed, the computational time of the simulation will increase substantially. Therefore, an optimum time step size must be found in order to obtain more precise results with as minimal amount of computational time as possible.

The geometry used for the grid independence study was also used for the time step size independence test. All simulations are run for 10 seconds simulated time, and time step size is varied for each simulation from 0.005 to 0.5s. Again, the Nusselt number was used a criterion for this test. Figure 4.8 and Figure 4.9 indicate the results of this study and indicates that a time step size of 0.01s (corresponding to 1,000 total time steps) is sufficient for this study. It is noted that the Nusselt number becomes constant well before the data is recorded for thermodynamics and heat transfer calculations, discussed further in Chapter 5.

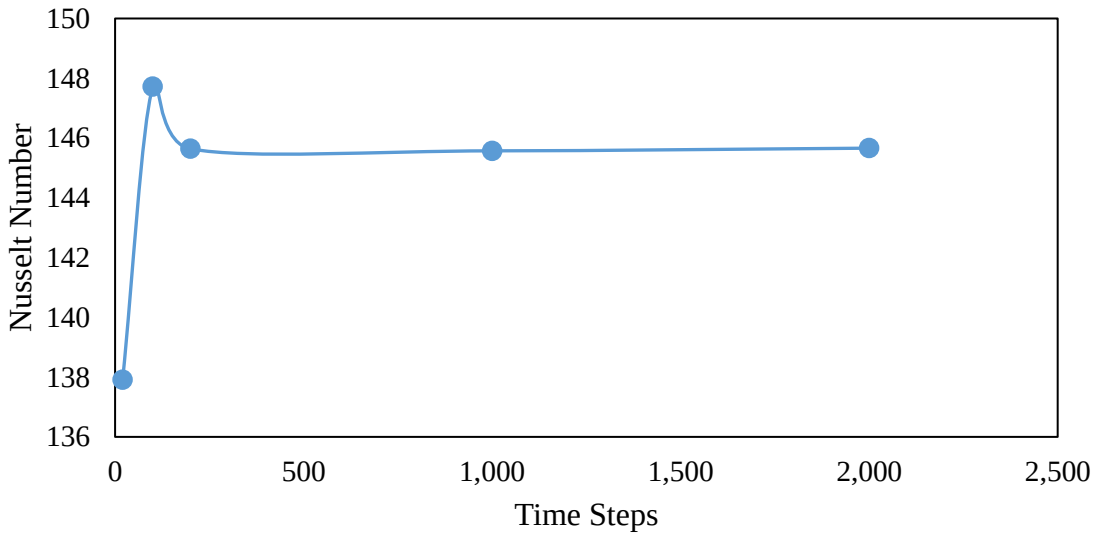

Figure 4. 8 Time step size independence study

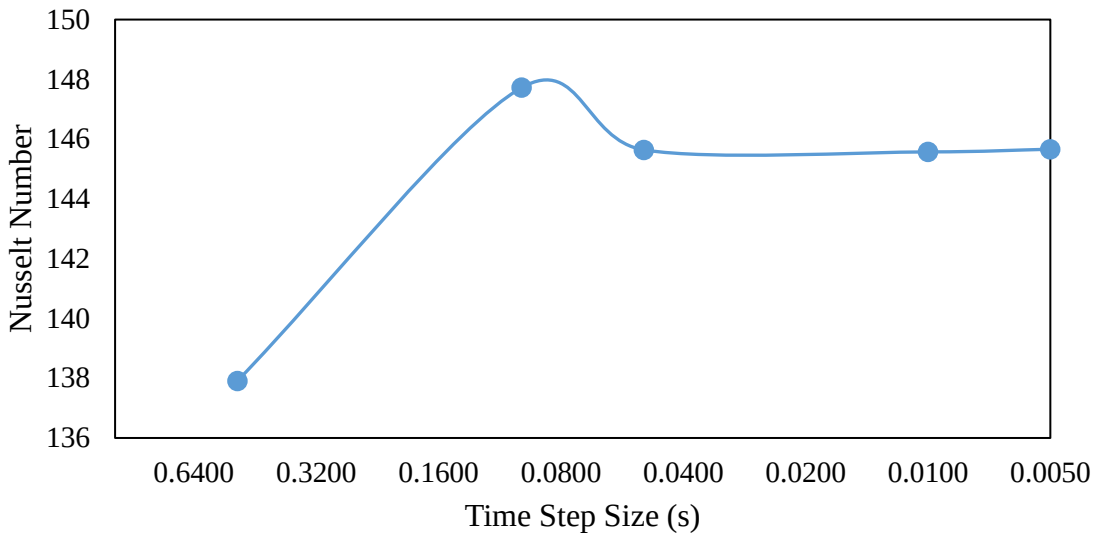

Figure 4. 9 Time step size independence study

Beside Nusselt number, the temperature contours are also examined for different time step sizes as seen in Fig. 4.10. It is clear from the figures that, whereas there is a considerable difference between 0.5s and 0.01s, the contours are virtually identical for the 0.01s and 0.005s cases. Therefore, the chosen time step size 0.001s is considered adequate for this study.

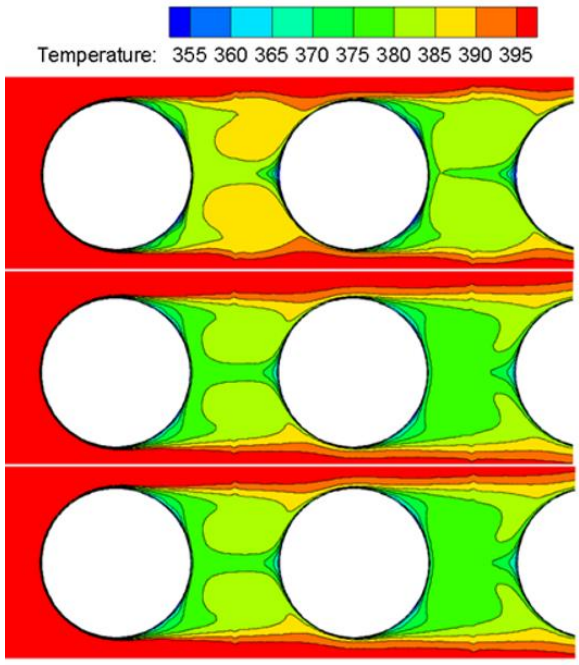

Figure 4. 10 Temperature contours for different time step size (top= 0.5s, middle= 0.01s, bottom= 0.005s)

Now that the governing equations, solutions procedures, and numerical independence tests have been discussed, the validation, results and associated discussion are presented in the next Chapter.

The material in this chapter has been co-authored by Dr. David MacPhee, Assistant Professor of mechanical engineering at the University of Alabama, and is currently being prepared for publication.

5 RESULTS AND DISCUSSION

In this chapter, the first and second laws of thermodynamics are presented in relation to a tube bundle in cross-flow considering various parameters, with a numerical method. First of all, energy efficiency will be calculated for different values of Reynolds number, pitch ratio, number of cylinders, and other such parameters. Subsequently, exergy efficiency (second law) will be examined for the same geometries and parameters.

Before starting with the results, the models' validation needs to be performed, in order to ensure that the models are accurately employed.

5.1 Model Validation

5.1.1 Nusselt number

Nusselt number and pressure drop values were used as parameters to compare the different models' validation. As demonstrated in equations (5.1) and (5.2), the Nusselt number can be calculated using data recorded in Fluent, e.g. total heat flux and outlet and inlet temperatures. Among several Nusselt number correlations, the widely known Zukauskas (1987) correlation was used. Table 5.1 indicates these correlations corresponding to Reynolds numbers values. The pitch ratio was then varied for each Reynolds number and the resulting Nusselt number was compared to the numerical results.

$$Nu = \frac{\dot{Q}_w D}{\Delta T_{ln} k} \tag{5.1}$$

$$\Delta T_{ln} = \frac{\left(T_w - \bar{T}_{out}\right) - \left(T_w - \bar{T}_{in}\right)}{ln\left[\left(T_w - \bar{T}_{out}\right) / \left(T_w - \bar{T}_{in}\right)\right]} \tag{5.2}$$

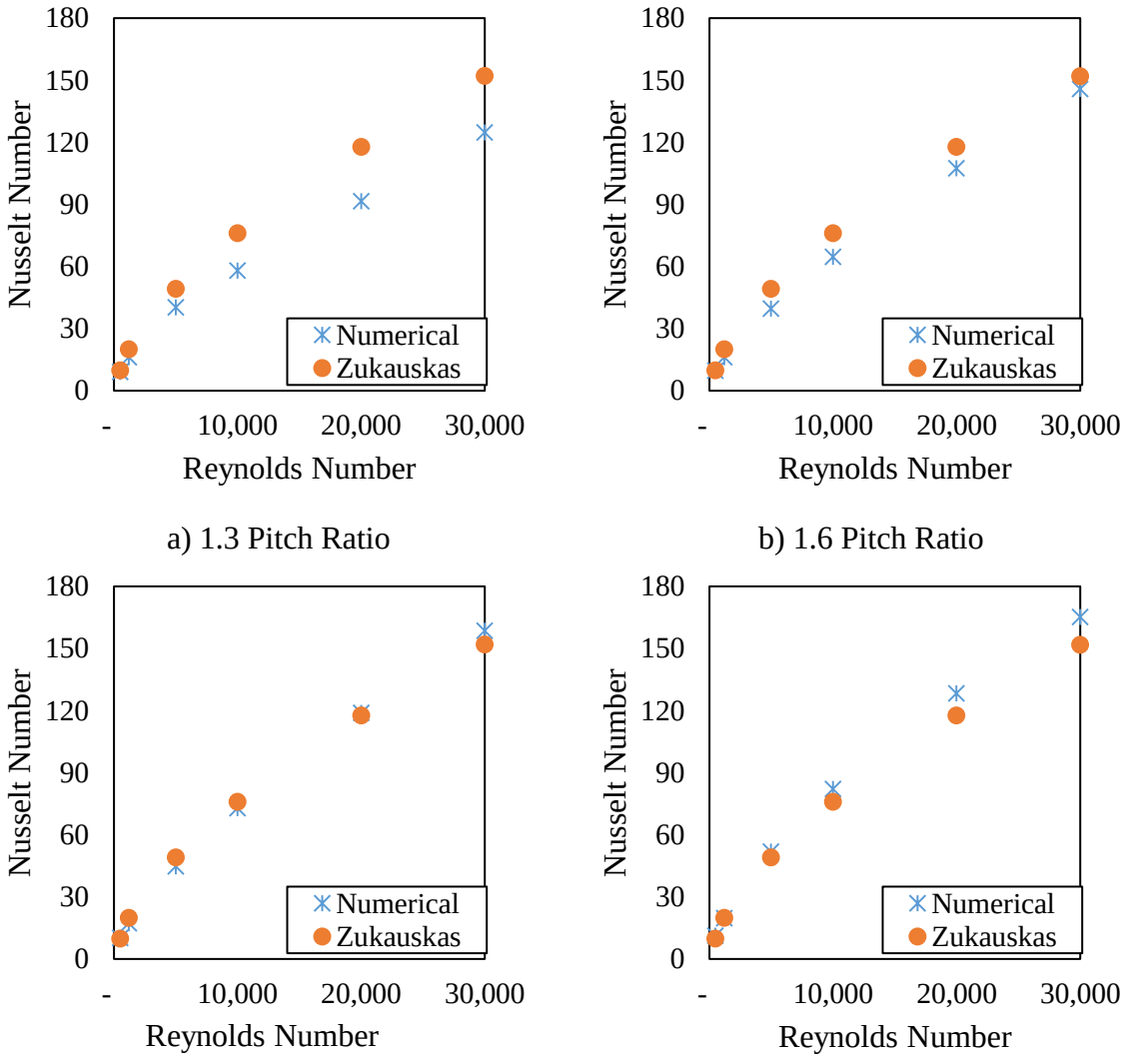

a) 1.3 Pitch Ratio

b) 1.6 Pitch Ratio

c) 2.0 Pitch Ratio

b) 3.0 Pitch Ratio

Figure 5. 1 Nusselt number validation

In many cases, the numerical and published results came quite close, and the difference between these results was less than 20% in all cases, barring a few on average, the numerical simulations agreed with (Žkauskas, 1987) to 24%. It can be observed from Fig.5.1.a) that the

difference between the published and numerical values for this case was nearly 23%. This error is caused by the small pitch ratio of 1.3; such low ratios act to push the boundary layers out to a less resolved portion of the mesh, decreasing the accuracy to some degree.

Table 5.1 Zukauskas Nusselt number correlations

Re_D	*Zukauskas Nusselt number correlation*
100–1,000	$Nu_D = 0.9\,\mathrm{Re}^{0.4}\,\mathrm{Pr}^{0.36}\left(\mathrm{Pr}/\,\mathrm{Pr}_s\right)^{0.25}$
1,000–2×10^5	$Nu_D = 0.52\,\mathrm{Re}^{0.5}\,\mathrm{Pr}^{0.36}\left(\mathrm{Pr}/\,\mathrm{Pr}_s\right)^{0.25}$

5.1.2 Pressure drop

Since the amount of viscous dissipation is an important factor in thermodynamics, the pressure drop losses between the inlet and exit of the tube array were compared in order to validate the results. An analytical relation for the pressure drop in the tube banks has been indicated with equation (5.3).

$$\Delta P = N_L f \chi \frac{\rho U_{max}^2}{2} \tag{5.3}$$

In this equation, f and χ denotes the friction factor and correction factor respectively. Zukauskas and Ulinskas (1985) provided a graph to obtain these two values. As it can be observed from equation (5.3), the maximum velocity of the fluid, which occurs between the tubes, is used in correspondence to the Reynolds number. After the calculation of the pressure drop with this equation, the results were compared with the ones obtained from simulations. As discussed earlier, the area-weighted-average values for pressure were recorded at the inlet and exit of the tube bank. Figure 5.2 illustrates the comparison between the numerical and analytical results of the pressure drop. It is evident from the graphs that the difference between the published and numerical values is less than 20% for most cases in fact, an average, the two agreed to within 24%. In spite of the fact that a high value of Reynolds number, 30,000 was used in this study, the highest difference between the numerical and published value was found to be

less than 24% for this Reynolds number. Hence, it can be stated that there was good agreement between the published values for both Nusselt number and pressure drop.

It should also be observed that although all cases were validated for this study, only eight cylinder cases have been discussed here for the purpose of validation, as they showed the poorest agreement among all cases considered. Validation information for four and three cylinders has been provided in Appendix A.

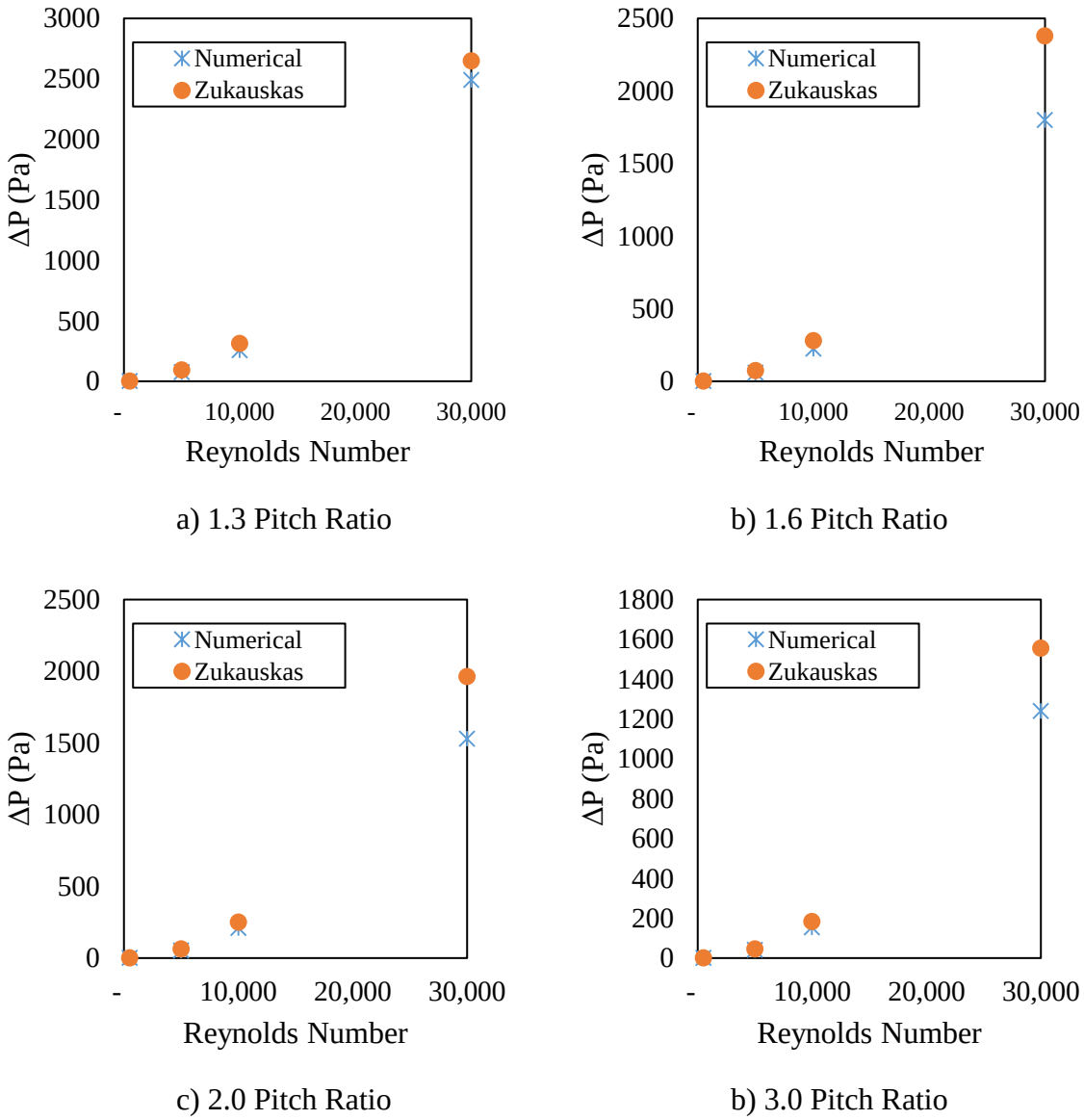

Figure 5. 2 Pressure drop validation

5.2 Energy Efficiency

Thermodynamic analyses were conducted using equations (4.20)–(4.24). The primary purpose was to investigate the change in energy and exergy efficiency with respect to the Reynolds number, pitch ratio, number of tubes, heat leakage, and inlet temperature of the HTF. Energy efficiency, one of the most important parameters for assessing a system's performance (MacPhee, Dincer, & Beyene, 2012), depends on the heat transfer from HTF to the cylinders, viscous dissipation, and heat leakage from the system to the environment.

The energy efficiency, as calculated in this study, ranged from 71.72%–99%. The lowest energy efficiency was obtained for a domain with eight cylinders, a pitch ratio of 3.0, a Reynolds number of 500, an inlet temperature of 400 K, and a heat transfer coefficient 100 W/m^2. The highest energy efficiency occurred with three cylinders, a pitch ratio of 1.3, a Reynolds number of 500, an inlet temperature of 500K, and without any heat leakage.

It is important to note that viscous heating and heat leakage, quite significant processes for this type of systems, were considered in this study. Heat leakage from a system to the environment always takes place in real-world systems. Hence, four different artificial heat leakage sources were applied to the given systems and the heat leakage's effect on energy efficiency was analyzed. Moreover, viscous heating or viscous dissipation is caused due to shear stress in the fluid domain. It can be expected that the viscous dissipation effect increases with increasing fluid velocity due to high pressure energy loss. It can be observed from most of the figures and tables that the highest velocity values lead to lowest energy efficiencies due to high viscous dissipation.

5.2.1 Reynolds number

In this section, the variation in energy efficiency will be illustrated for different values of Reynolds number, pitch ratio, and heat leakage.

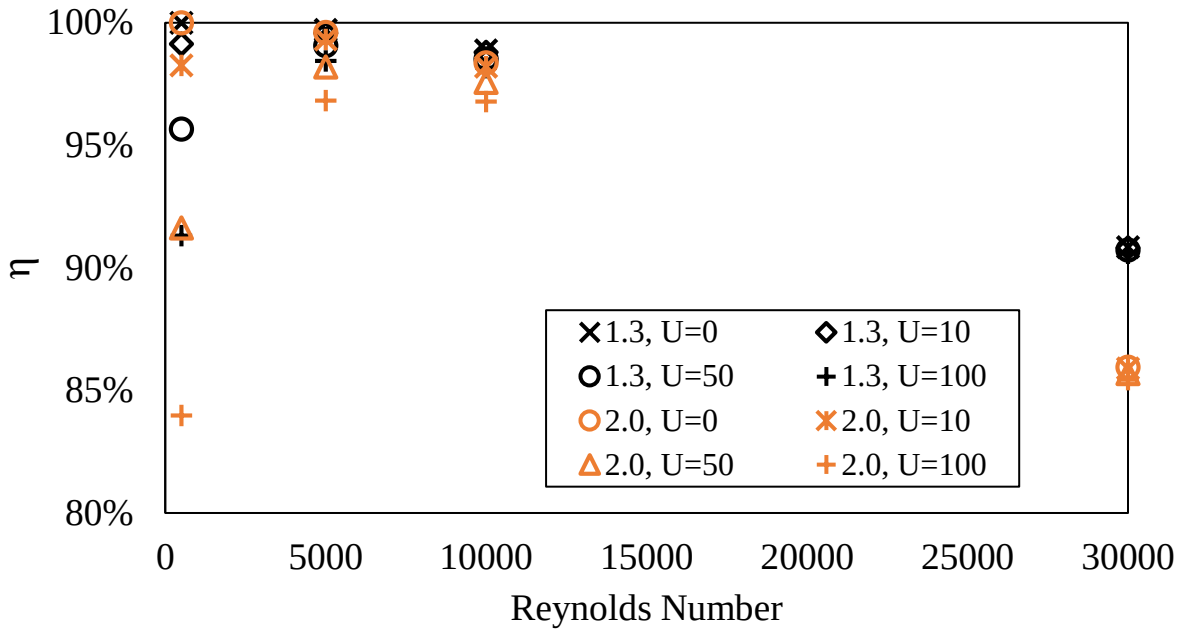

Figure 5. 3 Energy efficiency for the case T_{in} = 400K, 8 cylinders, pitch ratio 1.3 and 2.0 for different heat leakages

Figure 5.3 and 5.4 compare the energy efficiency in terms of heat leakage, pitch ratio, and Reynolds number for a domain with eight cylinders and an inlet temperature of 400 K. It is evident from these graphs that the energy efficiency values tend to decrease with increasing Reynolds number when the system is assumed to be adiabatic, i.e., no heat transfer from the system to the environment. The reason for this decreasing phenomenon is due to the fact that viscous dissipation increases with increasing Reynolds number. It can also be observed from Table 5.2 that energy efficiency depends on only heat transfer from the HTF to the cylinders and viscous dissipation for adiabatic systems. Hence, viscous dissipation has a considerable effect on the energy efficiency for cases with high Reynolds number; for instance, its proportion is greater than 18% for the pitch ratio of 3.0 and Re = 30,000. This is not surprising since viscous

dissipation depends on the volumetric flow rate and average pressure difference, both of which increase with higher Re.

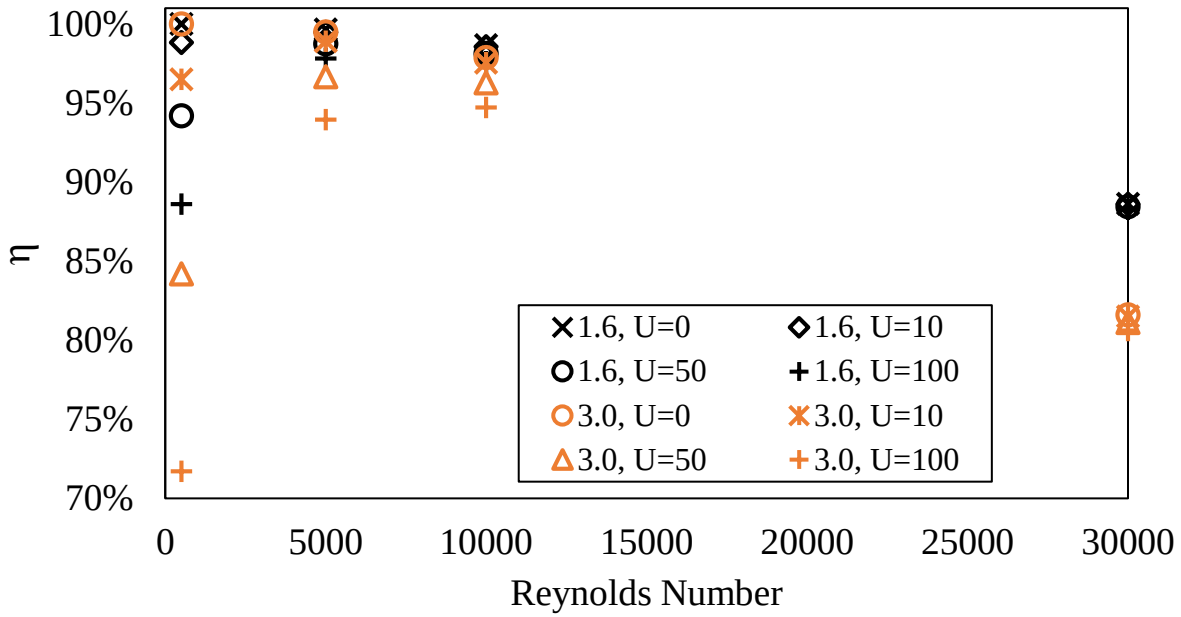

Figure 5. 4 Energy efficiency for the case T_{in} = 400 K, eight cylinders, pitch ratio of 1.6 and 3.0 for different heat leakages.

It should be noted that while the highest energy efficiencies were obtained with Re = 5,000 for most cases, the differences in the efficiency values were relatively close when Re = 5,000 and Re = 10,000 were compared. The main reason behind this can be explained through analysis of Table 5.2. Moreover, even though small amounts of heat leakage were applied to the systems, the efficiency of the low Reynolds number cases decreased since convective heat transfer effects are not significant for low Reynolds number cases. For instance, the proportion of the heat leakage for 3.0 pitch ratio and Reynolds number of 500 cases with a heat transfer coefficient of 10 W/m^{2}K and 50 W/m^{2}K were 3.5% and 18.3% respectively.

Table 5.2 Effect of heat transfer, heat loss, and viscous dissipation on energy efficiency (T_{in} = 400 K, eight cylinder)

		Heat leakage											
		U = 0			U = 10 W/m^{2}K			U = 50 W/m^{2}K			U = 100 W/m^{2}K		
		Percentage effect on energy efficiency											
Pitch ratio	Reynolds number	HT	VD	HL	HT	VD	HL	HT	VD	HL	HT	VD	HL
1.30	500	100%	0%	0%	99%	0%	1%	96%	0%	4%	91%	0%	9%
1.30	5,000	100%	0%	0%	100%	0%	0%	99%	0%	1%	98%	0%	1%
1.30	10,000	99%	1%	0%	99%	1%	0%	99%	1%	0%	98%	1%	1%
1.30	30,000	91%	9%	0%	91%	9%	0%	91%	9%	0%	91%	9%	0%
1.60	500	100%	0%	0%	99%	0%	1%	94%	0%	6%	89%	0%	11%
1.60	5,000	100%	0%	0%	99%	0%	0%	99%	0%	1%	98%	0%	2%
1.60	10,000	99%	1%	0%	99%	1%	0%	98%	1%	1%	98%	1%	1%
1.60	30,000	89%	11%	0%	89%	11%	0%	88%	11%	0%	88%	11%	0%
2.00	500	100%	0%	0%	98%	0%	2%	92%	0%	8%	84%	0%	16%
2.00	5,000	100%	0%	0%	99%	0%	0%	98%	0%	1%	97%	0%	3%
2.00	10,000	98%	2%	0%	98%	2%	0%	98%	2%	1%	97%	2%	2%
2.00	30,000	86%	14%	0%	86%	14%	0%	86%	14%	0%	85%	14%	1%
3.00	500	100%	0%	0%	97%	0%	3%	84%	0%	16%	72%	0%	28%
3.00	5,000	99%	1%	0%	99%	1%	1%	97%	0%	3%	94%	0%	6%
3.00	10,000	98%	2%	0%	98%	2%	0%	96%	2%	2%	95%	2%	3%
3.00	30,000	82%	18%	0%	82%	18%	0%	81%	18%	1%	81%	18%	1%

The last point of analysis in this section are the energy efficiencies with varying heat leakage. It is clear from Table 5.2 that the lowest energy efficiencies were obtained in the case of a Reynolds number 30,000 for all cases, except in the case of the heat leakage with the heat transfer coefficient of 100 W/m^{2}K. In this case, the lowest efficiencies were obtained for the Reynolds number of 500 as the proportion of heat leakage dominated the heat transfer from HTF to the cylinders and the viscous heating.

The author also compared the cases with four cylinders and an inlet temperature of 500 K as well as a case with three cylinders and an inlet temperature of 600 K. However, they have not

been mentioned here because the trend was extremely similar to the ones of 400 K presented here. These two cases have been included in Appendix B.

5.2.2 Number of cylinders

Figures 5.5, 5.6, and 5.7 compare the energy efficiencies with varying number of in-line cylinders for different pitch ratios, heat transfer coefficients, and inlet temperatures. It is obvious from the first two graphs that energy efficiency increases with increasing number of in-line cylinders due to the heat transfer fluid's high velocity. Figure 5.5 and 5.6 present cases where Reynolds numbers is 30,000 and 10,000, respectively. The velocity of the fluid was relatively high for these Reynolds numbers, and this caused higher heat transfer from HTF to the cylinders. Hence, increasing the number of cylinders resulted in higher efficiency.

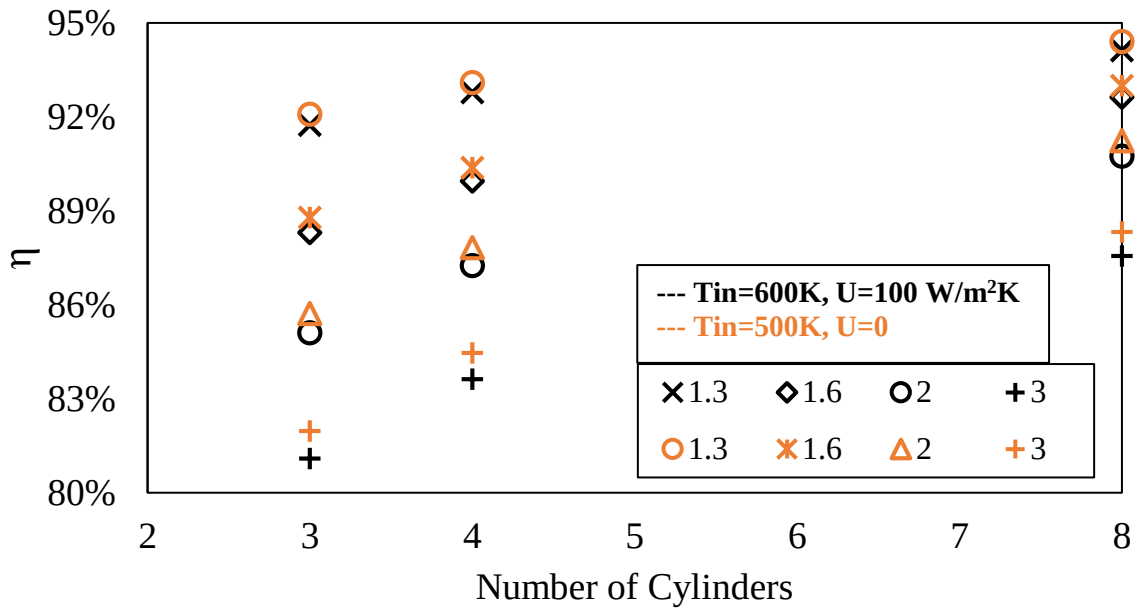

Figure 5. 5 Energy efficiency for the case of *Re* = 30,000 with varying number of cylinders for all four pitch ratios.

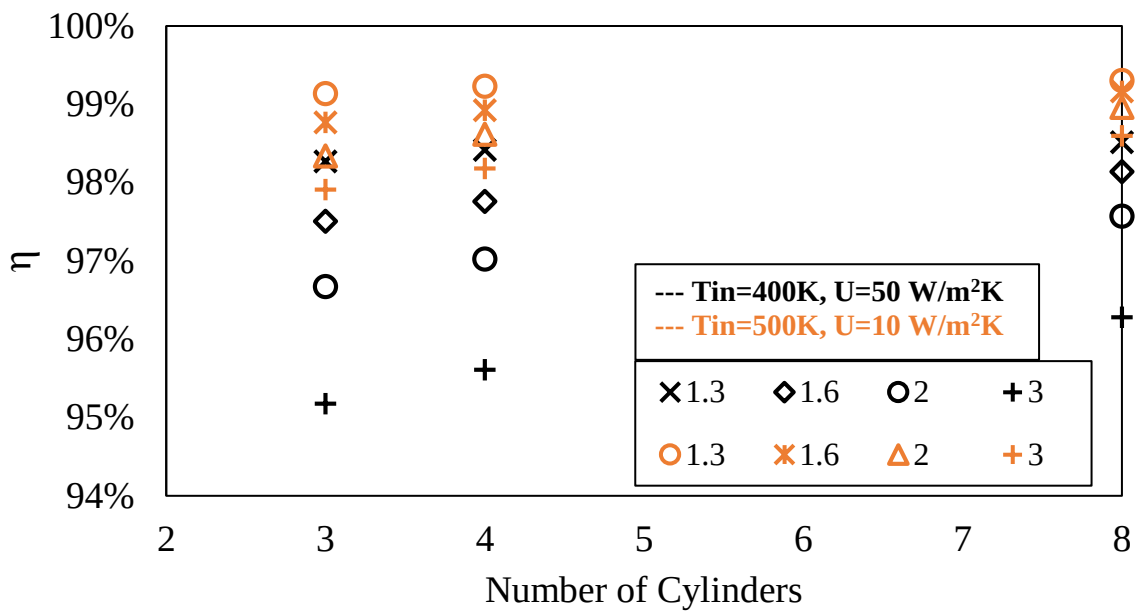

Figure 5. 6 Energy efficiency for the case *Re* = 10,000 with varying number of cylinders for all four pitch ratios.

Nevertheless, when a low Reynolds number is considered, such as 500, the system's efficiency decreases with an increasing number of cylinders, since the heat transfer fluid's velocity is low, and this leads to lower heat transfer. Moreover, the pressure drop increases with increasing number of cylinders. However, the effect of the pressure drop (viscous dissipation) was the lowest for three in-line cylinders for low Reynolds numbers. Even though this aspect was extremely similar even if the system was assumed to be adiabatic, this decreasing trend was exhibited by systems with a heat transfer coefficient of 100 W/m^{2}K.

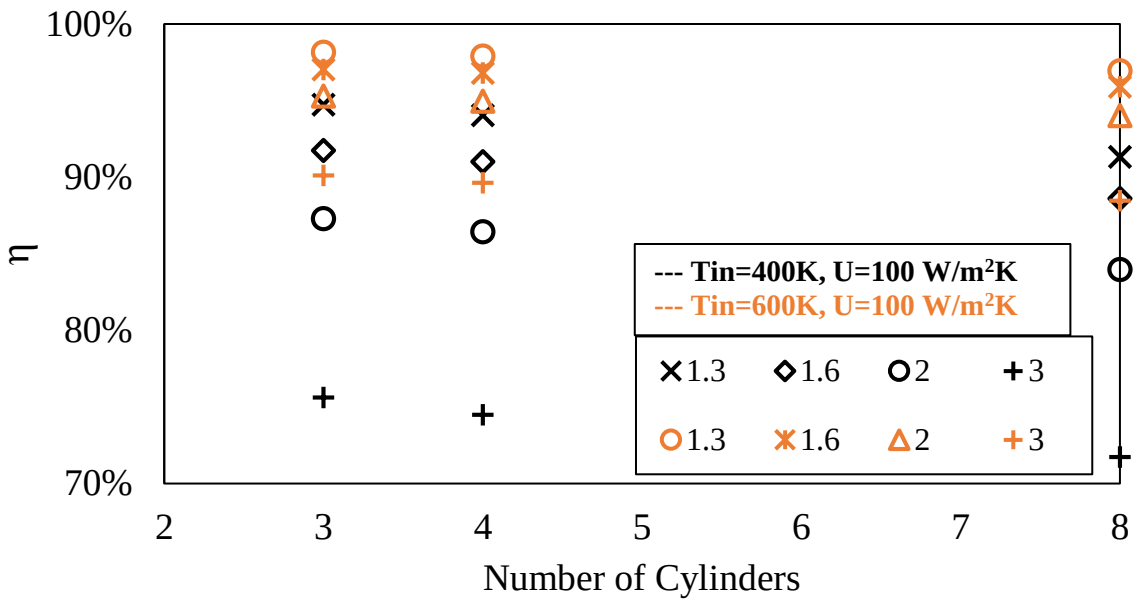

Figure 5. 7 Energy efficiency for the case *Re* = 500 with varying number of cylinders for all four pitch ratios.

5.2.3 Heat leakage

As previously mentioned, most analyses of this type assume an adiabatic or well insulated system. However, it is not easy to find systems free of heat leakage, as heat leakage always happens from systems to the environment or vice versa. In this study, an artificial heat leakage was applied to the given domains and the amount of the heat leakage was calculated using equation (4.22). Moreover, three different amounts of heat leakage were selected corresponding to three different heat transfer coefficients; 10, 50, and 100 W/m^{2}K, and all these heat leakage values were applied to the all pitch ratios, Reynolds numbers, and inlet temperatures. Results from these simulations can then be compared to the adiabatic cases.

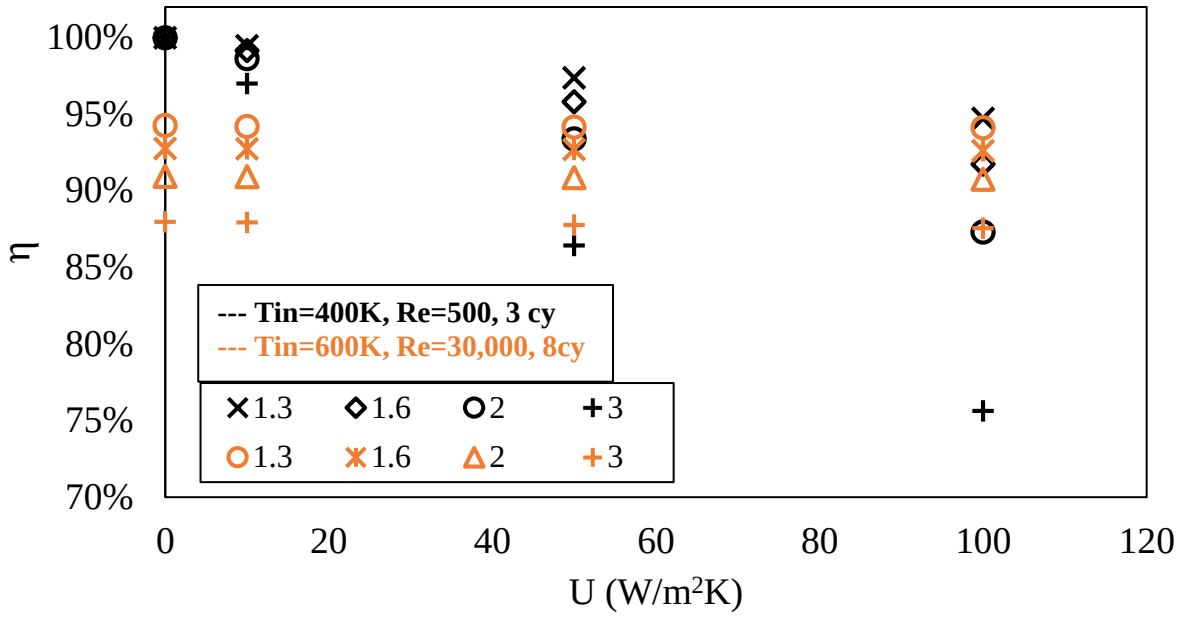

Figure 5. 8 Energy efficiency for varying heat transfer coefficients for all four pitch ratios

Figure 5.8 compares the variation in energy efficiency with heat leakage, inlet temperature, and pitch ratio. Not surprisingly, it is evident from the graph that the efficiency always decreases with increasing values of the heat transfer coefficient, whereas while the heat transfer from HTF to the cylinders and viscous dissipation remains the same, the heat leakage increases. Hence, this leads to overall decreased energy efficiency. Furthermore, the decreasing energy efficiency is more obvious for the Reynolds number of 500, since heat leakage has a considerable effect on this low Reynolds number value. Table 5.3 indicates the energy alterations for a domain with eight cylinders and a Reynolds numbers of 500 and 30,000. Even though the decrease in the efficiency in the Re = 30,000 case is not as obvious as that for the Re = 500 case, a small decrease is observed for this case as well. The main reason behind this small change is the low effect of heat leakage, since the HTF's velocity is considerably high for high Reynolds number cases and the effect of convective heat transfer and viscous dissipation are quite higher than the heat leakage effect for these cases.

Table 5.3 Effect of heat transfer, heat loss, and viscous dissipation on energy efficiency in terms of the heat transfer coefficient

		Inlet Temperature					
		T_{in} = 400 K(3 cy, *Re* = 500)			T_{in} = 600 K (8 cy, *Re* = 30,000)		
		Percentage effect on energy efficiency					
Pitch ratio	Heat transfer coefficient(W/m^2K)	HT	VD	HL	HT	VD	HL
1.3 × 1.3	0	100.00%	0.00%	0.00%	94.26%	5.74%	0.00%
1.3 × 1.3	10	99.47%	0.00%	0.52%	94.20%	5.79%	0.01%
1.3 × 1.3	50	97.37%	0.00%	2.63%	94.16%	5.79%	0.05%
1.3 × 1.3	100	94.73%	0.00%	5.27%	94.12%	5.79%	0.09%
1.6 × 1.6	0	100.00%	0.00%	0.00%	92.76%	7.24%	0.00%
1.6 × 1.6	10	99.15%	0.00%	0.85%	92.74%	7.24%	0.01%
1.6 × 1.6	50	95.80%	0.00%	4.19%	92.69%	7.24%	0.07%
1.6 × 1.6	100	91.74%	0.00%	8.26%	92.62%	7.24%	0.14%
2.0 × 2.0	0	100.00%	0.00%	0.00%	90.95%	9.05%	0.00%
2.0 × 2.0	10	98.63%	0.00%	1.37%	90.93%	9.05%	0.02%
2.0 × 2.0	50	93.38%	0.00%	6.61%	90.85%	9.04%	0.11%
2.0 × 2.0	100	87.30%	0.00%	12.69%	90.75%	9.03%	0.22%
3.0 × 3.0	0	99.99%	0.01%	0.00%	87.97%	12.03%	0.00%
3.0 × 3.0	10	97.01%	0.01%	2.99%	87.93%	12.03%	0.05%
3.0 × 3.0	50	86.43%	0.00%	13.57%	87.76%	12.01%	0.23%
3.0 × 3.0	100	75.62%	0.00%	24.37%	87.56%	11.98%	0.46%

5.2.4 Pitch ratio

In this section, the energy efficiencies with varying pitch ratios for different inlet temperatures and Reynolds numbers are compared. Before discussing the changes in energy, the viscous heating will be discussed in a detailed manner.

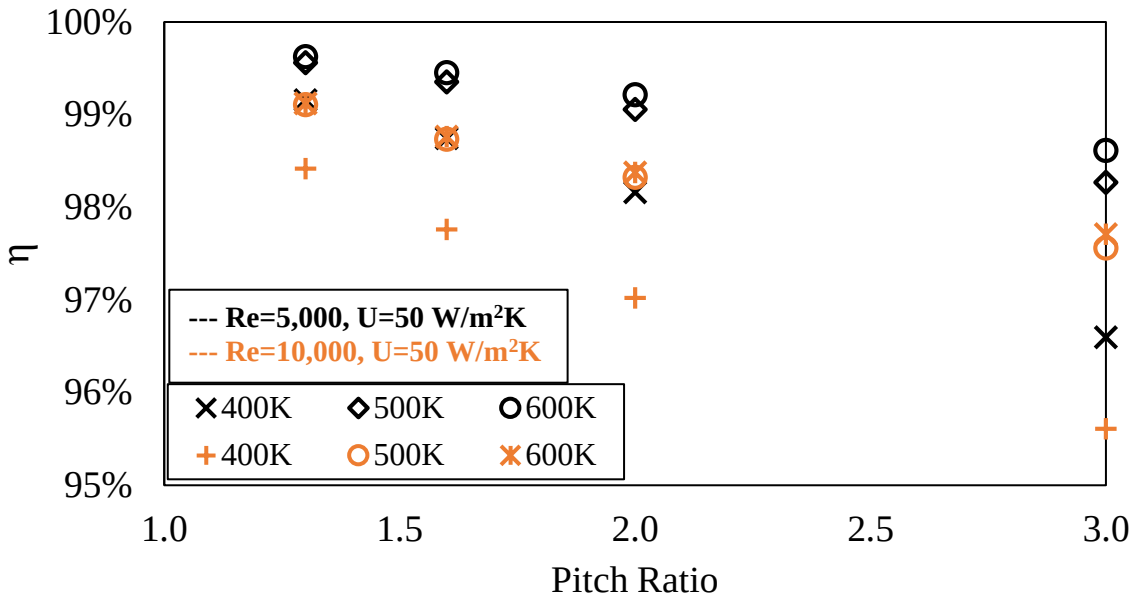

Figure 5. 9 Energy efficiency for cases with varying pitch ratio for all three inlet temperatures for the four cylinder case

As mentioned earlier, viscous heating or viscous dissipation is caused due to shear stress in the fluid domain. The velocity differences in a fluid lead to heat generation, since friction acts between adjacent molecules traveling at different velocities. Nevertheless, heat generation is not possible without energy transfer across system boundaries, according to the first law of thermodynamics. This is the reason for pressure decrease along any pipe or duct flow. In order to conserve the total energy, the pressure energy must be converted into heat energy with viscous dissipation. Furthermore, for fluids with greater velocity generally have greater viscous dissipation. It should also be noted that the viscous heating also depends on the fluid domain's geometry, as depicted in Table 5.4. However, it is evident from Figures 5.9 and 5.11 that viscous heating depends more on the fluid's velocity than the tube geometry (pitch ratio). This is the main reason why the fluid domains with the highest flow rates, namely the domains with a pitch ratio of 3.0, achieve the most viscous dissipation and hence the lowest energy efficiencies. Again, this can be explained with the viscous dissipation equation, which is the product of

volumetric flow rate and pressure gradient between the inlet and outlet of tube banks. Although the pressure difference is higher for small pitch ratios, viscous dissipation was less due to lower volumetric flow rate.

Table 5.4 Effect of heat transfer, heat loss, and viscous dissipation on energy efficiency in terms of the pitch ratio (T_{in} =600K, 8 cylinders, Re = 30,000, U = 10 W/m^{2}K)

Pitch ratio	HT	VD	HL
1.3 × 1.3	94.20%	5.79%	0.01%
1.6 × 1.6	92.74%	7.24%	0.01%
2.0 × 2.0	90.93%	9.05%	0.02%
3.0 × 3.0	87.93%	12.03%	0.05%

Lastly, Figure 5.10 illustrates the energy efficiency for a laminar flow with a Reynolds number of 500. It is apparent from the figure that the energy efficiencies for different pitch ratios were extremely close; thus, it can be said that viscous heating does not have a considerable effect on cases with low-speed velocity. However, when the velocity increased to 5,000, the viscous heating had a significant effect on the energy efficiency, as depicted in Figure 5.11.

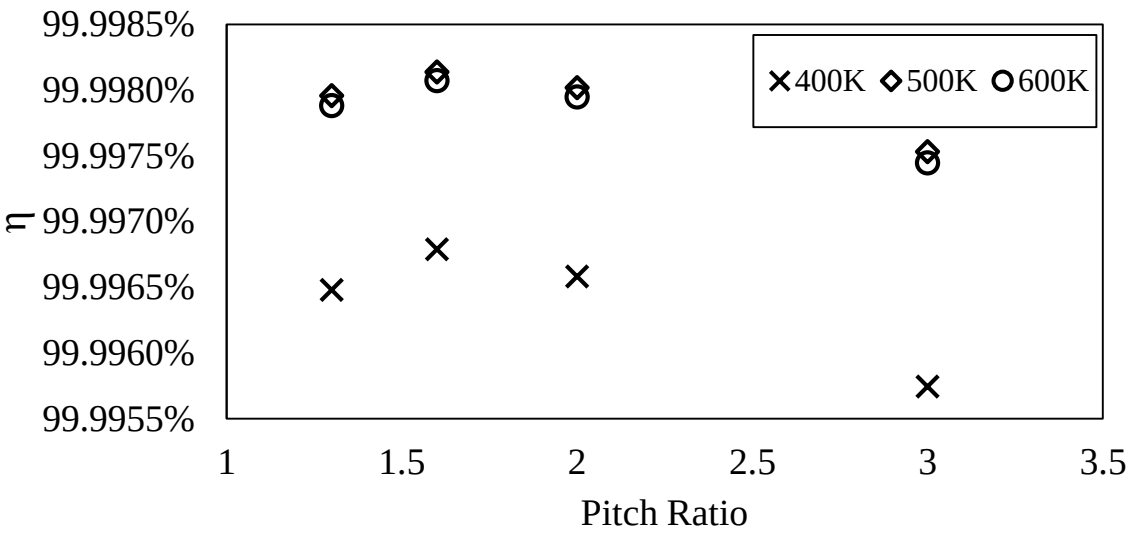

Figure 5. 10 Energy efficiency for cases with varying pitch ratios for all three inlet temperatures at *Re*=500 and eight cylinder case (adiabatic).

Consequently, it can be stated that the energy efficiency decreases with increasing pitch ratio, except for a few cases.

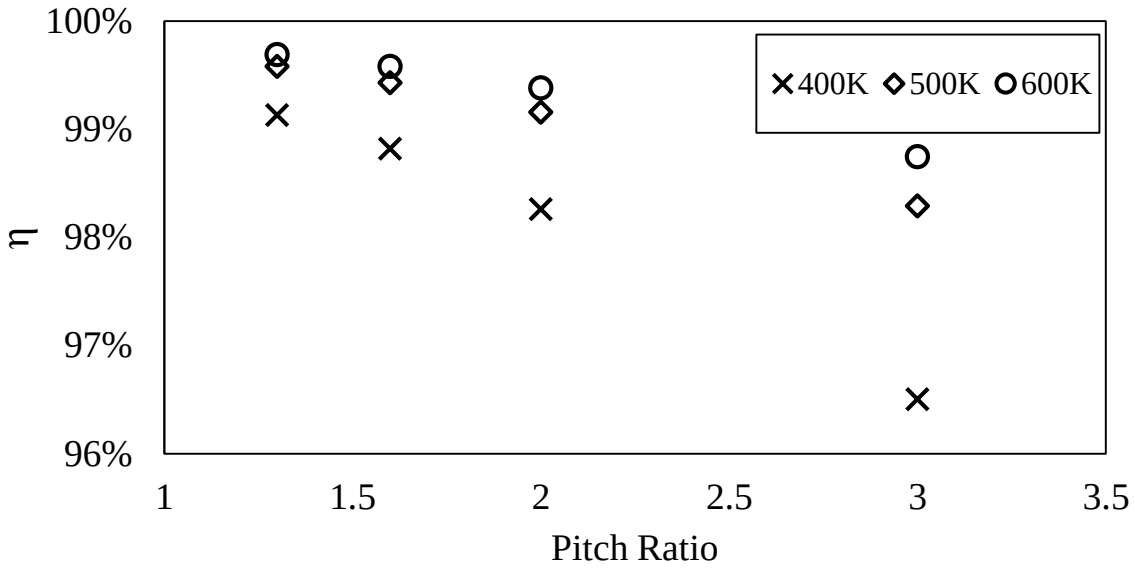

Figure 5. 11 Energy efficiency for cases with varying pitch ratio for all three inlet temperatures at *Re* = 5,000 and the eight cylinder case (adiabatic).

5.2.5 Inlet temperature

According to Newton's Law of Cooling, the rate of heat transfer between an object and a convective flow shares a positive relation with the temperature difference between the cylinder's surface and flow. Therefore, it can be said that more heat transfer occurred from the fluids to the cylinders when the inlet temperature of the fluid was increased in the case with a constant tube surface temperature.

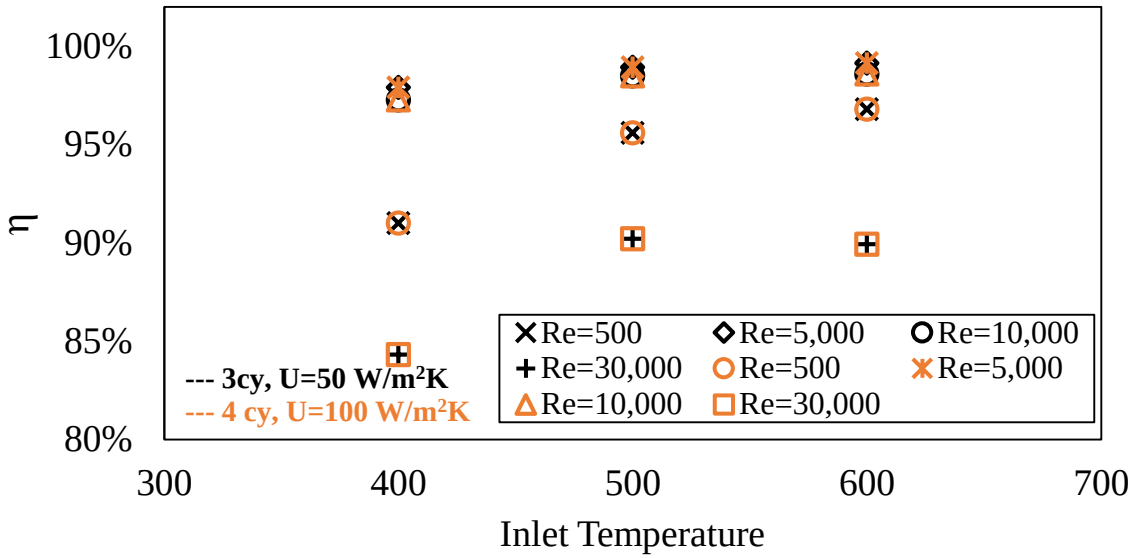

Figure 5. 12 Energy efficiency for cases with varying inlet temperatures for all four Reynolds number with a pitch ratio of 1.6

Figure 5.12 compares the energy efficiencies of domains with a pitch ratio of 1.6 for different Reynolds numbers, number of cylinders, and heat transfer coefficients. From the graph, it is evident that energy efficiency increases with increasing inlet temperature, since the heat transfer rate increases and exerts the highest effect on efficiency. This trend is valid for each case, except adiabatic systems, and the cases with a Reynolds number of 30,000. This is why different number of cylinders and heat transfer coefficient cases were illustrated in this graph. Although the heat leakage and viscous dissipation also increase with increasing inlet temperature, since the fluid's velocity increases due to the Reynolds number, the increasing ratio of the convective heat transfer is considerably more than the total increasing ratio of the viscous dissipation and heat leakage.

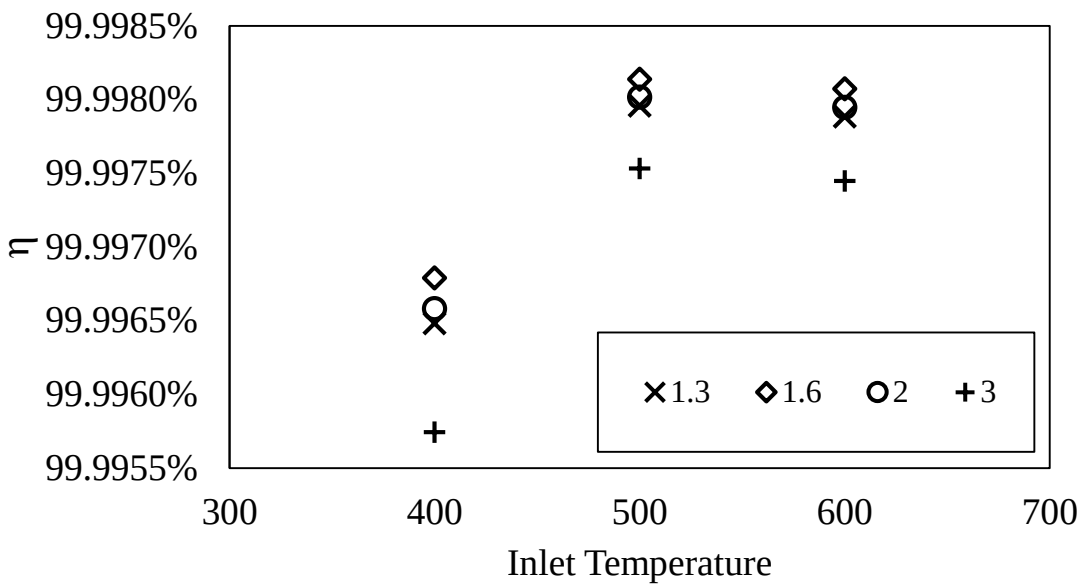

Figure 5. 13 Energy efficiency for cases with varying inlet temperatures for all four pitch ratios at *Re* = 500 and eight cylinder case (adiabatic).

Conversely, an important consideration must be made for adiabatic systems. As can be observed from figures 5.13 and 5.14, the highest energy efficiencies were obtained at 500 K in each case. The primary reason for this is that the changes in velocity and HTF's properties depend on the mean temperature of tube bundles' inlets and outlets. In adiabatic systems, the effect of the viscous dissipation on efficiency is higher in cases with 500 K compared to the other two inlet temperature cases.

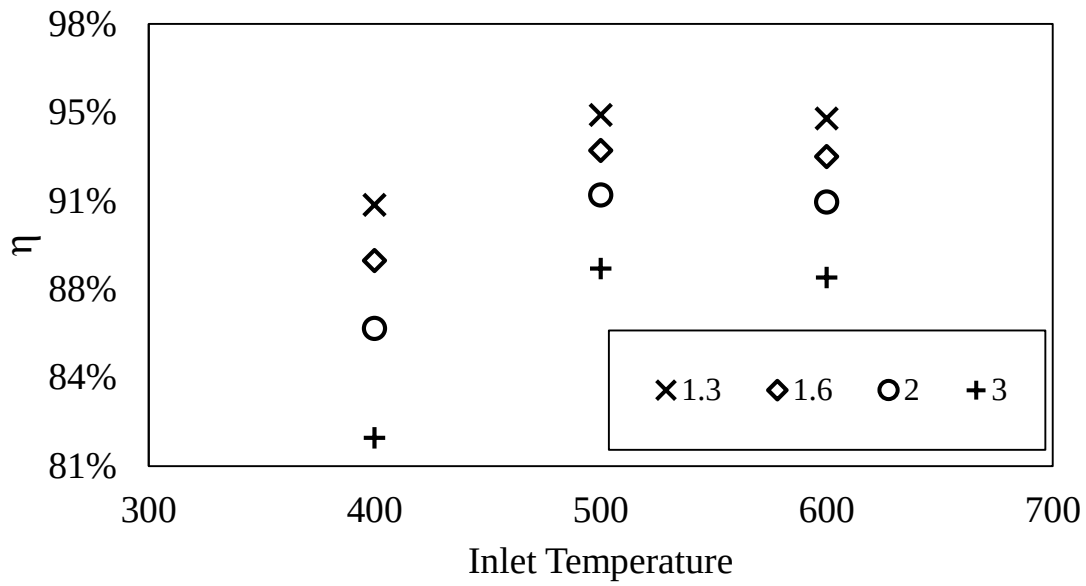

Figure 5. 14 Energy efficiency for varying inlet temperature cases for all four pitch ratios at *Re* = 30,000 and eight cylinder case (adiabatic).

It is also interesting to note that the highest efficiency was obtained at 500 K for each pitch ratio case until the Reynolds number reached 10,000 and the heat transfer coefficient was 10 W/m^{2}K. From Figures 5.15 and 5.16, it is clear that when the heat transfer coefficient, that is, the heat leakage, is increased to 50 W/m^{2}K, the highest efficiencies are obtained at 600 K (Figure 5.16). As expected, the convective heat transfer rate decreases with increasing heat leakage, causing lower energy efficiency. Therefore, the effect of convective heat transfer rate increases with increasing inlet temperature for higher values of heat leakage (heat transfer coefficient).

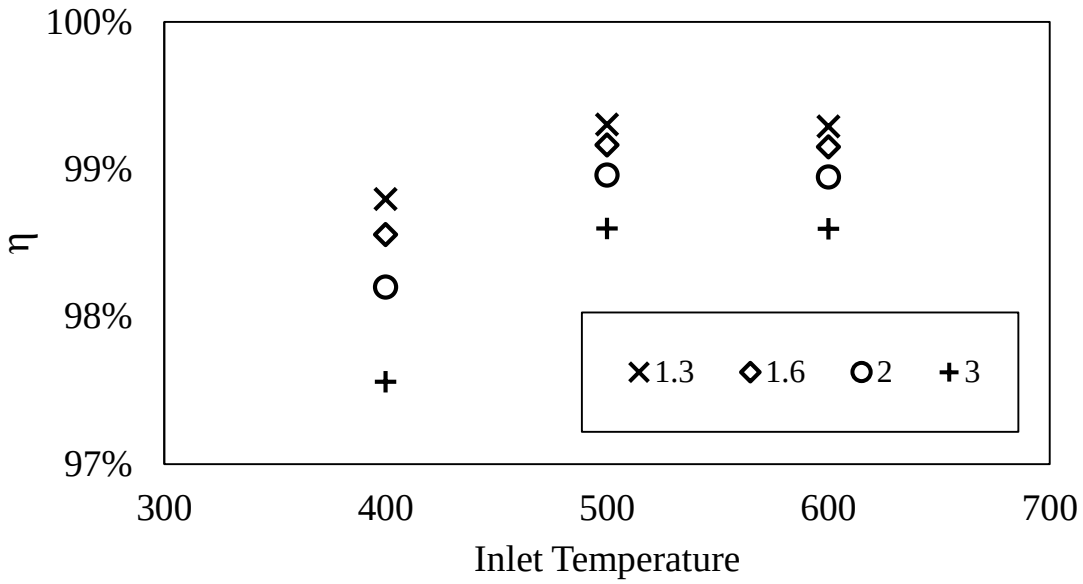

Figure 5. 15 Energy efficiency for cases with varying inlet temperatures for all four pitch ratios at *Re* = 10,000 and eight cylinders, U = 10 W/m^{2}K

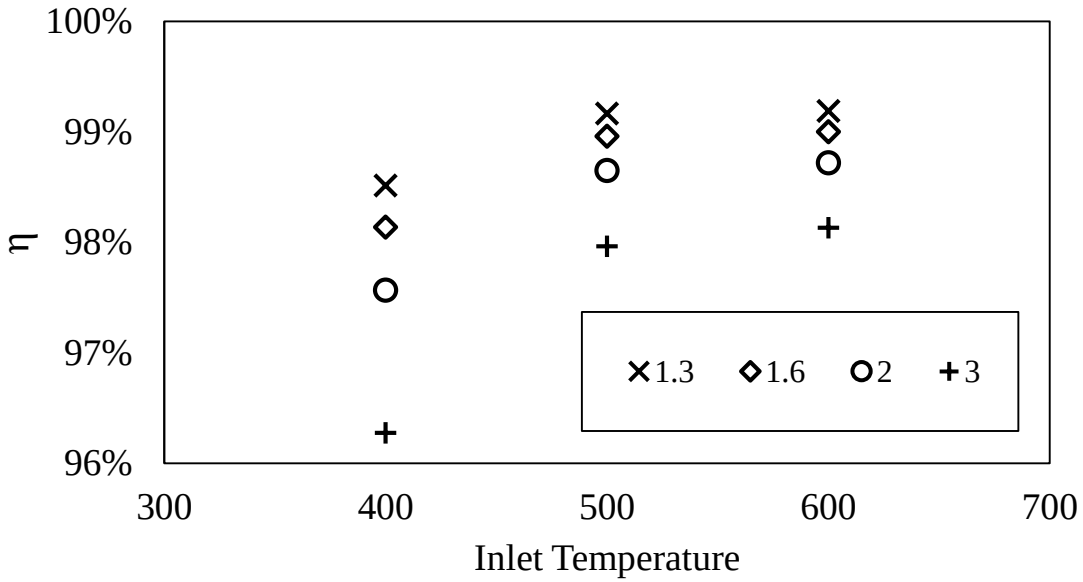

Figure 5. 16 Energy efficiency for cases with varying inlet temperatures for all four pitch ratios at *Re* = 10,000 and eight cylinders, U = 50 W/m^{2}K

5.3 Exergy Efficiency

In this section, the exergy analysis will be conducted using equations (4.25)–(4.36). Exergy analyses can be more beneficial than energy analyses, since they assess both the quantity and usefulness of energy. Dincer and Rosen (2013) defined exergy as a measure of energy's

usefulness or quality. Since exergy quantifies the locations, types, and magnitudes of wastes and losses, it can be useful in enhancing the efficiency of energy resources' utilization. Moreover, it presents a measure of a system's potential to cause change, as a result of not being in complete equilibrium in relation to a reference environment. Therefore, the reference environment (state) must be introduced completely. It is also interesting to note that exergy is not conserved like energy. It is consumed or destroyed due to the irreversibility of any system.

The exergy efficiencies in this study ranged from 26%–70% and, in general were, considerably lower than the corresponding energy efficiencies. This disparity is a direct result of exergy destruction, caused due to real processes' irreversibilities (MacPhee et al., 2012); it is calculated according to equations (4.30)–(4.35). In most cases, entropy generation due to viscous dissipation was not significant; however, it does form a crucial parameter for those systems, especially for those with high Reynolds numbers. It should be noted that the highest and lowest exergy efficiencies were obtained in cases with the Reynolds number 500. While the highest one was found in a case with a 400 K inlet temperature and no heat leakage, the lowest was obtained in 600 K with a heat transfer coefficient of 100 W/m^2K.

Again, the effects of the mass flow rate (Reynolds number), pitch ratio, number of cylinders, heat leakage, and inlet temperature of the HTF on exergy efficiency will be addressed in this section. Although there is large amount of data and simulations, only significant trends will be discussed. For further information regarding all cases with exergy efficiency, Appendix C can be examined.

5.3.1 Reynolds number

Figures 5.17–5.19 illustrate the exergy efficiencies varying with the Reynolds number for different pitch ratios, heat leakage, and inlet temperatures. It is evident from the figures that

exergy efficiency decreases with increasing Reynolds number for all adiabatic cases, as was the case for energy efficiency.

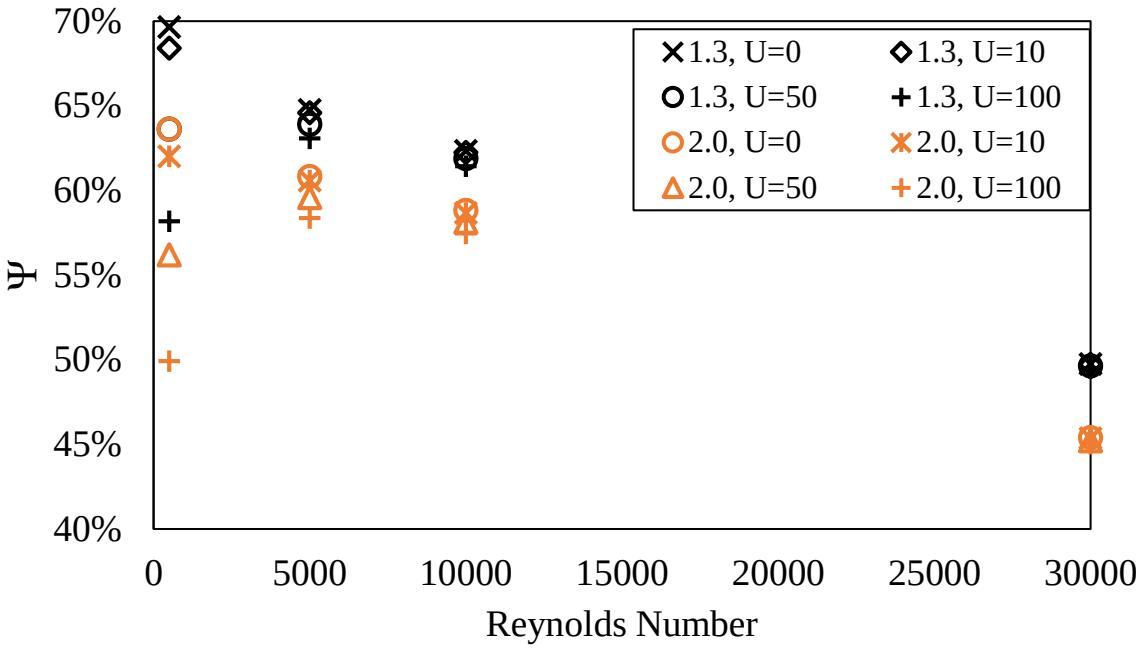

Figure 5. 17 Exergy efficiency for the case T_{in} = 400 K, with eight cylinders, pitch ratio of 1.3 and 2.0 for different heat leakages

It should be observed that the effect of exergy destruction on exergy efficiency is considerably higher than the viscous effect on energy efficiency. The primary reason behind this is the high effect of exergy destruction sources. As briefly explained in section 4.3.2, the exergy destruction is caused due to entropy generation, which is a direct result of viscous dissipation and heat transfer. As can be observed in Table 5.5, the exergy destruction ratio increases with increasing Reynolds number, since viscous dissipation also increases with the mass flow rate. For instance, the proportion of exergy destruction in relation to exergy efficiency is nearly 54% in the 400 K cases, with a Reynolds number of 30,000, due to high viscous dissipation. In the following section, the effect of entropy generation due to heat transfer and entropy generation due to viscous dissipation will be compared.

Table 5.5 Effect of heat transfer, heat loss, and exergy destruction on exergy efficiency (T_{in} = 400 K, 8 cylinders)

		Heat leakage											
		U = 0			U = 10 W/m^{2}K			U =50 W/m^{2}K			U = 100 W/m^{2}K		
		Percentage effect on exergy efficiency											
Pitch ratio	Reynolds number	HT	E,D	HL	HT	E,D	HL	HT	E,D	HL	HT	E,D	HL
1.30	500	70%	30%	0%	68%	30%	2%	64%	28%	8%	58%	26%	16%
1.30	5,000	65%	35%	0%	65%	35%	0%	64%	35%	1%	63%	34%	3%
1.30	10,000	62%	38%	0%	62%	38%	0%	62%	37%	1%	61%	37%	1%
1.30	30,000	50%	50%	0%	50%	50%	0%	50%	50%	0%	50%	50%	0%
2.00	500	64%	36%	0%	62%	36%	2%	56%	32%	11%	50%	29%	21%
2.00	5,000	61%	39%	0%	61%	39%	0%	60%	38%	2%	58%	38%	4%
2.00	10,000	59%	41%	0%	59%	41%	0%	58%	41%	1%	57%	40%	2%
2.00	30,000	45%	55%	0%	45%	55%	0%	45%	54%	0%	45%	54%	1%

Figure 5.18 and 5.19 compare the exergy efficiencies for the 500 K and 600 K cases. While the highest exergy efficiencies were obtained for the lowest Reynolds number (Re=500), in adiabatic systems, it was obtained at Re=5,000 when U=50 W/m^{2}K, and a 500 K inlet temperature. The main reason behind this phenomenon is similar to that discussed earlier resulting from decreasing Reynolds number. A similar phenomenon can be clearly observed in Figure 5.19 for the 600 K case. In this case, however, while most of the highest exergy efficiencies were obtained at Re=500, when the heat transfer coefficient was selected as 100 W/m^{2}K, the highest exergy efficiencies were obtained at Re=5,000 for the cases with pitch ratio greater than 2.0. Another important point here is that the exergy efficiency decreases with increasing inlet temperature, the comparison having been presented in Figures 5.17 and 5.18. Further details about the inlet temperature effect are discussed in section 5.3.5.

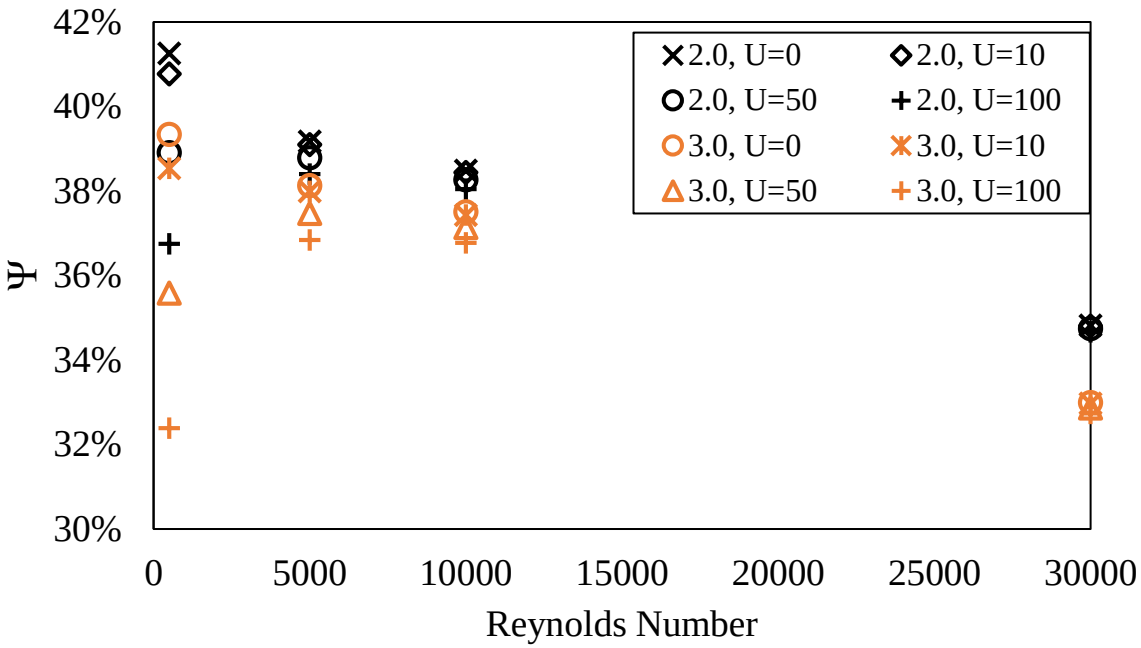

Figure 5. 18 Exergy efficiency for the case T_{in} = 500 K, eight Cylinders, pitch ratio of 1.3 and 2.0 for different heat leakages

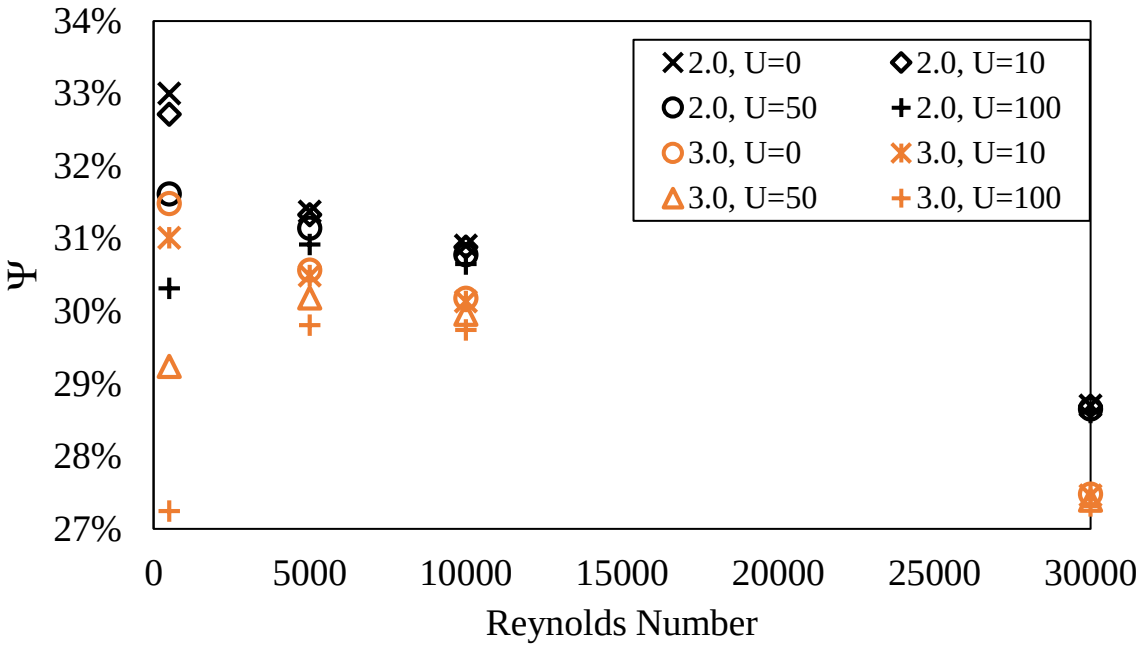

Figure 5. 19 Exergy efficiency for the case T_{in} = 600 K, eight cylinders, pitch ratio of 1.3 and 2.0 for different heat leakages

5.3.2 Number of cylinders

Figure 5.20 compares the exergy efficiency of an adiabatic system with an inlet temperature of 400 K and a Reynolds number of 500 for all three numbers of in-line cylinders. The graph clearly demonstrates that the exergy efficiency increases with the number of cylinders, since the heat transfer also rises with an increase in the number of cylinders, as expected.

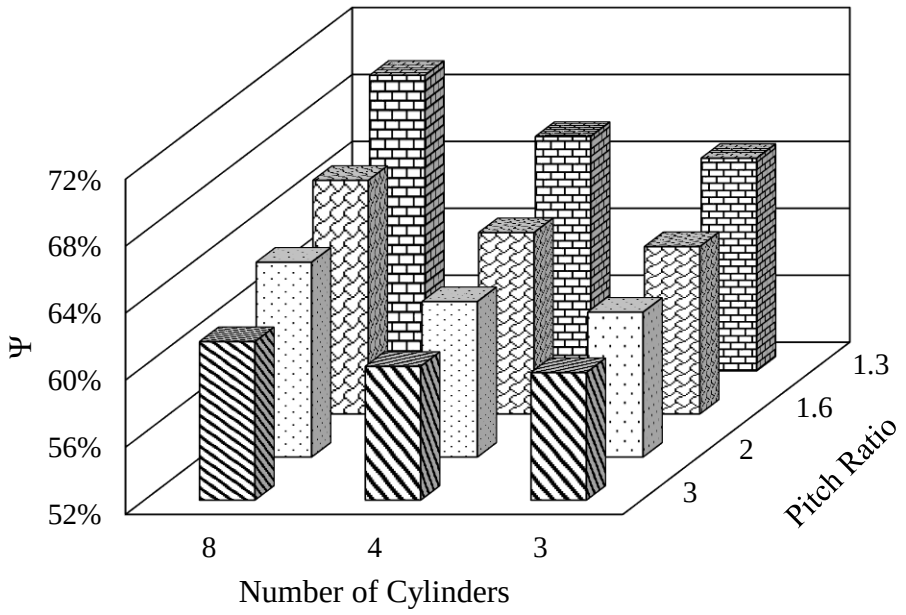

Figure 5. 20 Exergy efficiency for the case of *Re* = 500 varying number of cylinders for all four pitch ratios (T_{in} = 400 K, U = 0 W/m^{2}K)

Again, this argument can be proven by examining the exergy change between the computational domain's inlet and outlet. As it was stated in equation (4.36), exergy efficiency represents the proportion of exergy generation due to the heat transfer to the exergy flow difference between the fluid domain's inlet and outlet. Considering equation (4.29), the exergy flow difference is higher in cases with a lower temperature difference between the inlet and outlet. Not surprisingly, a higher number of in-line cylinders induces a lower outlet temperature, as greater heat transfer happens from the HTF to the cylinders. However, the effect of convection

heat transfer is higher than exergy destruction. Therefore, a higher number of in-line cylinder results in higher exergy efficiencies.

Table 5.6 presents the ratio of entropy generation due to viscous dissipation to the total entropy generation. It is evident in this case that the ratio increases with increasing Reynolds number. It is surprising that even though the pressure difference is lower for the three in-line tubes, the entropy generation ratio due to viscous dissipation is the highest due to the low heat transfer effect in total entropy generation. Increasing the number of cylinders in a domain results in increased convective heat transfer, leading to higher entropy generation; however, the viscous dissipation effect on the total entropy generation decreases with increasing number of cylinders.

Table 5.6 The ratio of entropy generation due to viscous dissipation to the total entropy generation (T_{in} = 400 K, U = 0 W/m^{2}K)

Number of cylinders	Pitch ratio	Reynolds number			
		$S_{gen,diss}/S_{gen,Total}$			
		500	5,000	10,000	30,000
8	1.3 × 1.3	0.040%	2.42%	7.32%	23.29%
	1.6 × 1.6	0.028%	2.17%	7.04%	23.58%
	2.0 × 2.0	0.024%	2.28%	7.56%	24.68%
	3.0 × 3.0	0.028%	2.83%	9.40%	27.60%
4	1.3 × 1.3	0.026%	1.99%	6.61%	23.14%
	1.6 × 1.6	0.022%	2.10%	7.14%	24.29%
	2.0 × 2.0	0.022%	2.36%	8.18%	26.64%
	3.0 × 3.0	0.028%	3.11%	10.41%	29.68%
3	1.3 × 1.3	0.023%	1.99%	6.78%	23.61%
	1.6 × 1.6	0.022%	2.20%	7.51%	25.07%
	2.0 × 2.0	0.022%	2.51%	8.74%	27.66%
	3.0 × 3.0	0.028%	3.28%	10.98%	30.47%

Although all cases showed similar trends in terms of the number of cylinders, another case with 600 K with a heat transfer coefficient of 100 W/m^{2}K has been illustrated in Figure 5.21

to consolidate this finding for the readers. Exergy efficiency for these case varied from 27%–31%.

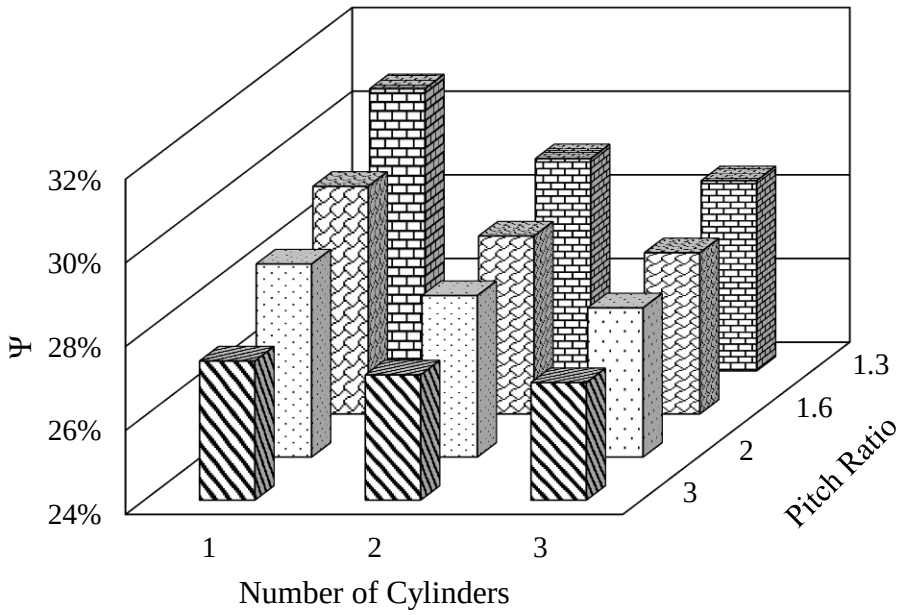

Figure 5. 21 Exergy efficiency for the case with *Re* = 30,000 and varying number of cylinders for all four pitch ratios (T_{in} =600 K, U = 100 W/m^{2}K).

5.3.3 Heat leakage

This section investigates the effect of heat leakage on exergy efficiency. As anticipated, a reverse ratio between heat leakage and exergy efficiency was found, as was the case with energy efficiency. As previously mentioned in section 4.3.3, the heat leakage effects are more obvious for cases with low Reynolds numbers, since heat leakage dominates the heat transfer from HTF to the cylinders as well as viscous dissipation. In order to indicate this, Figure 5.22 was selected as the case with the lowest Reynolds number, 500. As depicted by this graph, the exergy efficiency can be increased to nearly 20% using a well-insulated (adiabatic) system.

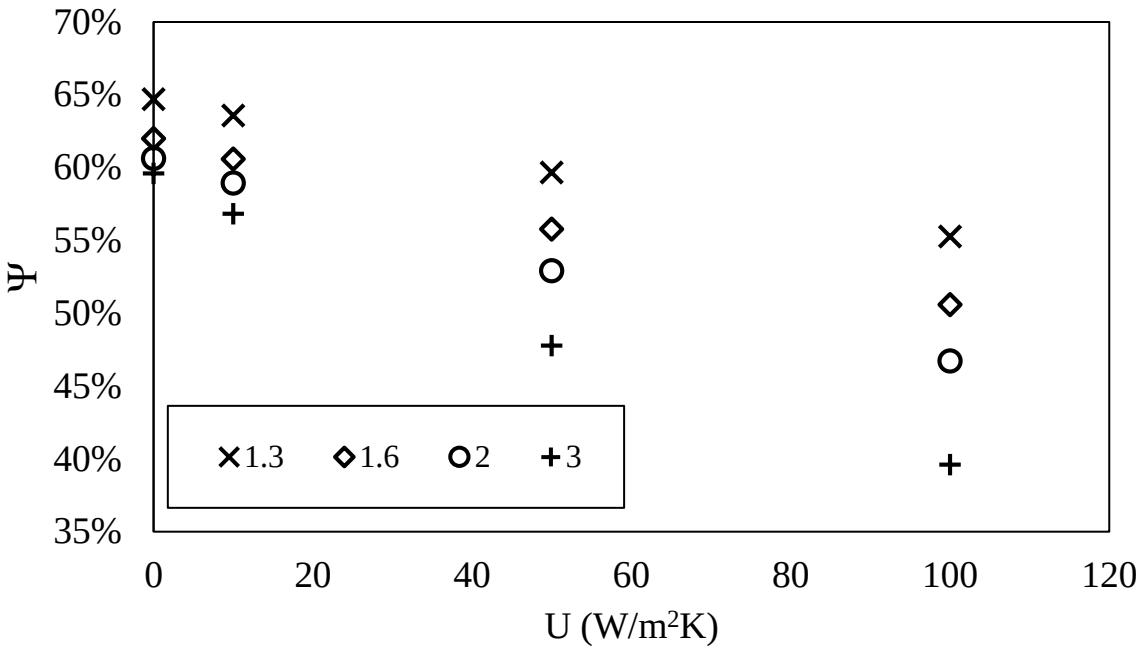

Figure 5. 22 Exergy efficiency for cases with varying heat transfer coefficient for all four pitch ratios (T_{in} = 400K, three cylinders).

Figure 5.23 demonstrates the effect of heat leakage in exergy efficiency. Undoubtedly, the heat leakage effect increases with increasing pitch ratio, since the surface area of the domain is higher for higher pitch ratios. Another important aspect here is the extent of the heat leakage effect. In the case of three cylinders, a pitch ratio of 3.0, and a heat transfer coefficient of 100 W/m^2K, it was nearly 35%, which represents an extremely high loss value for this type of system. This is why the system's insulation plays a significant role in their efficiencies.

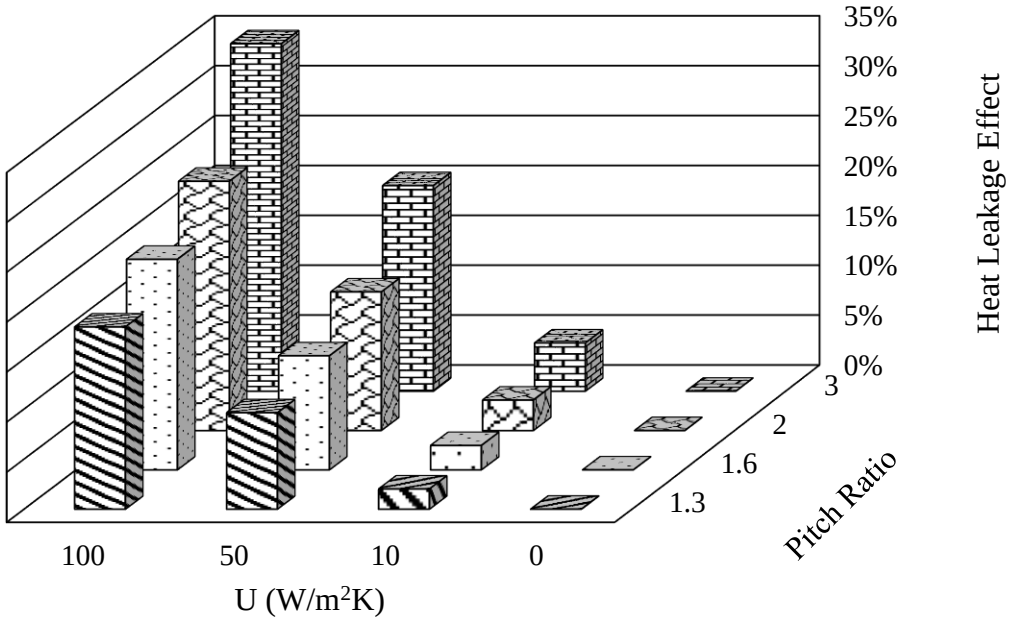

Figure 5. 23 Heat leakage effect on exergy efficiency for cases with varying heat transfer coefficient for all four pitch ratios (T_{in} = 400 K, three cylinders).

5.3.4 Pitch ratio

Figure 5.24 illustrates the exergy efficiency with a varying pitch ratio in terms of inlet temperature and heat leakage. Surprisingly, the lowest pitch ratios attained the highest exergy efficiencies, due to the high effect of heat leakage and destructed exergy on the efficiency calculation.

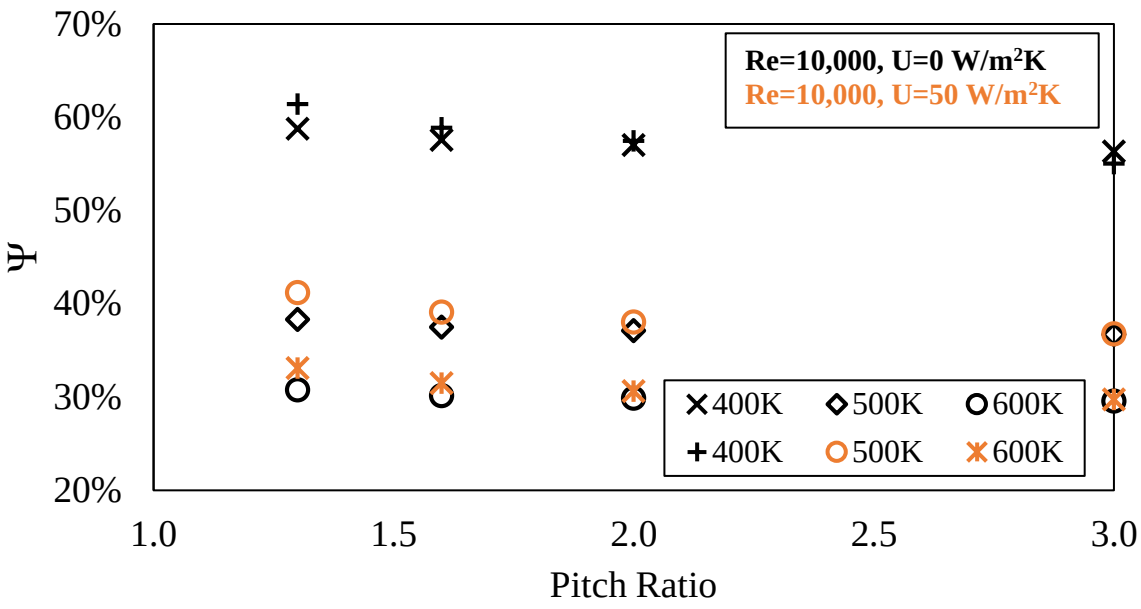

Figure 5. 24 Energy efficiency for cases with varying pitch ratios for all three inlet temperatures for the case with eight cylinders.

Analyzing the heat leakage effects on the system, it is apparent that increasing the dimensionless pitch ratio causes an increase in heat leakage, leading to greater entropy generation and hence lower exergy efficiency. Furthermore, the heat leakage effect in exergy analysis becomes more severe than that witnessed in the case of energy, as demonstrated by Figure 5.25. While the heat leakage effect was nearly 6% in energy efficiency for the lowest pitch ratio, it was more than 18% in the case of exergy efficiency, since the exergy calculation also depends on the dead-state temperature.

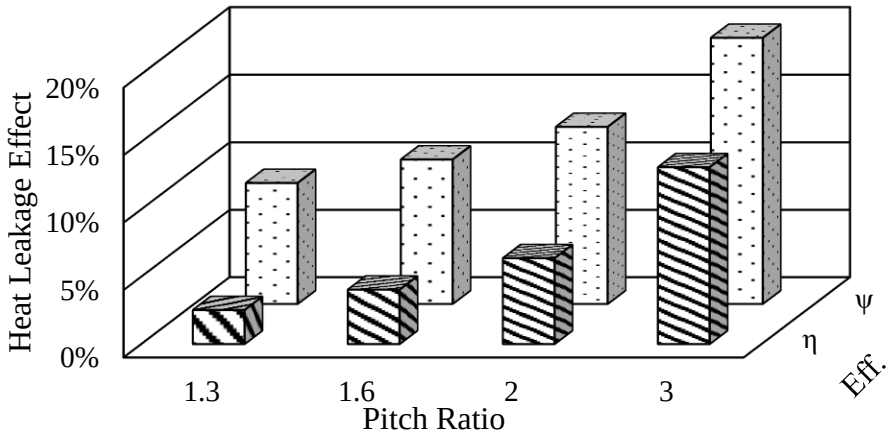

Figure 5. 25 Effect of heat leakage in energy and exergy efficiencies (T_{in} = 500 K, U = 100 W/m^{2}K, three cylinders).

As discussed in section 5.2.4, the Reynolds number remained constant in all cases, and it mainly depends on the maximum velocity in the fluid flow. The uniform inlet velocity was calculated according to equation (4.6), which depends on the transverse pitch ratio and the tubes' diameter. Therefore, the inlet velocity of the HTF is different for each inlet temperature case due to the different thermophysical properties in accordance to the inlet temperature and pitch ratio. Hence, it can be easily concluded that viscous dissipation is always higher for higher pitch ratios due to high inlet velocity. In Figure 5.26, the ratio of entropy generation due to viscous dissipation to the total entropy generation has been illustrated. It is evident that the effect of entropy generation due to viscous dissipation always increases with the pitch ratio. Furthermore, it decreases with increasing inlet temperature, since entropy generation due to heat transfer from HTF to the cylinder is considerably higher than the entropy generation due to viscous dissipation. This result is not surprising because entropy generation due to heat transfer, as represented in equation (4.33), mainly depends on the temperature gradients between the domain's inlet and outlet, and it increases with the HTF's rising inlet temperatures.

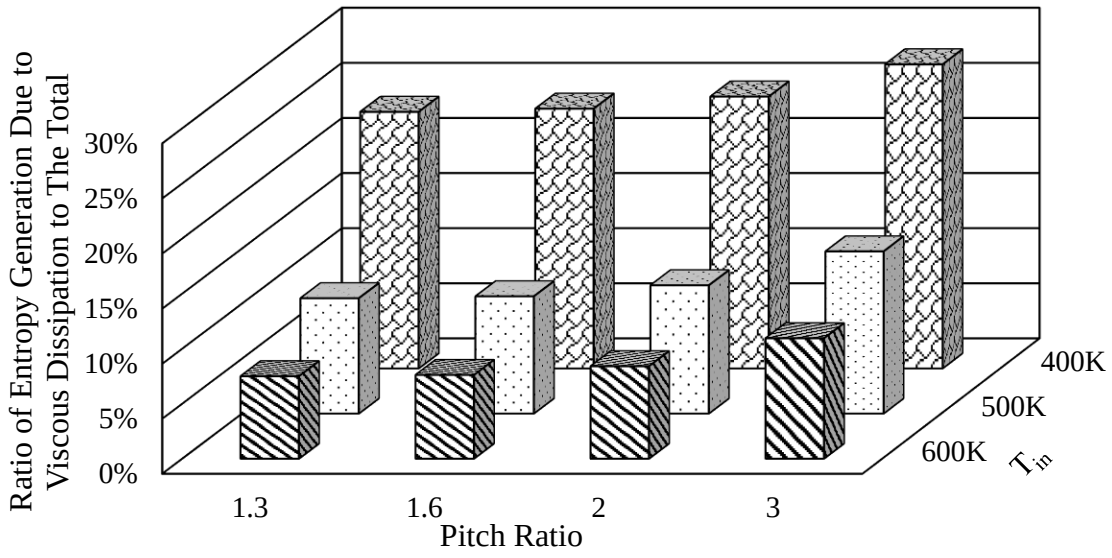

Figure 5. 26 Effect of entropy generation due to viscous heating on total entropy generation

Consequently, there is an inverse relationship between the exergy efficiency and dimensionless pitch ratio, as was also the case with energy efficiency. The reason for this is the increase in the volumetric flow rate; in this case, the flow rate and associated viscous dissipation is more important here than it was in the energy analysis, even more than the pressure differential.

5.3.5 Inlet temperature

HTF's inlet temperature is the most significant factor in this study, since the HTF's thermophysical parameters, such as density, thermal conductivity, and dynamic viscosity, vary with the inlet temperature. Hence, the HTF's velocity field changes. As indicated by Figure 5.27, exergy efficiency decreases with increasing inlet temperature. As previously mentioned in section 5.3.4, although the exergy flow due to heat transfer increases with increasing inlet temperature, exergy production experiences a greater variation between the inlet and outlet of the domain due to the higher temperature gradients for higher temperatures.

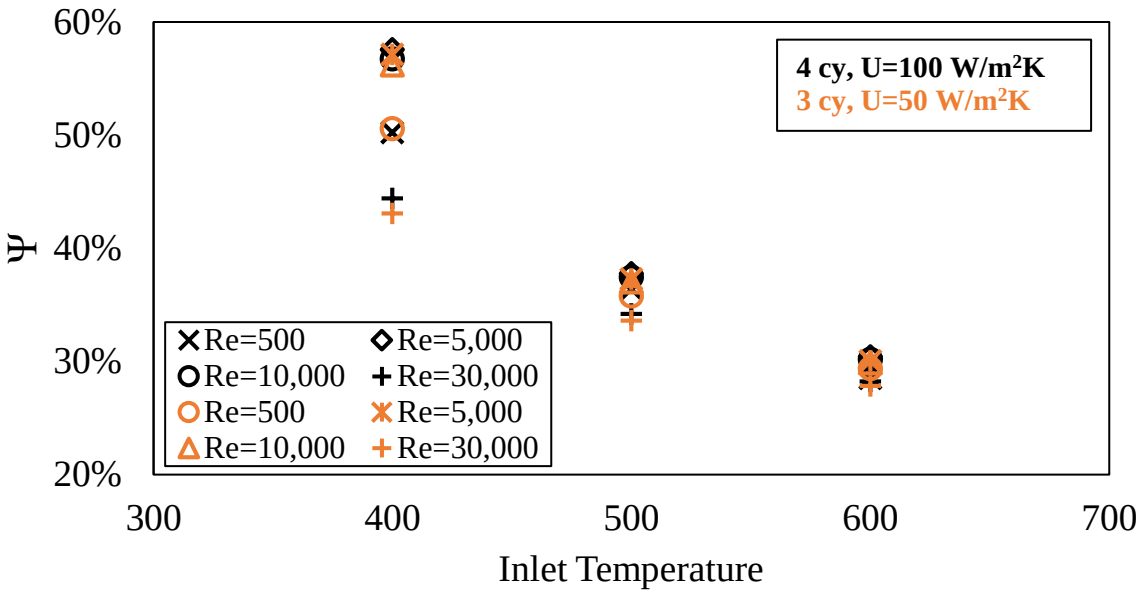

Figure 5. 27 Exergy efficiency for cases with varying inlet temperatures for all four Reynolds numbers with a pitch ratio of 1.6

It should be observed that while the exergy efficiency varies according to the pitch ratio, Reynolds number, heat leakage, and number of in-line cylinders, these effects are extremely low in comparison to the changes in HTF's inlet temperature. Figure 5.27 shows that the difference in the exergy efficiency between the 400 K and 600 K cases was nearly 27%. Furthermore, Figure 5.28 clearly demonstrates that while the exergy efficiency changed in the range 40%–70% for the 400 K case, it was considerably lower for the 500 K and 600 K cases, which witnessed an efficiency variation ranging from 30%–47% and 26%–38% respectively.

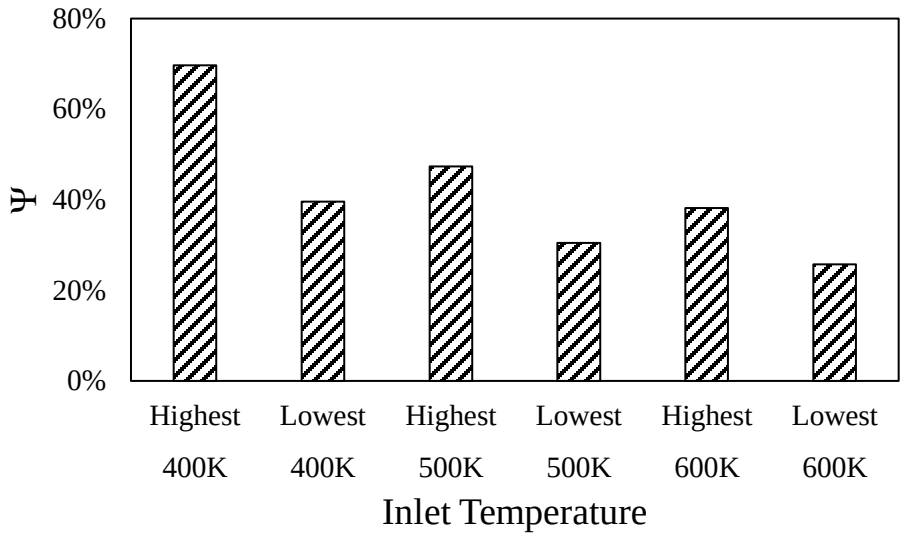

Figure 5. 28 Highest and lowest exergy efficiencies for different inlet HTF temperatures

The material in this chapter has been co-authored by Dr. David MacPhee, Assistant Professor of mechanical engineering at the University of Alabama, and is currently being prepared for publication.

6 CONCLUSIONS

In this study, both empirical and thermodynamic analyses were conducted for in-line tube banks. ANSYS Fluent 18.2 was used to create the geometry and solve the transient computational problem. Air was selected as the heat transfer fluid with an inlet temperature of 400 K, corresponding to the typical low-temperature waste heat temperatures. Furthermore, higher inlet temperatures, 500 K and 600 K, of HTF were studied to investigate the effect of inlet temperature on energy and exergy efficiencies. Furthermore, several simulations were conducted by varying the Reynolds number, pitch ratio, and number of cylinders. The Reynolds number was varied between 500 and 30,000, the pitch ratio between 1.3 and 3.0, and the number of tubes between three and eight. Artificial heat leakages also form an important factor in this analysis. Although most systems are assumed to be adiabatic, three different heat leakages with three different heat transfer coefficients of 10, 50, and 100 W/m^2K respectively were applied to all cases along with the adiabatic simulations. Most simulations were completed in 1.5–2 h of real time; in total, 576 simulations were conducted. Therefore, the total computational time taken by all simulations was more than 1,200 h. In order to validate these results, the Nusselt number and pressure drop values were compared with the experimental data and a good agreement was found. Grid independence and time-step independence studies were conducted to ensure the model's validity. The model, while transient in nature, produced steady results, and steady-state thermodynamic calculations were performed using time-averaged values, only subsequent to the achievement of steady simulation results.

Once all simulations were performed, all systems were investigated from a thermodynamic standpoint in order to gain a more realistic performance of each system. Thermodynamic analyses can offer meaningful insight into the overall performance, especially energy and exergy analysis, as the exergy analysis is directly concerned with irreversibilities.

Starting with energy efficiency, it was observed that the efficiencies varied from 72%–99% across all cases. In this study, the energy losses in the system took place as a result of heat leakage and the HTF's viscous heating. While no heat leakage was witnessed in some systems, the viscous dissipation effect was always considered in all systems. Viscous heating did not have a considerable effect on the cases with low Reynolds numbers, for which, it was less than 0.001% of the energy transferred via heat transfer to the tubes. However, it was significant for cases with high Reynolds number. In some cases, the proportion of the viscous dissipation exceeded 18% of the total energy. Furthermore, viscous heating is an important element in each case, even those with low Reynolds numbers, since it causes a pressure drop after the HTF passes the cylinders, and this pressure drop is related to the fluid power requirement of the system.

Since energy efficiency is directly related to viscous dissipation and heat leakage, the geometries with higher pitch ratios produced higher inlet velocities. While this higher velocity leads to higher convective heat transfer, the amount of viscous dissipation ratio was considerably higher than the heat transfer ratio. Furthermore, the amount of heat leakage increases with increasing pitch ratio, since it depends on the HTF's surface area. Thus, it was observed that, in terms of pitch ratio, the energy efficiency decreases with increasing dimensionless pitch ratio due to high viscous dissipation and heat leakage.

The Reynolds number was found to have a significant effect on energy efficiency, as it contributes to the amount of vicious dissipation. For higher values of Reynolds number, the pressure drops was considerably higher, and this caused an increase in viscous heating. In adiabatic systems, the energy efficiency decreases with increasing Reynolds number, since only viscous effect is considered as a loss in these systems. However, when a heat leakage happened from the systems to the environment, the highest efficiency was obtained for Re = 5,000 in most cases. Heat leakage is extremely important in this type of processes, and its effect increases with increasing pitch ratio and decreasing Reynolds number. In some cases, the effect of heat leakage in the efficiency was more than 28%, and it dominated the viscous dissipation for low values of Reynolds numbers. Thus, it is to be expected that an increase in the heat leakage amount will lead to a decrease in the energy efficiency.

The last two considerations are the effect of the number of in-line cylinders and the HTF's inlet temperature. A positive relation was observed between the number of cylinders and energy efficiency, since the convective heat transfer increases with cylinder numbers. Although greater pressure drop was experienced in such cases, and thus greater viscous dissipation, the increasing ratio of convective heat transfer was considerably higher than the viscous heating and heat loss. Conversely, the inlet temperature was found to have has a considerable effect on efficiency. Furthermore, it can be said that it exerts the highest effect among all parameters. Again, a positive relation was determined between the inlet temperature and efficiency. Hence, the highest inlet temperature cases produced the highest energy efficiency. However, it should also be observed that this situation is not valid for Re = 30,000 cases, since a high mass flow rate causes higher viscous dissipation. Furthermore, the highest energy efficiency was obtained at

500 K for all adiabatic systems cases for Reynolds number up to 10,000 and a heat leakage with a heat transfer coefficient of 10 W/m^2K.

In the evaluation of the exergy efficiency of the systems, it was found that exergy efficiency differs greatly from its energy counterparts. First of all, it was observed that while the energy efficiency was higher than 70% in all cases, the exergy efficiency values ranged from 26%–70%. The reason behind this lower efficiency is the systems' exergy destruction. In this study, three different exergy terms were involved, due to convective heat transfer, heat leakage, and entropy generation. In order to find the optimum design for the given systems, the exergy destruction must be minimized.

With regard to pitch ratio, it was found that exergy efficiency decreases with increasing pitch ratio, since heat leakage and destroyed exergy becomes significantly higher for higher pitch ratios. As mentioned earlier, entropy generation had two sources: the first is heat transfer and the second is viscous dissipation. Predictably, viscous dissipation increased with increasing pitch ratio and it exerted a greater effect on entropy generation due to the convective heat transfer. While the effect of heat leakage in energy efficiency was about 6% for the lowest pitch ratio, it was more than 18% for exergy efficiency. Hence, it can be concluded that heat leakage effect is more pronounced in exergy efficiency. Again, it is not surprising that, the efficiency decreases with increasing heat leakage.

Another important parameter was the Reynolds number, and the exergy efficiency decreased with increasing Reynolds numbers for all adiabatic systems, as it was in energy efficiency. However, in exergy efficiency, the difference between the highest and lowest Reynolds number cases was higher than that for energy efficiency, since the exergy destruction effect in exergy is greater than the viscous heating effect in entropy generation. For instance, the

proportion of destroyed exergy in the efficiency was about 54% in one case. The main reason behind this phenomena is that exergy destruction had two sources, as stated earlier. However, when the systems suffered heat leakage, the highest efficiency was obtained at 5,000 Reynolds number.

The number of cylinders is also a crucial parameter. It was observed that the exergy efficiency increases with the number of cylinders, as the convective heat transfer increases with the increased cylinder numbers. It is surprising that even though the pressure difference was lower for three in-line tubes, the entropy generation ratio due to viscous dissipation was the highest due to the low heat transfer effect in total entropy generation. Increasing the number of cylinders in a domain results in greater convective heat transfer, leading to higher entropy generation; however, the viscous dissipation effect on the total entropy generation decreases with increasing number of cylinders.

The HTF's inlet temperature is the most important among all other parameters, as the thermophysical properties of the HTF change with its mean temperature. This is why all uniform inlet velocities were different for each inlet temperature case, even though the Reynolds number remained the same. It was found that the exergy efficiency decreases with increasing inlet temperature, since the exergy flow difference was higher for high inlet temperatures. The primary reason behind this is that the exergy flow difference increases when the temperature gradient between the inlet and outlet of the tube bundle increase. Lastly, exergy efficiency differences between the 400 K and 600 K case were nearly 27%, a value which was not obtained with any other parameter changes.

The main findings of this study can be summarized as follows:

- While the highest energy and exergy efficiencies were obtained at the Reynolds number value of 500 in adiabatic cases, they were obtained at 5,000 Reynolds number when the artificial heat leakage was applied to the systems.
- While the energy efficiency varied from 72%–99%, the exergy efficiency ranged from 26%–70%.
- The most efficient system from an energy standpoint was obtained in a domain containing three cylinders, a pitch ratio of 1.3, a Reynolds number of 500, an inlet temperature of 500 K, and in a system without heat leakage.
- The most efficient system from an exergy standpoint was achieved in a domain with eight cylinders, a pitch ratio of 1.3, a Reynolds number of 500, an inlet temperature of 400 K; this system did not have heat leakage.
- An increase in heat leakage led to a decrease in both energy and exergy efficiencies.
- A positive relation exists between the number of cylinders and energy and exergy efficiencies.
- While increasing the pitch ratio always decreases the exergy efficiency, the same decreasing phenomenon is similar for exergy efficiency, except for a few cases.
- While increasing inlet temperature enhances the energy efficiency, it leads to a reduction in the exergy efficiency.

REFERENCES

Abdel-rehim, Z. S. (2013). Heat Transfer Characteristics and Fluid Flow past Staggered Flat-Tube Bank Using CFD. *International Journal of Mechanical, Aerospace, Industrial, Mechatronic and Manufacturing Engineering*, *7*(10).

Abu-Hijleh, B. A. (1998). Entropy Generation In Laminar Convection From An Isothermal Cylinder In Cross Flow. *Energy*, *23*(10), 851–857.

Ahmed, M. A., Yaseen, M. M., & Yusoff, M. Z. (2017). Numerical study of convective heat transfer from tube bank in cross flow using nanofluid. *Case Studies in Thermal Engineering*, *10*(September), 560–569. http://doi.org/10.1016/j.csite.2017.11.002

Aiba, S., Tsuchida, H., & Ota, T. (1982a). Heat Transfer Around Tubes in Inline Tube Banks. *Bulletin of the JSME*, *25*(204), 919–924. http://doi.org/10.1299/jsme1958.25.919

Aiba, S., Tsuchida, H., & Ota, T. (1982b). Heat Transfer around Tubes in Staggered Tube Banks. *Bulletin of the JSME*, *25*(204), 927–933. http://doi.org/10.1299/jsme1958.25.927

Ambesi, D., & Kleijn, C. R. (2012). Laminar forced convection heat transfer to ordered and disordered single rows of cylinders. *International Journal of Heat and Mass Transfer*, *55*(21–22), 6170–6180. http://doi.org/10.1016/j.ijheatmasstransfer.2012.06.038

ANSYS FLUENT Theory Guide. (2011). Canonsburg.

Bacellar, D., Aute, V., & Radermacher, R. (2014). CFD-Based Correlation Development For Air Side Performance Of Finned And Finless Tube Heat Exchangers With Small Diameter Tubes. In *International Refrigeration and Air Conditioning Conference*.

Bahaidarah, H. M. S. (2004). *A Numerical Study of Heat and Momentum Transfer Over a Bank of Flat Tubes a Numerical Study of Heat and Momentum Transfer*.

Bahaidarah, H. M. S., Anand, N. K., & Chen, H. C. (2005). A Numerical Study of Fluid Flow and Heat Transfer over a Bank of Flat Tubes. *Numerical Heat Transfer, Part A: Applications*, *48*(4), 359–385. http://doi.org/10.1080/10407780590957134

Balabani, S. (1996). A*n experimental investigation of tube bundles*.

Beale, S. B. (1992). *Fluid Flow and Heat Transfer in Tube Banks*.

Beale, S. B., & Spalding, D. B. (1998). Numerical study of fluid flow and heat transfer in tube

banks with stream-wise periodic boundary conditions. *Transactions of the CSME*, *22*(4A), 397–416.

Benarji, N., Balaji, C., & Venkateshan, S. P. (2008). Unsteady fluid flow and heat transfer over a bank of flat tubes. *Heat and Mass Transfer*, *44*(4), 445. http://doi.org/https://doi.org/10.1007/s00231-007-0256-5

Bergelin, O. P., Davis, E. S., & Hull, H. L. (1949). A study of three tube arrangements in unbaffled tubular heat exchangers. *Trans.ASME*, *71*, 369–374.

Bergman, T. L., Lavine, A. S., Incropera, F. P., & Dewitt, D. P. (2011). *Introduction to Heat Transfer* (6th ed.). NJ: John Wiley & Sons.

Buyruk, E. (2002). Numerical study of heat transfer characteristics on tandem cylinders, inline and staggered tube banks in cross-flow of air. *International Communications in Heat and Mass Transfer*, *29*(3), 355–366. http://doi.org/10.1016/S0735-1933(02)00325-1

Cengel, Y. A., & Boles, M. A. (2015). *Thermodynamics : An Engineering Approach* (8th ed.). New York: McGraw-Hill Education.

Cengel, Y. A., & Ghajar, A. J. (2015). *Heat and Mass Transfer Fundamentals & Applications* (5th ed.). New York: McGraw-Hill Education.

Chakrabarty, S. G., & Wankhede, U. S. (2012). Flow and heat transfer behaviour across circular cylinder and tube banks with and without splitter plate. *International Journal of Modern Engineering Research*, *2*(4), 1529–1533.

Chorin, A. J. (1968). Numerical Solution of the Navier-Stokes Equation. *Mathematics of Computation*, *22*, 745–762.

Churchill, S. W. (2002). Free Convection Around Immersed Bodies. In *Heat Exchanger Design Handbook, Section 2.5.9*. New York: Begell House. http://doi.org/10.1615/hedhme.a.000174

Churchill, S. W., & Bernstein, M. (1977). A Correlating Equation for Forced Convection From Gases and Liquids to a Circular Cylinder in Crossflow. *Journal of Heat Transfer*, *99*(2), 300–306. http://doi.org/10.1115/1.3450685

Churchill, S. W., & Chu, H. H. S. (1975a). Correlating equations for laminar and turbulent free convection from a horizontal cylinder. *International Journal of Heat and Mass Transfer*, *18*(9), 1049–1053. http://doi.org/https://doi.org/10.1016/0017-9310(75)90222-7

Churchill, S. W., & Chu, H. H. S. (1975b). Correlating equations for laminar and turbulent free convection from a vertical plate. *International Journal of Heat and Mass Transfer*, *18*(11), 1323–1329. http://doi.org/10.1016/0017-9310(75)90243-4

Colburn, A. P. (1933). A method of correlating forced convection heat transfer data and a comparison with fluid friction. *International Journal of Heat and Mass Transfer*, *7*, 1359–1384. Retrieved from http://ci.nii.ac.jp/naid/10007717209/en/

Dincer, I., & Kanoglu, M. (2010). *Refrigeration Systems and Applications* (2nd ed.). John Wiley & Sons, Ltd. http://doi.org/10.1002/9780470661093

Dincer, I., & Rosen, M. A. (2013). *Exergy: Energy, Environment And Sustainable Development* (2nd ed.). Elsevier.

Dittus, F.W. and Boelter, L. M. K. (1985). Heat Transfer in Automobile Radiators of the Tubular Type. *International Communications in Heat and Mass Transfer*, *12*(1), 3–22. http://doi.org/https://doi.org/10.1016/0735-1933(85)90003-X

Dubovsky, V., Ziskind, G., & Letan, R. (2011). Analytical model of a PCM-air heat exchanger. *Applied Thermal Engineering*, *31*(16), 3453–3462. http://doi.org/https://doi.org/10.1016/j.applthermaleng.2011.06.031

El-Shaboury, A. M. F., & Ormiston, S. J. (2005). Analysis of Laminar Forced Convection of Air Crossflow in In-Line Tube Banks with NonSquare Arrangements. *Numerical Heat Transfer, Part A: Applications*, *48*(2), 99–126. http://doi.org/10.1080/10407780590945452

Fowler, A. J., & Bejan, A. (1994). Correlation of optimal sizes of bodies with external forced convection heat transfer. *International Communications in Heat and Mass Transfer*, *21*(1), 17–27.

Fujii, M., Fujii, T., & Nagata, T. (1984). A NUMERICAL ANALYSIS OF LAMINAR FLOW AND HEAT TRANSFER OF AIR IN AN IN-LINE TUBE BANK. *Numerical Heat Transfer*, *7*(1), 89–102. http://doi.org/10.1080/01495728408961813

Fujii, T., Uehara, H., Hirata, K., & Oda, K. (1972). Heat transfer and flow resistance in condensation of low pressure steam flowing through tube banks. *International Journal of Heat and Mass Transfer*, *15*(2), 247–260. http://doi.org/10.1016/0017-9310(72)90072-5

Gharbi, N. El, Kheiri, A., Ganaoui, M. El, & Blanchard, R. (2015). Numerical optimization of heat exchangers with circular and non-circular shapes. *Case Studies in Thermal Engineering*, *6*, 194–203. http://doi.org/10.1016/j.csite.2015.09.006

Gholami, A., Wahid, M. A., Mohammed, H. A., Saat, A., Mohd Yasin, M. F., Sies, M. M., … Rahman, M. M. (2016). Numerical evaluation of thermo-hydraulic performance in fin-and-tube compact heat exchangers with different tube cross-sections. *Jurnal Teknologi*, *78*(8–4), 113–118. http://doi.org/10.11113/jt.v78.9592

Graetz, L. (1885). Ueber die Wärmeleitungsfähigkeit von Flüssigkeiten. *Annalen Der Physik*, *261*(7), 337–357. http://doi.org/10.1002/andp.18852610702

Grannis, V. B., & Sparrow, E. M. (1991). NUMERICAL SIMULATION OF FLUID FLOW THROUGH AN ARRAY OF DIAMOND-SHAPED PIN FINS. *Numerical Heat Transfer, Part A: Applications*, *19*(4), 381–403. http://doi.org/10.1080/10407789108944856

Grimison, E. D. (1937). Correlation and Utilization of New Data on Flow Resistance and Heat Transfer for Cross Flow of Gases Over Tube Banks. *Journal of Dynamic Systems, Measurement and Control*, *59*, 583–594.

Hausen, H. (1983). *Heat Transfer in Counter Flow, Parallel Flow and Cross Flow*. New York: McGraw–Hill.

Huge, E. C. (1937). Experimental Investigation of Effects of Equipment Size on Convection Heat Transfer and Flow Resistance in Cross Flow of Gases Over Tube Banks. *Journal of Heat Transfer,ASME*, *59*, 573–581.

Iacovides, H., Launder, B., Laurence, D., & West, A. (2013). Alternative Strategies for Modelling Flow over In-Line Tube Banks. In *Proceedings of the 8th International Symposium on Turbulence and Shear Flow Phenomena (TSFP-8)* (pp. 1–6). Poitiers, France.

Ibrahim, E., & Moawed, M. (2009). Forced convection and entropy generation from elliptic tubes with longitudinal fins. *Energy Conversion and Management*, *50*(8), 1946–1954. http://doi.org/https://doi.org/10.1016/j.enconman.2009.04.021

Ibrahim, T. A., & Gomaa, A. (2009). Thermal performance criteria of elliptic tube bundle in crossflow. *International Journal of Thermal Sciences*, *48*(11), 2148–2158. http://doi.org/10.1016/j.ijthermalsci.2009.03.011

Jang, J.-Y., Wu, M.-C., & Chang, W.-J. (1996). Numerical and experimental studies of three dimensional plate-fin and tube heat exchangers. *International Journal of Heat and Mass Transfer*, *39*(14), 3057–3066. http://doi.org/10.1016/0017-9310(95)00341-X

Kays, W. M., & London, A. L. (1964). *Compact Heat Exchangers*. New York: McGraw–Hill.

Khan, W. A., Culham, J. R., & Yovanovich, M. M. (2006). The Role of Fin Geometry in Heat Sink Performance. *Journal of Electronic Packaging*, *128*(4), 324–330. http://doi.org/doi:10.1115/1.2351896.

Khan, W. A., Culham, R. J., & Yovanovich, M. M. (2006). Analytical Model for Convection Heat Transfer from Tube Banks. *Journal of Thermophysics and Heat Transfer*, *20*(4), 720–727. http://doi.org/https://doi.org/10.2514/1.15453

Khan, W. A., Culham, R. J., & Yovanovich, M. M. (2007). Optimal Design of Tube Banks in Crossflow Using Entropy Generation Minimization Method. *Journal of Thermophysics and Heat Transfer*, *21*(2), 372–378. http://doi.org/10.2514/1.26824

Khan, W. A., Culham, R., & Yovanovich, M. (2006). Convection heat transfer from tube banks in cross flow: Analytical approach. *International Journal of Heat and Mass Transfer*, *49*(25–26), 4831–4838. http://doi.org/10.1016/j.ijheatmasstransfer.2006.05.042

Kim, T. (2013). Effect of longitudinal pitch on convective heat transfer in crossflow over in-line tube banks. *Annals of Nuclear Energy*, *57*, 209–215. http://doi.org/10.1016/j.anucene.2013.01.060

Korukcu, M. O. (2015). 2D Temperature Analysis of Energy and Exergy Characteristics of Laminar Steady Flow across a Square Cylinder under Strong Blockage. *Entropy*, *17*(5), 3124–3151. http://doi.org/10.3390/e17053124

Krishne Gowda, Y. T., Patnaik, B. S. V. P., Aswatha Narayana, P. A., & Seetharamu, K. N. (1998). Finite element simulation of transient laminar flow and heat transfer past an in-line tube bank. *International Journal of Heat and Fluid Flow*, *19*(1), 49–55. http://doi.org/10.1016/S0142-727X(97)10005-4

Kritikos, K., Albanakis, C., Missirlis, D., Vlahostergios, Z., Goulas, A., & Storm, P. (2010). Investigation of the thermal efficiency of a staggered elliptic-tube heat exchanger for aeroengine applications. *Applied Thermal Engineering*, *30*(2–3), 134–142. http://doi.org/10.1016/j.applthermaleng.2009.07.013

Lavasani, M. A., & Bayat, H. (2016). Numerical study of pressure drop and heat transfer from circular and cam-shaped tube bank in cross-flow of nanofluid. *Energy Conversion and Management*, *129*, 319–328. http://doi.org/10.1016/j.enconman.2016.10.029

Lavasani, M. A., Bayat, H., & Maarefdoost, T. (2014). Experimental study of convective heat transfer from in-line cam shaped tube bank in cross flow. *Applied Thermal Engineering*, *65*(1–2), 85–93. http://doi.org/10.1016/j.applthermaleng.2013.12.078

Lee, D., Ahn, J., & Shin, S. (2013). Uneven longitudinal pitch effect on tube bank heat transfer in cross flow. *Applied Thermal Engineering*, *51*(1–2), 937–947. http://doi.org/10.1016/j.applthermaleng.2012.10.031

Letan, R., & Ziskind, G. (2006). Thermal design and operation of a portable PCM cooler. In M. Kutz (Ed.), *Heat Transfer Calculations*. New York: McGraw-Hill.

Ljungkrona, L., & Sundén, B. (1993). Flow visualization and surface pressure measurement on two tubes in an inline arrangement. *Experimental Thermal and Fluid Science*, *6*(1), 15–27. http://doi.org/10.1016/0894-1777(93)90037-J

MacPhee, D., Dincer, I., & Beyene, A. (2012). Numerical simulation and exergetic performance assessment of charging process in encapsulated ice thermal energy storage system. *Energy*, *41*(1), 491–498. http://doi.org/10.1016/j.energy.2012.02.042

Mandhani, V. K., Chhabra, R. P., & Eswaran, V. (2002). Forced convection heat transfer in tube

banks in cross flow. *Chemical Engineering Science*, *57*(3), 379–391. http://doi.org/10.1016/S0009-2509(01)00390-6

Mangrulkar, C. K., Dhoble, A. S., Chakrabarty, S. G., & Wankhede, U. S. (2017). Experimental and CFD prediction of heat transfer and friction factor characteristics in cross flow tube bank with integral splitter plate. *International Journal of Heat and Mass Transfer*, *104*, 964–978. http://doi.org/https://doi.org/10.1016/j.ijheatmasstransfer.2016.09.013

McAdams, W. H. (1954). *Heat transmission* (3rd ed.). New York: McGraw-Hill.

Melhem, O. A., Sahin, A. Z., & Yilbas, B. S. (2017). Entropy Generation Due To External Fluid Flow and Heat Transfer From a Cylinder Between Parallel Planes. *Thermal Science*, *21*(2), 841–848. http://doi.org/10.2298/TSCI141104068M

Miyatake, O., & Iwashita, H. (1991). Laminar-flow heat transfer to a fluid flowing axially between cylinders with a uniform wall heat flux. *International Journal of Heat and Mass Transfer*, *34*(1), 322–327. http://doi.org/10.1016/0017-9310(91)90199-O

Nagamani, V., & Reddy, A. C. (2015). Turbulent and incompressible flow in a shell and tube heat exchanger. *International Journal of Advanced Research*, *3*(4), 676–683.

Ota, T., Nishiyama, H., & Taoka, Y. (1984). Heat transfer and flow around an elliptic cylinder. *International Journal of Heat and Mass Transfer*, *27*(10), 1771–1779. http://doi.org/10.1016/0017-9310(84)90159-5

Paul, S. S., Ormiston, S. J., & Tachie, M. F. (2008). Experimental and numerical investigation of turbulent cross-flow in a staggered tube bundle. *International Journal of Heat and Fluid Flow*, *29*(2), 387–414. http://doi.org/10.1016/j.ijheatfluidflow.2007.10.001

Pierson, O. L. (1937). Experimental Investigation of the Influence of Tube Arrangement on Convection Heat Transfer and Flow Resistance in Cross Flow of Gases Over Tube Banks. *Journal of Heat Transfer,ASME*, *59*, 563–572.

Poulikakos, D., & Johnson, J. M. (1989). Second law analysis of combined heat and mass transfer phenomena in external flow. *Energy*, *14*(2), 67–73. http://doi.org/10.1016/0360-5442(89)90080-7

Sandall, O. C. (1974). Transfer processes, D. K. Edwards, V. E. Denny, and A. F. Mills, Holt, Rinehart, Winston, Inc., New York (1973) 361 pages. $15.00. *AIChE Journal*, *20*(2), 414. http://doi.org/10.1002/aic.690200242

Sayed Ahmed, S. E., Ibrahiem, E. Z., Mesalhy, O. M., & Abdelatief, M. A. (2015). Effect of attack and cone angels on air flow characteristics for staggered wing shaped tubes bundle. *Heat and Mass Transfer*, *51*(7), 1001–1016. http://doi.org/10.1007/s00231-014-1473-3

Sayed Ahmed, S. A., Mesalhy, O. M., & Abdelatief, M. A. (2015). Effect of Longitudinal-

External-Fins on Fluid Flow Characteristics for Wing-Shaped Tubes Bundle in Crossflow. *Journal of Termodynamics*, *2015*. http://doi.org/10.1155/2015/542405

Selma, B., Désilets, M., & Proulx, P. (2014). Optimization of an industrial heat exchanger using an open-source CFD code. *Applied Thermal Engineering*, *69*(1–2), 241–250. http://doi.org/10.1016/j.applthermaleng.2013.11.054

Sieder, E. N., & Tate, G. E. (1936). Heat Transfer and Pressure Drop of Liquids in Tubes. *Industrial and Engineering Chemistry*, *28*(12), 1429–1435. http://doi.org/10.1021/ie50324a027

Tahseen, A. T., Ishak, M., & Rahman, M. M. (2013). Laminar forced convection heat transfer over staggered circular tube banks: A CFD approach. *Journal of Mechanical Engineering and Sciences*, *4*(June), 418–430. http://doi.org/10.15282/jmes.4.2013.6.0039

Tahseen, T. A., Ishak, M., & Rahman, M. M. (2015). An overview on thermal and fluid flow characteristics in a plain plate finned and un-finned tube banks heat exchanger. *Renewable and Sustainable Energy Reviews*, *43*, 363–380. http://doi.org/10.1016/j.rser.2014.10.070

Torresi, M., Saponaro, A., Camporeale, S. M., & Fortunato, B. (2008). CFD Analysis of the Flow Through Tube Banks of HRSG. *Proceedings of ASME Turbo Expo 2008, Berlin, Germany*, 327–337. http://doi.org/10.1115/GT2008-51300

V. Gnielinski. (1976). New Equations for Heat and Mass Transfer in Turbulent Pipe and Channel Flow. *International Chemical Engineering*, *16*, 359–368.

Välikangas, T. (2015). Simulation method development for Fin-and-Tube Heat Ex- changer with Open-source software.

Van Doormaal, J. P., & Raithby, G. D. (1984). ENHANCEMENTS OF THE SIMPLE METHOD FOR PREDICTING INCOMPRESSIBLE FLUID FLOWS. *Numerical Heat Transfer*, *7*(2), 147–163. http://doi.org/10.1080/01495728408961817

Welty, J. R., Rorrer, G. L., & Foster, D. G. (2013). *Fundamentals of Momentum, Heat, and Mass Transfer* (6th ed.). NJ: Wiley.

Whitaker, S. (1972). Forced convection heat transfer correlations for flow in pipes, past flat plates, single cylinders, single spheres, and for flow in packed beds and tube bundles. *AIChE Journal*, *18*(2), 361–371. http://doi.org/10.1002/aic.690180219

Will, J. B., Kruyt, N. P., & Venner, C. H. (2017). An experimental study of forced convective heat transfer from smooth, solid spheres. *International Journal of Heat and Mass Transfer*, *109*, 1059–1067. http://doi.org/10.1016/j.ijheatmasstransfer.2017.02.018

Wilson, A. S., & Bassiouny, M. K. (2000). Modeling of heat transfer for flow across tube banks. *Chemical Engineering and Processing*, *39*(1), 1–14. http://doi.org/10.1016/S0255-

2701(99)00069-0

Yilmaz, A., Kuru, M. N., Erdinc, M. T., & Yilmaz, T. (2016). Numerical Calculation of Heat Transfer and Pressure Drop in In-line Axially-Finned Tube. In *1st International Mediterranean Science and Engineering Congress*. Adana.

Yilmaz, A., & Yilmaz, T. (2016). Optimum Design of Cross-Flow In-Line Tube Banks at Constant Wall Temperature. *Heat Transfer Engineering*, *37*(6), 523–534. http://doi.org/10.1080/01457632.2015.1060753

Zhang, L.-Z., Zhong, W.-C., Chen, J.-M., & Zhou, J.-R. (2011). Fluid Flow and Heat Transfer in Plate-Fin and Tube Heat Exchangers in a Transitional Flow Regime. *Numerical Heat Transfer, Part A: Applications*, *60*(9), 766–784. http://doi.org/10.1080/10407782.2011.627802

Žkauskas, A. (1987). Heat Transfer from Tubes in Crossflow. In J. P. Hartnett & T. F. Irvine (Eds.) (Vol. 18, pp. 87–159). Elsevier. http://doi.org/10.1016/S0065-2717(08)70118-7

Žukauskas, A. (1972). Heat Transfer from Tubes in Crossflow. In J. P. Hartnett & T. F. Irvine (Eds.) (Vol. 8, pp. 93–160). Elsevier. http://doi.org/https://doi.org/10.1016/S0065-2717(08)70038-8

ŽUKAUSKAS, A., & ULINSKAS, R. (1985). Efficiency Parameters for Heat Transfer in Tube Banks. *Heat Transfer Engineering*, *6*(1), 19–25. http://doi.org/10.1080/01457638508939614

APPENDIX A

As stated in section 5.1, validation of the model has been provided for three and four number of in-line cylinders. While Figures A1 and A2 indicate the nusselt number validation, Figures A3 and A4 illustrate the validation in terms of pressure drop.

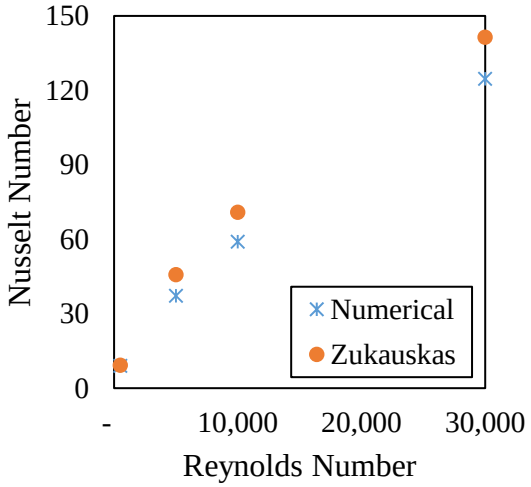

a) 1.3 Pitch Ratio

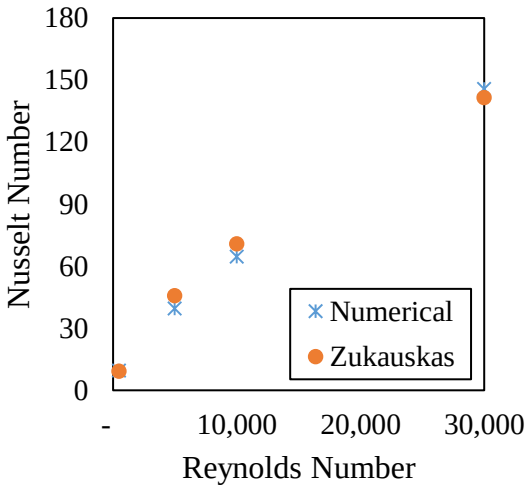

b) 1.6 Pitch Ratio

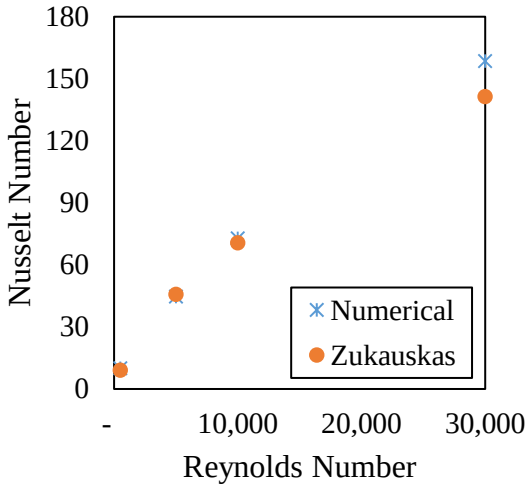

c) 2.0 Pitch Ratio

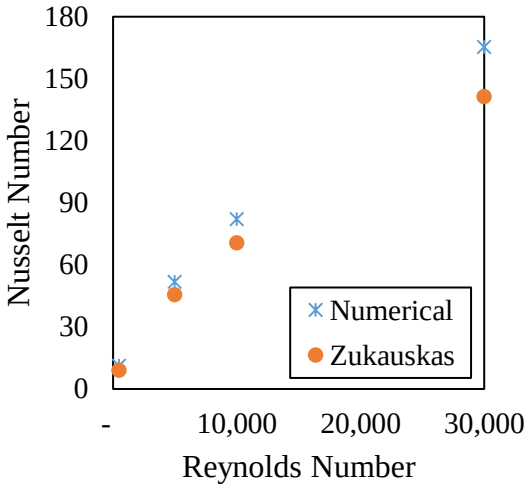

b) 3.0 Pitch Ratio

Figure A. 1 Nusselt number validation for four in-line cylinders

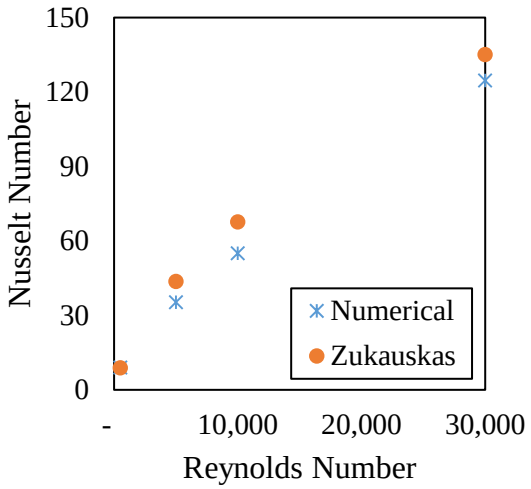

a) 1.3 Pitch Ratio

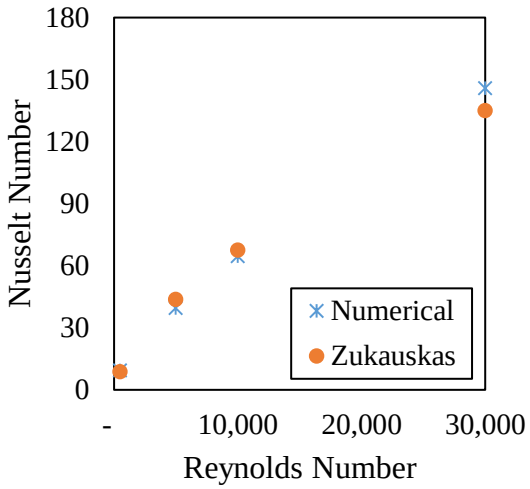

b) 1.6 Pitch Ratio

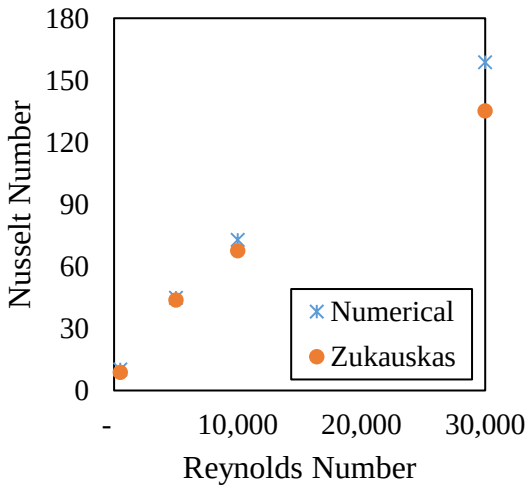

c) 2.0 Pitch Ratio

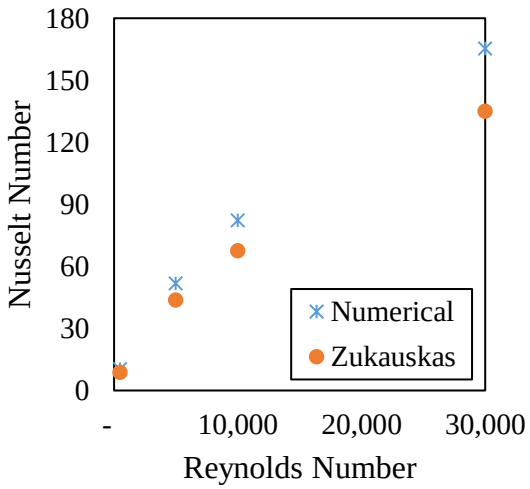

b) 3.0 Pitch Ratio

Figure A. 2 Nusselt number validation for three in-line cylinders

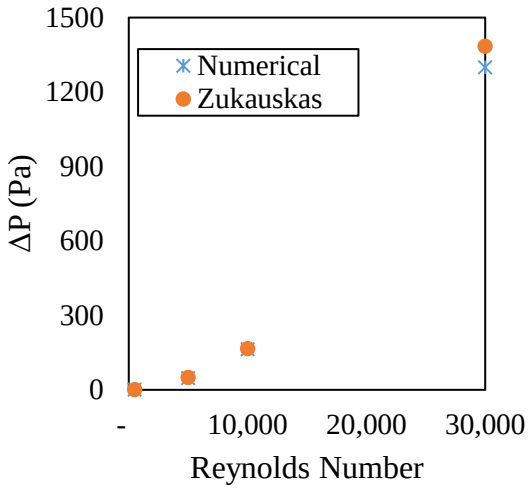

a) 1.3 Pitch Ratio

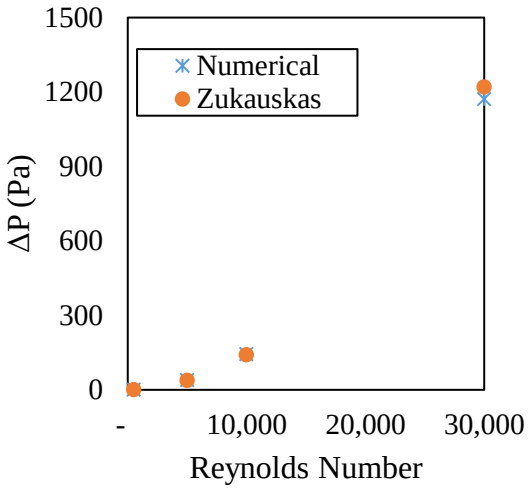

b) 1.6 Pitch Ratio

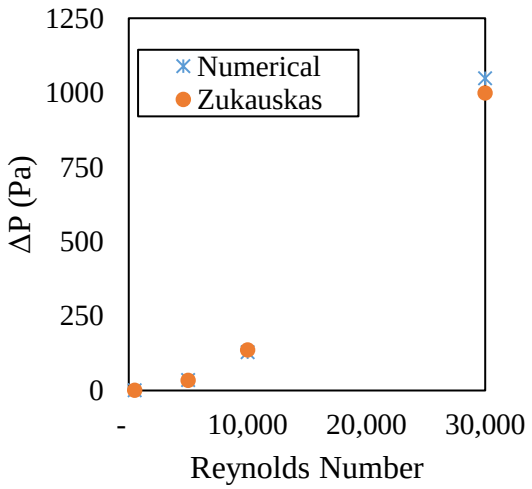

c) 2.0 Pitch Ratio

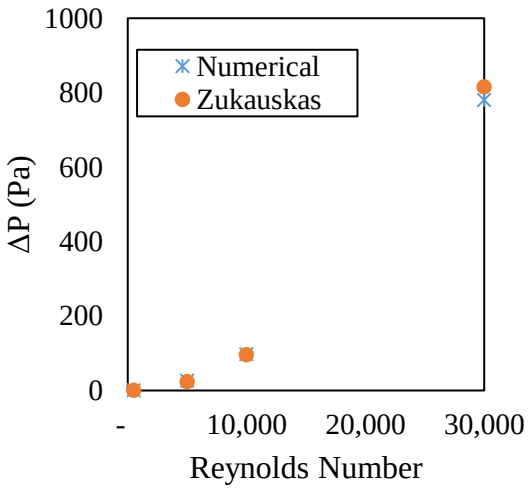

b) 3.0 Pitch Ratio

Figure A. 3 Pressure drop validation for four in-line cylinders

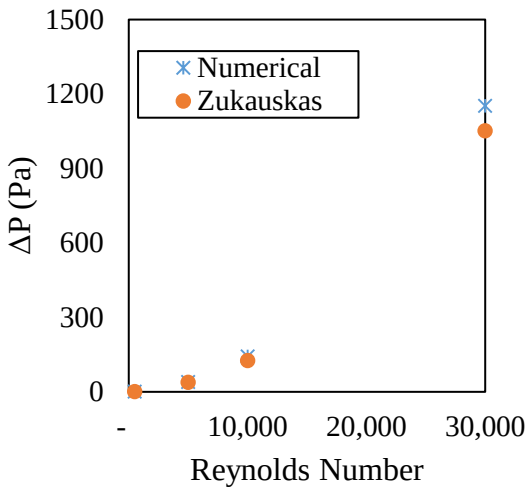

a) 1.3 Pitch Ratio

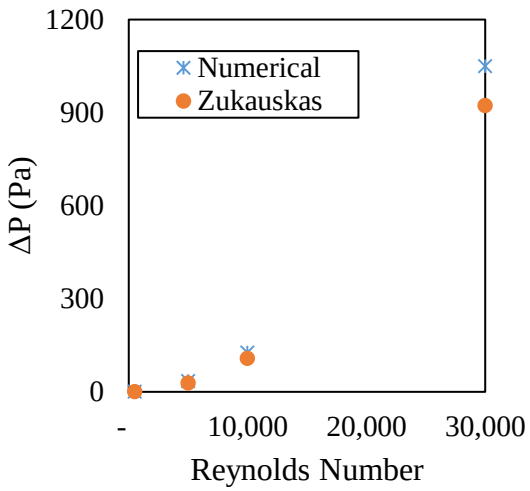

b) 1.6 Pitch Ratio

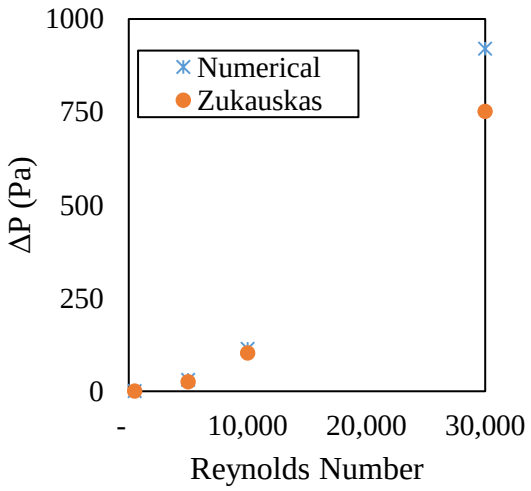

c) 2.0 Pitch Ratio

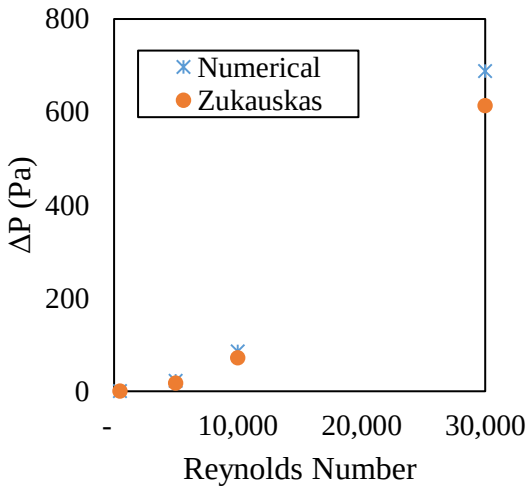

b) 3.0 Pitch Ratio

Figure A. 4 Pressure drop validation for three in-line cylinders

APPENDIX B

Since there are 576 simulations, it is not easy to show each case in result and discussion part. Therefore, the energy and exergy efficiency of each case is illustrated here. Moreover, the effect of viscous dissipation and heat leakage on the energy efficiency can be seen from tables.

- **T_{in}=400K**

8 cylinders		Heat Leakage											
		U=0			*U=10W/m²K*			*U=50W/m²K*			*U=100W/m²K*		
		Percentage Effect on Energy Efficiency											
Pitch Ratio	*Reynolds Number*	*HT*	*VD*	*HL*	*HT*	*VD*	*HL*	*HT*	*VD*	*HL*	*HT*	*VD*	*HL*
1.30	500	100%	0%	0%	99%	0%	1%	96%	0%	4%	91%	0%	9%
1.30	5,000	100%	0%	0%	100%	0%	0%	99%	0%	1%	98%	0%	1%
1.30	10,000	99%	1%	0%	99%	1%	0%	99%	1%	0%	98%	1%	1%
1.30	30,000	91%	9%	0%	91%	9%	0%	91%	9%	0%	91%	9%	0%
1.60	500	100%	0%	0%	99%	0%	1%	94%	0%	6%	89%	0%	11%
1.60	5,000	100%	0%	0%	99%	0%	0%	99%	0%	1%	98%	0%	2%
1.60	10,000	99%	1%	0%	99%	1%	0%	98%	1%	1%	98%	1%	1%
1.60	30,000	89%	11%	0%	89%	11%	0%	88%	11%	0%	88%	11%	0%
2.00	500	100%	0%	0%	98%	0%	2%	92%	0%	8%	84%	0%	16%
2.00	5,000	100%	0%	0%	99%	0%	0%	98%	0%	1%	97%	0%	3%
2.00	10,000	98%	2%	0%	98%	2%	0%	98%	2%	1%	97%	2%	2%
2.00	30,000	86%	14%	0%	86%	14%	0%	86%	14%	0%	85%	14%	1%
3.00	500	100%	0%	0%	97%	0%	3%	84%	0%	16%	72%	0%	28%
3.00	5,000	99%	1%	0%	99%	1%	1%	97%	0%	3%	94%	0%	6%
3.00	10,000	98%	2%	0%	98%	2%	0%	96%	2%	2%	95%	2%	3%
3.00	30,000	82%	18%	0%	82%	18%	0%	81%	18%	1%	81%	18%	1%

4 cylinders		Heat Leakage											
		U=0			*U=10W/m²K*			*U=50W/m²K*			*U=100W/m²K*		
		Percentage Effect on Energy Efficiency											
Pitch Ratio	*Reynolds Number*	*HT*	*VD*	*HL*	*HT*	*VD*	*HL*	*HT*	*VD*	*HL*	*HT*	*VD*	*HL*
1.30	500	100%	0%	0%	99%	0%	1%	97%	0%	3%	94%	0%	6%
1.30	5,000	100%	0%	0%	100%	0%	0%	99%	0%	1%	99%	0%	1%
1.30	10,000	99%	1%	0%	99%	1%	0%	98%	1%	0%	98%	1%	1%
1.30	30,000	89%	11%	0%	89%	11%	0%	89%	11%	0%	89%	11%	0%
1.60	500	100%	0%	0%	99%	0%	1%	95%	0%	5%	91%	0%	9%
1.60	5,000	100%	0%	0%	99%	0%	0%	99%	0%	1%	98%	0%	2%
1.60	10,000	98%	2%	0%	98%	2%	0%	98%	2%	0%	97%	2%	1%
1.60	30,000	85%	15%	0%	85%	15%	0%	84%	15%	0%	84%	15%	0%
2.00	500	100%	0%	0%	99%	0%	1%	93%	0%	7%	86%	0%	14%
2.00	5,000	99%	1%	0%	99%	1%	0%	98%	1%	1%	97%	1%	3%
2.00	10,000	98%	2%	0%	98%	2%	0%	97%	2%	1%	96%	2%	2%
2.00	30,000	81%	19%	0%	81%	19%	0%	81%	19%	0%	80%	19%	1%
3.00	500	100%	0%	0%	97%	0%	3%	86%	0%	14%	74%	0%	26%
3.00	5,000	99%	1%	0%	99%	1%	1%	97%	1%	3%	94%	1%	5%
3.00	10,000	97%	3%	0%	97%	3%	0%	96%	3%	2%	94%	3%	3%
3.00	30,000	76%	24%	0%	76%	24%	0%	76%	24%	1%	75%	24%	1%

3 cylinders		Heat Leakage											
		U=0			*U=10W/m²K*			*U=50W/m²K*			*U=100W/m²K*		
		Percentage Effect on Energy Efficiency											
Pitch Ratio	*Reynolds Number*	*HT*	*VD*	*HL*	*HT*	*VD*	*HL*	*HT*	*VD*	*HL*	*HT*	*VD*	*HL*
1.30	500	100%	0%	0%	99%	0%	1%	97%	0%	3%	95%	0%	5%
1.30	5,000	100%	0%	0%	100%	0%	0%	99%	0%	1%	99%	0%	1%
1.30	10,000	99%	1%	0%	99%	1%	0%	98%	1%	0%	98%	1%	1%
1.30	30,000	87%	13%	0%	87%	13%	0%	87%	13%	0%	87%	13%	0%
1.60	500	100%	0%	0%	99%	0%	1%	96%	0%	4%	92%	0%	8%
1.60	5,000	100%	0%	0%	99%	0%	0%	99%	0%	1%	98%	0%	2%
1.60	10,000	98%	2%	0%	98%	2%	0%	98%	2%	0%	97%	2%	1%
1.60	30,000	82%	18%	0%	82%	18%	0%	82%	18%	0%	82%	18%	0%
2.00	500	100%	0%	0%	99%	0%	1%	93%	0%	7%	87%	0%	13%
2.00	5,000	99%	1%	0%	99%	1%	0%	98%	1%	1%	97%	1%	3%
2.00	10,000	97%	3%	0%	97%	3%	0%	97%	3%	1%	96%	3%	1%
2.00	30,000	78%	22%	0%	78%	22%	0%	78%	22%	0%	77%	22%	1%

3.00	500	100%	0%	0%	97%	0%	3%	86%	0%	14%	76%	0%	24%
3.00	5,000	99%	1%	0%	99%	1%	1%	97%	1%	3%	94%	1%	5%
3.00	10,000	97%	3%	0%	96%	3%	0%	95%	3%	2%	94%	3%	3%
3.00	30,000	73%	27%	0%	73%	27%	0%	72%	27%	1%	72%	27%	1%

- **T_{in}=500K**

8 cylinders		Heat Leakage											
		U=0			*U=10W/m²K*			*U=50W/m²K*			*U=100W/m²K*		
		Percentage Effect on Energy Efficiency											
Pitch Ratio	*Reynolds Number*	*HT*	*VD*	*HL*	*HT*	*VD*	*HL*	*HT*	*VD*	*HL*	*HT*	*VD*	*HL*
1.30	500	100%	0%	0%	100%	0%	0%	98%	0%	2%	96%	0%	4%
1.30	5,000	100%	0%	0%	100%	0%	0%	100%	0%	0%	99%	0%	1%
1.30	10,000	99%	1%	0%	99%	1%	0%	99%	1%	0%	99%	1%	0%
1.30	30,000	94%	6%	0%	94%	6%	0%	94%	6%	0%	94%	6%	0%
1.60	500	100%	0%	0%	99%	0%	1%	97%	0%	3%	94%	0%	6%
1.60	5,000	100%	0%	0%	100%	0%	0%	99%	0%	0%	99%	0%	1%
1.60	10,000	99%	1%	0%	99%	1%	0%	99%	1%	0%	99%	1%	1%
1.60	30,000	93%	7%	0%	93%	7%	0%	93%	7%	0%	93%	7%	0%
2.00	500	100%	0%	0%	99%	0%	1%	96%	0%	4%	92%	0%	8%
2.00	5,000	100%	0%	0%	100%	0%	0%	99%	0%	1%	98%	0%	1%
2.00	10,000	99%	1%	0%	99%	1%	0%	99%	1%	0%	98%	1%	1%
2.00	30,000	91%	9%	0%	91%	9%	0%	91%	9%	0%	91%	9%	0%
3.00	500	100%	0%	0%	98%	0%	2%	92%	0%	8%	85%	0%	15%
3.00	5,000	100%	0%	0%	99%	0%	0%	98%	0%	1%	97%	0%	3%
3.00	10,000	99%	1%	0%	99%	1%	0%	98%	1%	1%	97%	1%	2%
3.00	30,000	88%	12%	0%	88%	12%	0%	88%	12%	0%	88%	12%	1%

4 cylinders		Heat Leakage											
		U=0			*U=10W/m²K*			*U=50W/m²K*			*U=100W/m²K*		
		Percentage Effect on Energy Efficiency											
Pitch Ratio	*Reynolds Number*	*HT*	*VD*	*HL*	*HT*	*VD*	*HL*	*HT*	*VD*	*HL*	*HT*	*VD*	*HL*
1.30	500	100%	0%	0%	100%	0%	0%	99%	0%	1%	97%	0%	3%
1.30	5,000	100%	0%	0%	100%	0%	0%	100%	0%	0%	99%	0%	1%
1.30	10,000	99%	1%	0%	99%	1%	0%	99%	1%	0%	99%	1%	0%
1.30	30,000	93%	7%	0%	93%	7%	0%	93%	7%	0%	93%	7%	0%
1.60	500	100%	0%	0%	100%	0%	0%	98%	0%	2%	96%	0%	4%
1.60	5,000	100%	0%	0%	100%	0%	0%	99%	0%	0%	99%	0%	1%

1.60	10,000	99%	1%	0%	99%	1%	0%	99%	1%	0%	98%	1%	0%
1.60	30,000	90%	10%	0%	90%	10%	0%	90%	10%	0%	90%	10%	0%
2.00	500	100%	0%	0%	99%	0%	1%	97%	0%	3%	93%	0%	7%
2.00	5,000	100%	0%	0%	100%	0%	0%	99%	0%	1%	98%	0%	1%
2.00	10,000	99%	1%	0%	99%	1%	0%	98%	1%	0%	98%	1%	1%
2.00	30,000	88%	12%	0%	88%	12%	0%	88%	12%	0%	88%	12%	0%
3.00	500	100%	0%	0%	98%	0%	2%	93%	0%	7%	86%	0%	14%
3.00	5,000	100%	0%	0%	99%	0%	0%	98%	0%	1%	97%	0%	3%
3.00	10,000	98%	2%	0%	98%	2%	0%	98%	2%	1%	97%	2%	2%
3.00	30,000	84%	16%	0%	84%	16%	0%	84%	15%	0%	84%	15%	1%

3 cylinders		Heat Leakage											
		U=0			*U=10W/m²K*			*U=50W/m²K*			*U=100W/m²K*		
		Percentage Effect on Energy Efficiency											
Pitch Ratio	*Reynolds Number*	*HT*	*VD*	*HL*	*HT*	*VD*	*HL*	*HT*	*VD*	*HL*	*HT*	*VD*	*HL*
1.30	500	100%	0%	0%	100%	0%	0%	99%	0%	1%	97%	0%	3%
1.30	5,000	100%	0%	0%	100%	0%	0%	100%	0%	0%	99%	0%	0%
1.30	10,000	99%	1%	0%	99%	1%	0%	99%	1%	0%	99%	1%	0%
1.30	30,000	92%	8%	0%	92%	8%	0%	92%	8%	0%	92%	8%	0%
1.60	500	100%	0%	0%	100%	0%	0%	98%	0%	2%	96%	0%	4%
1.60	5,000	100%	0%	0%	100%	0%	0%	99%	0%	0%	99%	0%	1%
1.60	10,000	99%	1%	0%	99%	1%	0%	99%	1%	0%	98%	1%	0%
1.60	30,000	89%	11%	0%	89%	11%	0%	89%	11%	0%	89%	11%	0%
2.00	500	100%	0%	0%	99%	0%	1%	97%	0%	3%	94%	0%	6%
2.00	5,000	100%	0%	0%	100%	0%	0%	99%	0%	1%	98%	0%	1%
2.00	10,000	100%	0%	0%	100%	0%	0%	99%	0%	0%	99%	0%	1%
2.00	30,000	86%	14%	0%	86%	14%	0%	86%	14%	0%	85%	14%	0%
3.00	500	100%	0%	0%	99%	0%	1%	93%	0%	7%	87%	0%	13%
3.00	5,000	100%	0%	0%	99%	0%	0%	98%	0%	1%	97%	0%	3%
3.00	10,000	98%	2%	0%	98%	2%	0%	97%	2%	1%	97%	2%	2%
3.00	30,000	82%	18%	0%	82%	18%	0%	82%	18%	0%	81%	18%	1%

- **T_{in}=600K**

8 cylinders		Heat Leakage											
		U=0			*U=10W/m²K*			*U=50W/m²K*			*U=100W/m²K*		
		Percentage Effect on Energy Efficiency											
Pitch Ratio	*Reynolds Number*	*HT*	*VD*	*HL*	*HT*	*VD*	*HL*	*HT*	*VD*	*HL*	*HT*	*VD*	*HL*
1.30	500	100%	0%	0%	100%	0%	0%	98%	0%	2%	97%	0%	3%
1.30	5,000	100%	0%	0%	100%	0%	0%	100%	0%	0%	99%	0%	0%
1.30	10,000	99%	1%	0%	99%	1%	0%	99%	1%	0%	99%	1%	0%
1.30	30,000	94%	6%	0%	94%	6%	0%	94%	6%	0%	94%	6%	0%
1.60	500	100%	0%	0%	100%	0%	0%	98%	0%	2%	96%	0%	4%
1.60	5,000	100%	0%	0%	100%	0%	0%	99%	0%	0%	99%	0%	1%
1.60	10,000	99%	1%	0%	99%	1%	0%	99%	1%	0%	99%	1%	0%
1.60	30,000	93%	7%	0%	93%	7%	0%	93%	7%	0%	93%	7%	0%
2.00	500	100%	0%	0%	99%	0%	1%	97%	0%	3%	94%	0%	6%
2.00	5,000	100%	0%	0%	100%	0%	0%	99%	0%	1%	99%	0%	1%
2.00	10,000	99%	1%	0%	99%	1%	0%	99%	1%	0%	98%	1%	1%
2.00	30,000	91%	9%	0%	91%	9%	0%	91%	9%	0%	91%	9%	0%
3.00	500	100%	0%	0%	99%	0%	1%	94%	0%	6%	88%	0%	12%
3.00	5,000	100%	0%	0%	99%	0%	0%	99%	0%	1%	98%	0%	2%
3.00	10,000	99%	1%	0%	99%	1%	0%	98%	1%	1%	98%	1%	1%
3.00	30,000	88%	12%	0%	88%	12%	0%	88%	12%	0%	88%	12%	0%

4 cylinders		Heat Leakage											
		U=0			*U=10W/m²K*			*U=50W/m²K*			*U=100W/m²K*		
		Percentage Effect on Energy Efficiency											
Pitch Ratio	*Reynolds Number*	*HT*	*VD*	*HL*	*HT*	*VD*	*HL*	*HT*	*VD*	*HL*	*HT*	*VD*	*HL*
1.30	500	100%	0%	0%	100%	0%	0%	99%	0%	1%	98%	0%	2%
1.30	5,000	100%	0%	0%	100%	0%	0%	100%	0%	0%	99%	0%	0%
1.30	10,000	99%	1%	0%	99%	1%	0%	99%	1%	0%	99%	1%	0%
1.30	30,000	93%	7%	0%	93%	7%	0%	93%	7%	0%	93%	7%	0%
1.60	500	100%	0%	0%	100%	0%	0%	98%	0%	2%	97%	0%	3%
1.60	5,000	100%	0%	0%	100%	0%	0%	99%	0%	0%	99%	0%	1%
1.60	10,000	99%	1%	0%	99%	1%	0%	99%	1%	0%	99%	1%	0%
1.60	30,000	90%	10%	0%	90%	10%	0%	90%	10%	0%	90%	10%	0%
2.00	500	100%	0%	0%	99%	0%	1%	97%	0%	3%	95%	0%	5%
2.00	5,000	100%	0%	0%	100%	0%	0%	99%	0%	0%	99%	0%	1%
2.00	10,000	99%	1%	0%	99%	1%	0%	98%	1%	0%	98%	1%	1%

2.00	30,000	87%	13%	0%	87%	13%	0%	87%	13%	0%	87%	13%	0%
3.00	500	100%	0%	0%	99%	0%	1%	95%	0%	5%	90%	0%	10%
3.00	5,000	100%	0%	0%	99%	0%	0%	99%	0%	1%	98%	0%	2%
3.00	10,000	98%	2%	0%	98%	2%	0%	98%	2%	1%	97%	2%	1%
3.00	30,000	84%	16%	0%	84%	16%	0%	84%	16%	0%	84%	16%	0%

3 cylinders		Heat Leakage											
		U=0			*U=10W/m²K*			*U=50W/m²K*			*U=100W/m²K*		
		Percentage Effect on Energy Efficiency											
Pitch Ratio	*Reynolds Number*	*HT*	*VD*	*HL*	*HT*	*VD*	*HL*	*HT*	*VD*	*HL*	*HT*	*VD*	*HL*
1.30	500	100%	0%	0%	100%	0%	0%	99%	0%	1%	98%	0%	2%
1.30	5,000	100%	0%	0%	100%	0%	0%	100%	0%	0%	99%	0%	0%
1.30	10,000	99%	1%	0%	99%	1%	0%	99%	1%	0%	99%	1%	0%
1.30	30,000	92%	8%	0%	92%	8%	0%	92%	8%	0%	92%	8%	0%
1.60	500	100%	0%	0%	100%	0%	0%	99%	0%	1%	97%	0%	3%
1.60	5,000	100%	0%	0%	100%	0%	0%	99%	0%	0%	99%	0%	1%
1.60	10,000	99%	1%	0%	99%	1%	0%	99%	1%	0%	98%	1%	0%
1.60	30,000	88%	12%	0%	88%	12%	0%	88%	12%	0%	88%	12%	0%
2.00	500	100%	0%	0%	100%	0%	0%	98%	0%	2%	95%	0%	5%
2.00	5,000	100%	0%	0%	100%	0%	0%	99%	0%	0%	99%	0%	1%
2.00	10,000	98%	2%	0%	98%	2%	0%	98%	2%	0%	98%	2%	1%
2.00	30,000	85%	15%	0%	85%	15%	0%	85%	15%	0%	85%	15%	0%
3.00	500	100%	0%	0%	99%	0%	1%	95%	0%	5%	90%	0%	10%
3.00	5,000	100%	0%	0%	99%	0%	0%	99%	0%	1%	98%	0%	2%
3.00	10,000	98%	2%	0%	98%	2%	0%	97%	2%	1%	97%	2%	1%
3.00	30,000	81%	19%	0%	81%	19%	0%	81%	19%	0%	81%	18%	0%

APPENDIX C

Again here, exergy efficiency and the effect of heat leakage and exergy destruction for each case is demonstrated in Appendix C.

- **T_{in}=400K**

8 Cylinders		Heat Leakage											
		U=0			*U=10W/m²K*			*U=50W/m²K*			*U=100W/m²K*		
		Percentage Effect on Exergy Efficiency											
Pitch Ratio	*Reynolds Number*	*HT*	*E,D*	*HL*	*HT*	*E,D*	*HL*	*HT*	*E,D*	*HL*	*HT*	*E,D*	*HL*
1.30	500	70%	30%	0%	68%	30%	2%	64%	28%	8%	58%	26%	16%
1.30	5,000	65%	35%	0%	65%	35%	0%	64%	35%	1%	63%	34%	3%
1.30	10,000	62%	38%	0%	62%	38%	0%	62%	37%	1%	61%	37%	1%
1.30	30,000	50%	50%	0%	50%	50%	0%	50%	50%	0%	50%	50%	0%
1.60	500	66%	34%	0%	64%	34%	2%	58%	33%	9%	52%	31%	17%
1.60	5,000	62%	38%	0%	62%	38%	0%	61%	37%	2%	60%	37%	3%
1.60	10,000	60%	40%	0%	60%	40%	0%	60%	40%	1%	59%	39%	2%
1.60	30,000	48%	52%	0%	48%	52%	0%	47%	52%	0%	47%	52%	1%
2.00	500	64%	36%	0%	62%	36%	2%	56%	32%	11%	50%	29%	21%
2.00	5,000	61%	39%	0%	61%	39%	0%	60%	38%	2%	58%	38%	4%
2.00	10,000	59%	41%	0%	59%	41%	0%	58%	41%	1%	57%	40%	2%
2.00	30,000	45%	55%	0%	45%	55%	0%	45%	54%	0%	45%	54%	1%
3.00	500	61%	39%	0%	59%	37%	4%	50%	31%	19%	42%	26%	32%
3.00	5,000	59%	41%	0%	59%	40%	1%	57%	39%	3%	55%	38%	7%
3.00	10,000	57%	43%	0%	57%	43%	0%	56%	42%	2%	55%	41%	4%
3.00	30,000	41%	59%	0%	41%	59%	0%	41%	59%	1%	40%	58%	1%

4 Cylinders		Heat Leakage											
		U=0			*U=10W/m²K*			*U=50W/m²K*			*U=100W/m²K*		
		Percentage Effect on Exergy Efficiency											
Pitch Ratio	*Reynolds Number*	*HT*	*E,D*	*HL*	*HT*	*E,D*	*HL*	*HT*	*E,D*	*HL*	*HT*	*E,D*	*HL*
1.30	500	66%	34%	0%	65%	33%	2%	60%	31%	9%	55%	29%	17%
1.30	5,000	62%	38%	0%	61%	38%	0%	61%	38%	2%	59%	37%	4%

1.30	10,000	60%	40%	0%	59%	40%	0%	59%	40%	1%	58%	40%	2%
1.30	30,000	47%	53%	0%	47%	53%	0%	47%	53%	0%	47%	53%	1%
1.60	500	63%	37%	0%	61%	36%	2%	56%	33%	11%	50%	30%	19%
1.60	5,000	60%	40%	0%	60%	40%	0%	59%	39%	2%	58%	38%	4%
1.60	10,000	58%	42%	0%	58%	42%	0%	57%	41%	1%	57%	41%	2%
1.60	30,000	45%	55%	0%	45%	55%	0%	45%	55%	0%	44%	55%	1%
2.00	500	61%	39%	0%	59%	38%	3%	53%	34%	13%	47%	30%	23%
2.00	5,000	59%	41%	0%	59%	40%	1%	58%	40%	3%	56%	39%	5%
2.00	10,000	57%	43%	0%	57%	42%	0%	57%	42%	2%	56%	41%	3%
2.00	30,000	44%	56%	0%	44%	56%	0%	44%	56%	0%	43%	56%	1%
3.00	500	60%	40%	0%	57%	38%	5%	48%	32%	20%	40%	27%	33%
3.00	5,000	59%	41%	0%	58%	41%	1%	56%	40%	4%	54%	38%	8%
3.00	10,000	57%	43%	0%	56%	43%	0%	55%	42%	2%	54%	41%	5%
3.00	30,000	41%	59%	0%	41%	59%	0%	41%	59%	1%	40%	58%	2%

3 Cylinders		Heat Leakage											
		U=0			*U=10W/m^{2}K*			*U=50W/m^{2}K*			*U=100W/m^{2}K*		
		Percentage Effect on Exergy Efficiency											
Pitch Ratio	*Reynolds Number*	*HT*	*E,D*	*HL*	*HT*	*E,D*	*HL*	*HT*	*E,D*	*HL*	*HT*	*E,D*	*HL*
1.30	500	65%	35%	0%	64%	34%	2%	60%	31%	10%	55%	27%	18%
1.30	5,000	61%	39%	0%	61%	39%	0%	60%	38%	2%	59%	37%	4%
1.30	10,000	59%	41%	0%	59%	41%	0%	58%	41%	1%	58%	40%	2%
1.30	30,000	46%	54%	0%	46%	54%	0%	45%	54%	0%	45%	54%	1%
1.60	500	62%	38%	0%	61%	37%	2%	56%	33%	11%	51%	28%	21%
1.60	5,000	60%	40%	0%	59%	40%	0%	58%	39%	2%	57%	38%	5%
1.60	10,000	58%	42%	0%	57%	42%	0%	57%	42%	1%	56%	41%	3%
1.60	30,000	43%	57%	0%	43%	57%	0%	43%	56%	0%	43%	56%	1%
2.00	500	61%	39%	0%	59%	38%	3%	53%	33%	14%	47%	28%	25%
2.00	5,000	59%	41%	0%	59%	41%	1%	57%	40%	3%	56%	38%	6%
2.00	10,000	57%	43%	0%	57%	43%	0%	56%	42%	2%	55%	41%	3%
2.00	30,000	43%	57%	0%	43%	57%	0%	43%	57%	1%	43%	56%	1%
3.00	500	60%	40%	0%	57%	38%	5%	48%	32%	21%	40%	26%	35%
3.00	5,000	58%	42%	0%	58%	41%	1%	56%	40%	4%	54%	38%	9%
3.00	10,000	56%	44%	0%	56%	43%	1%	55%	42%	3%	54%	41%	5%
3.00	30,000	40%	60%	0%	40%	60%	0%	40%	59%	1%	40%	59%	2%

- **T_{in}=500K**

8 Cylinders		Heat Leakage											
		U=0			*U=10W/m²K*			*U=50W/m²K*			*U=100W/m²K*		
		Percentage Effect on Exergy Efficiency											
Pitch Ratio	*Reynolds Number*	*HT*	*E,D*	*HL*	*HT*	*E,D*	*HL*	*HT*	*E,D*	*HL*	*HT*	*E,D*	*HL*
1.30	500	47%	53%	0%	47%	52%	1%	46%	51%	4%	44%	49%	8%
1.30	5,000	43%	57%	0%	43%	57%	0%	42%	57%	1%	42%	57%	1%
1.30	10,000	41%	59%	0%	41%	58%	0%	41%	58%	0%	41%	58%	1%
1.30	30,000	38%	62%	0%	38%	62%	0%	38%	62%	0%	37%	62%	0%
1.60	500	43%	57%	0%	43%	56%	1%	41%	54%	4%	39%	52%	8%
1.60	5,000	40%	60%	0%	40%	60%	0%	40%	59%	1%	40%	59%	2%
1.60	10,000	40%	60%	0%	39%	60%	0%	39%	60%	0%	39%	60%	1%
1.60	30,000	36%	64%	0%	36%	64%	0%	36%	64%	0%	36%	64%	0%
2.00	500	41%	59%	0%	41%	58%	1%	39%	55%	6%	37%	53%	11%
2.00	5,000	39%	61%	0%	39%	61%	0%	39%	60%	1%	38%	60%	2%
2.00	10,000	38%	62%	0%	38%	61%	0%	38%	61%	1%	38%	61%	1%
2.00	30,000	35%	65%	0%	35%	65%	0%	35%	65%	0%	35%	65%	0%
3.00	500	39%	61%	0%	39%	59%	2%	36%	55%	10%	32%	50%	18%
3.00	5,000	38%	62%	0%	38%	62%	0%	37%	61%	2%	37%	60%	3%
3.00	10,000	38%	62%	0%	37%	62%	0%	37%	62%	1%	37%	61%	2%
3.00	30,000	33%	67%	0%	33%	67%	0%	33%	67%	0%	33%	66%	1%

4 Cylinders		Heat Leakage											
		U=0			*U=10W/m²K*			*U=50W/m²K*			*U=100W/m²K*		
		Percentage Effect on Exergy Efficiency											
Pitch Ratio	*Reynolds Number*	*HT*	*E,D*	*HL*	*HT*	*E,D*	*HL*	*HT*	*E,D*	*HL*	*HT*	*E,D*	*HL*
1.30	500	43%	57%	0%	43%	56%	1%	42%	54%	4%	40%	52%	8%
1.30	5,000	40%	60%	0%	40%	60%	0%	40%	60%	1%	39%	59%	2%
1.30	10,000	39%	61%	0%	39%	61%	0%	39%	61%	1%	39%	60%	1%
1.30	30,000	36%	64%	0%	35%	64%	0%	35%	64%	0%	35%	64%	0%
1.60	500	41%	59%	0%	40%	59%	1%	38%	56%	5%	36%	54%	10%
1.60	5,000	39%	61%	0%	38%	61%	0%	38%	61%	1%	38%	60%	2%
1.60	10,000	38%	62%	0%	38%	62%	0%	38%	62%	1%	37%	61%	1%
1.60	30,000	34%	66%	0%	34%	66%	0%	34%	65%	0%	34%	65%	0%
2.00	500	39%	61%	0%	39%	60%	1%	37%	57%	7%	34%	53%	12%
2.00	5,000	38%	62%	0%	38%	62%	0%	37%	61%	1%	37%	61%	3%

2.00	10,000	37%	63%	0%	37%	63%	0%	37%	62%	1%	37%	62%	1%
2.00	30,000	34%	66%	0%	34%	66%	0%	34%	66%	0%	34%	66%	1%
3.00	500	38%	62%	0%	37%	60%	2%	34%	56%	10%	31%	50%	19%
3.00	5,000	37%	63%	0%	37%	62%	0%	37%	61%	2%	36%	60%	4%
3.00	10,000	37%	63%	0%	37%	63%	0%	36%	62%	1%	36%	62%	2%
3.00	30,000	33%	67%	0%	33%	67%	0%	32%	67%	0%	32%	67%	1%

3 Cylinders		Heat Leakage											
		U=0			*U=10W/m²K*			*U=50W/m²K*			*U=100W/m²K*		
		Percentage Effect on Exergy Efficiency											
Pitch Ratio	*Reynolds Number*	*HT*	*E,D*	*HL*	*HT*	*E,D*	*HL*	*HT*	*E,D*	*HL*	*HT*	*E,D*	*HL*
1.30	500	42%	58%	0%	42%	57%	1%	41%	55%	5%	39%	52%	9%
1.30	5,000	39%	61%	0%	39%	61%	0%	39%	60%	1%	38%	60%	2%
1.30	10,000	38%	62%	0%	38%	62%	0%	38%	61%	1%	38%	61%	1%
1.30	30,000	35%	65%	0%	35%	65%	0%	35%	65%	0%	35%	65%	0%
1.60	500	40%	60%	0%	39%	60%	1%	38%	57%	6%	36%	53%	11%
1.60	5,000	38%	62%	0%	38%	62%	0%	38%	61%	1%	37%	60%	2%
1.60	10,000	38%	62%	0%	37%	62%	0%	37%	62%	1%	37%	62%	1%
1.60	30,000	34%	66%	0%	34%	66%	0%	34%	66%	0%	34%	66%	1%
2.00	500	39%	61%	0%	38%	60%	1%	36%	57%	7%	34%	53%	13%
2.00	5,000	38%	62%	0%	38%	62%	0%	37%	61%	1%	37%	61%	3%
2.00	10,000	37%	63%	0%	37%	63%	0%	37%	62%	1%	37%	62%	2%
2.00	30,000	33%	67%	0%	33%	67%	0%	33%	66%	0%	33%	66%	1%
3.00	500	38%	62%	0%	37%	61%	2%	34%	55%	11%	30%	50%	20%
3.00	5,000	37%	63%	0%	37%	63%	0%	36%	61%	2%	36%	60%	4%
3.00	10,000	37%	63%	0%	37%	63%	0%	36%	62%	1%	36%	62%	3%
3.00	30,000	32%	68%	0%	32%	68%	0%	32%	67%	1%	32%	67%	1%

- **T_{in}=600K**

8 Cylinders		Heat Leakage											
		U=0			*U=10W/m²K*			*U=50W/m²K*			*U=100W/m²K*		
		Percentage Effect on Exergy Efficiency											
Pitch Ratio	*Reynolds Number*	*HT*	*E,D*	*HL*	*HT*	*E,D*	*HL*	*HT*	*E,D*	*HL*	*HT*	*E,D*	*HL*
1.30	500	38%	62%	0%	38%	61%	1%	37%	60%	3%	36%	58%	6%
1.30	5,000	34%	66%	0%	34%	66%	0%	34%	65%	0%	34%	65%	1%
1.30	10,000	33%	67%	0%	33%	67%	0%	33%	67%	0%	33%	66%	1%
1.30	30,000	31%	69%	0%	31%	69%	0%	31%	69%	0%	31%	69%	0%

1.60	500	35%	65%	0%	35%	65%	1%	34%	63%	3%	32%	61%	6%
1.60	5,000	32%	68%	0%	32%	68%	0%	32%	67%	1%	32%	67%	1%
1.60	10,000	32%	68%	0%	32%	68%	0%	32%	68%	0%	31%	68%	1%
1.60	30,000	30%	70%	0%	30%	70%	0%	29%	70%	0%	29%	70%	0%
2.00	500	33%	67%	0%	33%	66%	1%	32%	64%	4%	30%	62%	8%
2.00	5,000	31%	69%	0%	31%	69%	0%	31%	68%	1%	31%	68%	1%
2.00	10,000	31%	69%	0%	31%	69%	0%	31%	69%	0%	31%	69%	1%
2.00	30,000	29%	71%	0%	29%	71%	0%	29%	71%	0%	29%	71%	0%
3.00	500	31%	69%	0%	31%	67%	2%	29%	64%	7%	27%	59%	14%
3.00	5,000	31%	69%	0%	30%	69%	0%	30%	69%	1%	30%	68%	3%
3.00	10,000	30%	70%	0%	30%	70%	0%	30%	69%	1%	30%	69%	1%
3.00	30,000	27%	73%	0%	27%	72%	0%	27%	72%	0%	27%	72%	1%

4 Cylinders		Heat Leakage											
		U=0			*U=10W/m²K*			*U=50W/m²K*			*U=100W/m²K*		
		Percentage Effect on Exergy Efficiency											
Pitch Ratio	*Reynolds Number*	*HT*	*E,D*	*HL*	*HT*	*E,D*	*HL*	*HT*	*E,D*	*HL*	*HT*	*E,D*	*HL*
1.30	500	35%	65%	0%	35%	65%	1%	34%	63%	3%	33%	61%	6%
1.30	5,000	32%	68%	0%	32%	68%	0%	32%	68%	1%	32%	67%	1%
1.30	10,000	31%	69%	0%	31%	69%	0%	31%	68%	0%	31%	68%	1%
1.30	30,000	29%	71%	0%	29%	71%	0%	29%	71%	0%	29%	71%	0%
1.60	500	32%	68%	0%	32%	67%	1%	31%	65%	4%	29%	64%	7%
1.60	5,000	31%	69%	0%	31%	69%	0%	31%	69%	1%	30%	68%	2%
1.60	10,000	30%	70%	0%	30%	69%	0%	30%	69%	0%	30%	69%	1%
1.60	30,000	28%	72%	0%	28%	72%	0%	28%	72%	0%	28%	71%	0%
2.00	500	31%	69%	0%	31%	68%	1%	30%	65%	5%	28%	62%	9%
2.00	5,000	30%	70%	0%	30%	69%	0%	30%	69%	1%	30%	68%	2%
2.00	10,000	30%	70%	0%	30%	70%	0%	30%	70%	1%	30%	69%	1%
2.00	30,000	28%	72%	0%	28%	72%	0%	28%	72%	0%	28%	72%	0%
3.00	500	31%	69%	0%	30%	68%	2%	28%	64%	8%	26%	59%	15%
3.00	5,000	30%	70%	0%	30%	70%	0%	30%	69%	1%	29%	68%	3%
3.00	10,000	30%	70%	0%	30%	70%	0%	29%	70%	1%	29%	69%	2%
3.00	30,000	27%	73%	0%	27%	73%	0%	27%	73%	0%	27%	72%	1%

3 Cylinders		Heat Leakage											
		U=0			*U=10W/m²K*			*U=50W/m²K*			*U=100W/m²K*		
		Percentage Effect on Exergy Efficiency											
Pitch Ratio	*Reynolds Number*	*HT*	*E,D*	*HL*	*HT*	*E,D*	*HL*	*HT*	*E,D*	*HL*	*HT*	*E,D*	*HL*
1.30	500	34%	66%	0%	34%	66%	1%	33%	64%	3%	32%	62%	7%
1.30	5,000	31%	69%	0%	31%	69%	0%	31%	68%	1%	31%	68%	1%
1.30	10,000	31%	69%	0%	31%	69%	0%	31%	69%	0%	31%	69%	1%
1.30	30,000	29%	71%	0%	29%	71%	0%	29%	71%	0%	29%	71%	0%
1.60	500	32%	68%	0%	32%	68%	1%	31%	65%	4%	29%	63%	8%
1.60	5,000	31%	69%	0%	30%	69%	0%	30%	69%	1%	30%	68%	2%
1.60	10,000	30%	70%	0%	30%	70%	0%	30%	69%	1%	30%	69%	1%
1.60	30,000	28%	72%	0%	28%	72%	0%	28%	72%	0%	28%	72%	0%
2.00	500	31%	69%	0%	31%	68%	1%	29%	65%	5%	28%	62%	10%
2.00	5,000	30%	70%	0%	30%	70%	0%	30%	69%	1%	30%	68%	2%
2.00	10,000	30%	70%	0%	30%	70%	0%	30%	70%	1%	30%	69%	1%
2.00	30,000	28%	72%	0%	28%	72%	0%	28%	72%	0%	28%	72%	0%
3.00	500	30%	70%	0%	30%	68%	2%	28%	64%	8%	26%	59%	15%
3.00	5,000	30%	70%	0%	30%	70%	0%	29%	69%	2%	29%	68%	3%
3.00	10,000	30%	70%	0%	30%	70%	0%	29%	70%	1%	29%	69%	2%
3.00	30,000	27%	73%	0%	27%	73%	0%	27%	73%	0%	27%	72%	1%